Dense Wireless Network Design and Evaluation – An Aircraft Cabin Use Case

Tezcan Cogalan

A thesis submitted for the degree of Doctor of Philosophy.
The University of Edinburgh.
March 2018

Abstract

One of the key requirements of fifth generation (5G) systems is having a connection to mobile networks without interruption at anytime and anywhere, which is also known as seamless connectivity. Nowadays, fourth generation (4G) systems, Long Term Evolution (LTE) and Long Term Evolution Advanced (LTE-A), are mature enough to provide connectivity to most terrestrial mobile users. However, for airborne mobile users, there is no connection that exists without interruption. According to the regulations, mobile connectivity for aircraft passengers can only be established when the altitude of the aircraft is above 3000 m. Along with demands to have mobile connectivity during a flight and the seamless connectivity requirement of 5G systems, there is a notable interest in providing in-flight wireless services during all phases of a flight. In this thesis, many issues related to the deployment and operation of the onboard systems have been investigated.

A measurement and modelling procedure to investigate radio frequency (RF) propagation inside an aircraft is proposed in this thesis. Unlike in existing studies for in-cabin channel characterization, the proposed procedure takes into account the deployment of a multi-cell onboard system. The proposed model is verified through another set of measurements where reference signal received power (RSRP) levels inside the aircraft are measured. The results show that the proposed model closely matches the in-cabin RSRP measurements. Moreover, in order to enforce the distance between a user and an interfering resource, cell sectorization is employed in the multi-cell onboard system deployment. The proposed propagation model is used to find an optimum antenna orientation that minimizes the interference level among the neighbouring evolved nodeBs (eNBs).

Once the optimum antenna deployment is obtained, comprehensive downlink performance evaluations of the multi-cell, multi-user onboard LTE-A system is carried out. Techniques that are proposed for LTE-A systems, namely enhanced inter-cell interference coordination (eICIC) and carrier aggregation (CA), are employed in the system analysis. Different numbers of eNBs, antenna mounting positions and scheduling policies are examined. A scheduling algorithm that provides a good tradeoff between fairness and system throughput is proposed. The results show that the downlink performance of the proposed onboard LTE-A system achieves not only 75% of the theoretical limits of the overall system throughput but also fair user data rate performance, irrespective of a passenger's seat location.

In order to provide the seamless connectivity requirement of 5G systems, compatibility between the proposed onboard system deployment and the already deployed terrestrial networks is investigated. Simulation based analyses are carried out to investigate power leakage from the onboard systems while the aircraft is in the parked position on the apron. According to the regulations, the onboard system should not increase the noise level of the already deployed terrestrial system by 1 dB. Results show that the proposed onboard communication system can be operated while the aircraft is in the parked position on the apron without exceeding the 1 dB increase in the noise level of the already deployed terrestrial 4G network. Furthermore, handover parameters are obtained for different transmission power levels of both the terrestrial and

onboard systems to make the transition from one system to another without interruption while a passenger boards or leaves the aircraft. Simulation and measurement based analyses show that when the RSRP level of the terrestrial system is below -65 dBm around the aircraft, a boarding passenger can be smoothly handed over to the onboard system and vice versa. Moreover, in order to trigger the handover process without interfering with the data transmission, a broadcast control channel (BCCH) power boosting feature is proposed for the in-cabin eNBs. Results show that employing the BCCH power boosting feature helps to trigger the handover process as soon as the passengers step on board the aircraft.

Lay summary

During the evolution of wireless communications, the way people use their mobile devices changed from voice-oriented to data-oriented services. In today's world, every mobile user wants to stay connected to online services at anytime and anywhere. In other words, an uninterrupted, seamless connectivity is desired. Although the current form of the fourth generation (4G) networks can provide such connectivity to the majority of terrestrial users, having an onboard connection for passengers has recently been proposed. Therefore, a lot of questions regarding how to deploy and when to operate onboard systems are gaining attention from both industry and academia. An aircraft cabin is characterised by a high user density. This poses a particular challenge to fairly distribute the user data rate inside the aircraft. Another challenge is the unusual propagation environment due to the construction materials of the aircraft including the metal hull, which is an excellent reflector of radio frequency (RF) waves. As a result, interference may become the system throughput limiting factor. Hence, in-cabin RF propagation characteristics and interference mitigation techniques are of primary importance.

This thesis focuses on the fundamental downlink characteristics of the onboard 4G system which consists of multiple cells. Firstly, in order to investigate the channel propagation characteristics inside the aircraft, a measurement and channel modelling procedure is proposed. The proposed channel model is used to find an optimum antenna orientation that minimizes the received power level of a neighbouring cell. The received power level generated by the proposed channel model is verified through on-site, multi-cell deployment measurements. The results show that the modelled power levels closely match the measured received power levels. Afterwards, a scheduling algorithm that provides a good tradeoff between the fair user data rate distribution and total system throughput is proposed. According to comprehensive downlink performance evaluations, the proposed scheduling algorithm achieves a better tradeoff between the fairness and system throughput than the commonly considered scheduling algorithms.

In order to establish the seamless connectivity for passengers, interference between the system in the aircraft and terrestrial networks is another focus point of this thesis. Based on regulations, an onboard system could only be in operation when the altitude of the aircraft is above 3000 m in order to mitigate harmful interference from onboard systems to terrestrial networks. In this thesis, power leakage from onboard to terrestrial systems and vice versa are investigated by computer simulations and on-site measurements while the aircraft is in the parked position on the apron. Furthermore, handover parameters are also investigated to provide a smooth, uninterrupted transition from one system to another as soon as users step on board or leave the aircraft. The results show that (1) the proposed onboard system can coexist within the already deployed terrestrial network without causing a harmful interference while the aircraft is in the parked position; and (2) a boarding passenger can be smoothly handed over to the onboard system and vice versa. Consequently, it can be advised that the legislation that prohibits the operation of onboard systems should be reviewed, so that the necessary steps can be taken to provide seamless mobile connectivity.

Declaration of originality

I hereby declare that the research recorded in this thesis and the thesis itself were composed and originated entirely by myself in Light-Fidelity (Li-Fi) Research and Development (R&D) Centre, Institute for Digital Communications, School of Engineering, University of Edinburgh.

The only exception to the above is the MATLAB code used as a basis for the simulation setup, which is based on a previous effort by Dr. Stefan Videv.

Tezcan Cogalan

Acknowledgements

First and foremost, I would like to offer my sincerest gratitude to my wife, Gokcen, and my parents, Ferda and Tahsin, who have always supported me, and boosted my pursuit for any aspirations that I have/had. No matter what has happened, they have always been by my side to encourage me and without them I could never accomplished this thesis.

I owe my undying gratitude to Professor Harald Haas, my supervisor, who has guided me throughout my studies. Having the opportunity to work with him over the years was intellectually rewarding and fulfilling. With his guidance and support, I have had a chance to improve and perfect not only my research, but also my professional attitude and working efficiency. I sincerely appreciate his enthusiasm and encouragement to think outside the box.

In addition, special thanks go to Dr. Stefan Videv from the LiFi Research and Development Centre, Mr. Erhard Bassow and Mr. Stefan Schulz from Airbus Operations GmbH, Buxtehude for their close cooperation and support during this thesis. Without their cooperation and support, the contribution of this thesis would be unconvincing. I would also thank to Ms. Hannah Brown for supporting not only my writing skills throughout this thesis, but also the administrative formalities involved in the school. Also, I would like to acknowledge the support of Mohamed Sufyan Islim and Sovan Das in conducting the on-site measurements.

I am indebted to Professor Erdal Panayirci for encouraging me to pursue a PhD degree. Last but not least, I would like to thank my friends, Ahmet, Anil, Burak, Ekrem, Gokhan, Kerem, Melike, Muhammed, Oguzhan, Sinan and Tulin, who have helped me to enjoy my experience in Edinburgh.

Finally, I would like to acknowledge the financial support of Airbus Operations GmbH, Buxtehude and the School of Engineering at the University of Edinburgh.

Contents

List of figures

List of tables

Acronyms and abbreviations

3GPP	third generation partnership project
1G	first generation
2G	second generation
3G	third generation
4G	fourth generation
5G	fifth generation
ABS	almost blank subframe
AMC	adaptive modulation and coding
AR	augmented reality
BCCH	broadcast control channel
BLER	block error ratio
CA	carrier aggregation
CAGR	compound annual growth rate
CC	carrier component
CDF	cumulative distribution function
CDL	clustered delay line
CDMA	code division multiple access
CoMP	coordinated multi-point transmission
CB	coordinated beamforming
CFI	control format indicator
CQI	channel quality indicator
CRE	cell range extension
CRS	cell-specific reference signal
CS	coordinated scheduler

CSI	channel state information
CW	continuous wave
DPS	dynamic point selection
ECC	Electronic Communications Committee
EARFCN	evolved universal terrestrial radio access absolute radio frequency channel number
eICIC	enhanced inter-cell interference coordination
EIRP	effective isotropic radiated power
EM	electro-magnetic
EMI	electro-magnetic interference
eNB	evolved nodeB
EPC	evolved packet core
EPRE	energy per resource element
E-UTRA	evolved universal terrestrial radio access
E-UTRAN	evolved universal terrestrial radio access network
EVM	error vector magnitude
DA2GC	direct air-to-ground communication
FAA	Federal Aviation Administration
FCC	Federal Communications Commission
FDD	frequency division duplex
FDMA	frequency division multiple access
FFR	fractional frequency reuse
GSM	Global System for Mobile Communications
HPBW	half power beamwidth
IB	ideal backhaul
IE	information element
i.i.d.	identical and independently distributed
ICIC	inter-cell interference coordination
IP	internet protocol

IoT	internet of things
JP	joint processing
JT	joint transmission
LoS	line of sight
LSB	least significant bit
LTE	Long Term Evolution
LTE-A	Long Term Evolution Advanced
MAC	medium access control
MCS	modulation and coding scheme
MIMO	multiple input multiple output
MLE	maximum likelihood estimation
MME	mobility management entity
MSB	most significant bit
MTC	machine-type communication
NCU	network control unit
NFV	network function virtualization
NIB	non-ideal backhaul
NLoS	non-line of sight
NSF	normal subframes
OFDM	orthogonal frequency division multiplexing
OFDMA	orthogonal frequency division multiple access
PCI	physical cell ID
PCS	proportional fair based coordinated scheduler
PDCCH	physical downlink control channel
PDCP	packet data convergence protocol
PDF	probability distribution function
PDSCH	physical downlink shared channel
PF	proportional fair
PGW	packet data network gateway

PHY	physical layer
PLMN	public land mobile network
QAM	quadrature amplitude modulation
QoS	quality of service
QPSK	quadrature phase shift keying
RA	resource allocation
RB	resource block
RBG	RB group
RE	resource element
RF	radio frequency
RIV	resource indication value
RLC	radio link control
RP-ABS	reduced power-ABS
RR	round-robin
RRC	radio resource control
RS	reference signal
RSRP	reference signal received power
RSRQ	reference signal received quality
RSSI	received signal strength indicator
SCFDMA	single carrier frequency division multiple access
SDN	software defined network
SGW	serving gateway
SIB	system information block
SINR	signal-to-noise-plus-interference ratio
SIR	signal-to-interference ratio
TBS	transport block size
TDD	time division duplex
TDMA	time division multiple access
TS	time slot

TTI	transmission time interval
UE	user equipment
UMTS	Universal Mobile Telecommunications System
VR	virtual reality
VRB	virtualized resource block
WINNER	Wireless World Initiative New Radio

Nomenclature

a_i	power delay value
A_{PL}	path loss exponent for terrestrial systems
$b_{u,j}^{c}$	indicator MCS index j is used for user u in cell c
B_{PL}	intercept determined by the free space path loss for the reference distance
$B\left(\cdot,\cdot,\cdot,\cdot\right)$	3-D antenna pattern gain
$B_{\phi}(\cdot,\cdot)$	antenna azimuth pattern gain
$B_{\theta}(\cdot,\cdot)$	antenna elevation pattern gain
B_0	maximum antenna front-to-back attenuation
B_r	bandwidth of a RB
c	nominal index
$\acute{c}$	nominal index of cell that uses reduced transmission power
c^*	nominal index for connected cells
c_n	nominal index for aggregated channels
$c_n^{(i,j)}$	nominal index for channel aggregation
C^n	number of channels that can be aggregated
$\mathcal{C}$	set of cells
$\mathcal{C}^n$	set of channels that can be aggregated
$\mathcal{C}_x$	set of cells that are considered for the simulation case x
$\mathcal{C}_x^r$	set of cells that use RB r for the simulation case x
C_{PL}	frequency dependent path loss for terrestrial systems
C	number of cells
$C_{\mathrm{RE}}^{\mathrm{RB}}$	number of PDSCH subcarriers per RB in a subframe
$\mathrm{CIO}_{\mathrm{in}}$	*cellIndividualOffset* of in-cabin eNBs
$\mathrm{CIO}_{\mathrm{out}}$	*cellIndividualOffset* of terrestrial eNBs
d	distance in m
$d_{\mathrm{K-S}}$	Kolmogorov-Smirnov test result
d_{in}	distance between wall to the indoor terminal
d_i	nominal location index
$d_{\mathrm{BP}}^{'}$	effective break point distance

d_{BP}	break point distance
$\mathcal{D}_x$	distribution parameters set of a distribution function x
$\hat{\mathcal{D}}_x$	estimated distribution parameters set of a distribution function x
f_c	carrier frequency
f_{AMC}	AMC function
$\tilde{f}_{\text{AMC}}(\cdot, p)$	power reduction level based limited AMC function
$f_{\text{AMC}}^{\text{256QAM}}$	AMC function that has maximum modulation order of 256QAM
$f_{\text{CQI,RA}}$	RBG and subband mapping function
$f_{\text{eff}}(\cdot)$	effective RB SINR mapping function
f_x^{PDF}	PDF of a distribution function x
$f_{\text{exponential}}^{\text{PDF}}$	PDF of exponential distribution
$f_{\text{nakagami}}^{\text{PDF}}$	PDF of Nakagami-m distribution
$f_{\text{rayleigh}}^{\text{PDF}}$	PDF of Rayleigh distribution
$f_{\text{weibull}}^{\text{PDF}}$	PDF of Weibull distribution
$F(\cdot)$	CDF
$F_{\text{PL}}(d_0)$	free-space path loss at reference distance d_0
g	nominal index
$G^{(c)}$	number of RBGs in cell c
G_{rx}	receive antenna gain
G_{tx}	transmit antenna gain
$\mathcal{G}^{(c)}$	set of RBGs in cell c
$h'(t)$	time-domain channel response
h_{BS}	antenna height of eNB
h_{MS}	antenna height of UE
$h_{\text{BS}}^{'}$	effective antenna height of eNB
$h_{\text{MS}}^{'}$	effective antenna height of UE
h_{w_i}	random variable
$H_{u,r}^{c}$	channel gain from cell c to user u on RB r
$H_{\text{RB}}^{\text{A}}(\cdot,\cdot)$	channel frequency response of eNBs inside aircraft
$H_{\text{RB}}^{\text{T}}(\cdot)$	channel frequency response of terrestrial eNBs
$H_0(\cdot)$	frequency-domain fast fading channel information of terrestrial eNBs
I^c	indicator cell c uses reduced transmission power level
j	nominal index

j^*	chosen MCS index
j_p	MCS index of the limited modulation order with the highest spectral efficiency
k	Boltzmann's constant
k_{wei}	shaping parameter of Weibull distribution
k_j	spectral efficiency of CQI index j
K_g	number of RBs in RBG g
l	nominal index
L	vector length
L_{cable}	total RF cable loss
M	number of selected bands
$M_{f_{\text{AMC}}}$	modulation order
$M_{f^p_{\text{AMC}}}$	modulation order that depends on power reduction level
n	path loss exponent
n_{Fl}	floor index
$N^{\text{PDSCH}}_{\text{CRS,RE}}$	number of CRS REs among PDSCH subcarriers
N_r	noise power on RB r
N_{RB}	number of RBs
$N_{\text{RB},c}$	number of RBs in cell c
$N^{\text{symbol}}_{\text{RE}}$	number of REs in a symbol
$N^{\text{PDCCH}}_{\text{symbol}}$	number of PDCCH symbols
$N^{\text{subframe}}_{\text{symbol}}$	number of symbols in a subframe
N_U	number of users between given antenna location points
p	transmission power reduction level for RP-ABS in dB
$p^{\acute{c}}_{\text{offset}}$	transmission power offset
P_A	UE-specific power allocation parameter
P_B	cell-specific power allocation parameter
P_c	transmission power of cell c
P^c_r	transmitted power of cell c on RB r
$P_{(\cdot),\text{LoS}}$	LoS link probability of WINNER scenarios
P_{rx}	measured received power level
$\overline{P_{\text{rx}}}$	average measured received power level
P_{tx}	measured transmit power level at antenna port
P_{Tx}	transmit power on CRS EPRE

$P_{u,c,r}$	received power on RB r from cell c to user u
$P_{u,x}^{\text{RSSI}}$	RSSI of a user u for a simulation case x
P_{u}^{RSRP}	RSRP of a user u
$\text{PL}_{\text{aircraft}}(\cdot,\cdot)$	path loss of in-cabin system
$\text{PL}_{\text{terrestrial}}$	path loss for terrestrial systems
$Q_{u^*}^{c}$	maximum MCS index among all RBGs for user u
$Q_{u,g}^{c}$	MCS index of RBG g for user u in cell c
$\tilde{Q}_{u,g}^{c}$	maximum MCS index among all RBGs for user u when eICIC techniques are used
$\tilde{Q}_{\acute{u},g}^{\acute{c}}$	maximum MCS index among all RBGs for users that are connected to cell which uses reduced transmission power
r	nominal index
R^{c}	number of RBs in cell c
$\mathcal{R}^{(c_n^{i,j})}$	resource set when channels i and j are aggregated
$\text{RSRP}_{\text{measured}}$	measured RSRP values
$\text{RSRP}_{\text{modelled}}$	modelled RSRP values
RSRP_{in}	RSRP level of in-cabin eNBs
RSRP_{out}	RSRP level of terrestrial eNBs
$\mathcal{R}$	set of RBs
s	nominal index
S	number of subbands
$\mathcal{S}$	set of subbands
$t_{u,g,j}^{c}$	auxiliary variable
T	temperature in Kelvin
$\overline{T}_{\text{PL}}(\theta)$	harmonic mean of the path loss difference for a given antenna tilt angle θ
u	nominal index
$\acute{u}$	nominal index of users that are connected to cell which uses reduced transmission power
$U^{(c)}$	number of users in cell c
U^{c^*}	ideal number of users per channel for an even user-channel bandwidth distribution
U_{RR}^{c}	vector that turns users in the circular order
$\mathcal{U}^{(c)}$	set of users in cell c

$\mathcal{U}^{(c_n^{i,j})}$	set of users when channels i and j are aggregated
V	constant
w_u^c	scheduling metric of user u in cell c
X	environment dependent term for terrestrial systems
$X_{\sigma_{\text{SF}}}$	log-normal shadowing variable
$x_{u,g}^c$	indicator RBG g in cell c is allocated to user u
$y_{u,g}^{c,\acute{c}}$	auxiliary variable
$Z(\theta)$	utility function of a given antenna tilt angle θ
$\overline{Z}_{\text{PL}}(\theta)$	harmonic mean of the path loss for a given antenna tilt angle θ
α^*	user-resource parity
χ_{σ_L}	large-scale signal fluctuations
Δ_ϕ	antenna azimuth HPBW
$\delta_{\text{power-offset}}$	transmission scheme based power offset
Δ_θ	antenna elevation HPBW
ΔP_{rx}	the ratio of the received power variation
$\ell(\cdot)$	log-likelihood function
$\gamma_{u,r}^c$	SINR of a user u in cell c on a RB r
$\tilde{\gamma}_{\acute{u},r}^{\acute{c}}$	SINR expression for RB r for user u in cell $\acute{c}$ when eICIC techniques are used
$\tilde{\gamma}_{u,r}^c$	SINR expression for RB r for user u in cell c when eICIC techniques are used
$\Gamma_{u,r}^c$	effective SINR of user u in cell c on RB r
$\Gamma_{u,g}^c$	effective SINR of user u in cell c on RBG g
$\tilde{\Gamma}_{u,g}^c$	effective SINR of user u in cell c on RBG g when eICIC techniques are used
$\tilde{\Gamma}_{u,r}^c$	effective SINR of user u in cell c on RB r when eICIC techniques are used
κ_{RB}	frequency-domain power variation term of a RB
λ_{exp}	scaling parameter of exponential distribution
λ_{wei}	scaling parameter of Weibull distribution
ω	spread controlling parameter of Nakagami-m distribution
ϕ	angle between transmitter and receiver in azimuth plane
Φ	antenna azimuth orientation
$\rho_{(\cdot)}$	PDSCH EPRE to cell-specific RS EPRE ratio
σ_{ray}	scaling parameter of Rayleigh distribution
σ_{SF}	shadowing standard deviation for terrestrial systems
σ_L	standard deviation of large-scale signal fluctuations term

τ_i	delay variable
Θ	antenna elevation orientation
θ	angle between transmitter and receiver in elevation plane
Ξ_{th}	data rate threshold constant
$\xi_{u,g}^{c}$	achievable rate on RBG g for user u in cell c
$\bar{\xi}_{u}^{c}$	average data rate for user u in cell c over a certain averaging period
$\tilde{\xi}_{\acute{u},g}^{\acute{c}}$	achievable rate on RBG g for users that are connected to cell which uses reduced transmission power
$\tilde{\xi}_{u,g}^{c}$	achievable rate on RBG g for user u in cell c when eICIC techniques are used
$\lceil \cdot \rceil$	ceiling function
$\min(\cdot,\cdot)$	function to take the minimum of two input values

Chapter 1
Introduction

1.1 Motivation

The demand for high data rates is an inherent result of the increasing number of mobile subscriptions and recent developments in video and gaming technology. Long Term Evolution (LTE), also known as fourth generation (4G), is proposed to fulfill the required data rates and improve mobile user experience in the long term. LTE is also designed to provide a smooth transition to fifth generation (5G) mobile wireless technology through different phases such as Long Term Evolution Advanced (LTE-A) and LTE-A Pro. The key component of 5G technology is unlimited access to information and the sharing of data anywhere and anytime for anyone and anything [6]. Although LTE technology is mature, it has only recently been proposed for use in aircraft [7–10], so, further development is required to satisfy the unlimited access requirement of 5G technology.

The main reasons to postpone in-flight connectivity are the prohibition of mobile device use within the aircraft, the cost of providing a high speed backhaul link to the aircraft and interference from the onboard system to terrestrial networks. However, today, customer demand coupled with new business models in the airline industry such as the "bring your own device" initiative and onboard shopping are responsible for increasing the interest around in-flight connectivity.

In 1963, the first regulation on using mobile devices onboard an aircraft was published by the Federal Aviation Administration (FAA). Although it is commonly believed that mobile devices are prohibited for security reasons, in actuality, the regulation is based on the fact that the onboard mobile devices have a potential to interfere with terrestrial wireless networks [11]. In 1991, the Federal Communications Commission (FCC) released its rules which banned the airborne use of mobile devices [12]. At that time, time division multiple access (TDMA) was used as the access technology. In TDMA, once a user is assigned for transmission, they benefit the whole operated frequency channel for a given period. Also, adaptive power allocation was not used at that time. Therefore, concerns about interference caused by using mobile devices onboard an aircraft to terrestrial networks were reasonable.

However, LTE systems use orthogonal frequency division multiple access (OFDMA) in downlink and the single carrier frequency division multiple access (SCFDMA) scheme in uplink directions. The orthogonality feature of both of the schemes provide efficient use of the operated frequency band and manage the interference among deployed cells as well as mobile devices. Moreover, along with the enhancements in LTE systems, deploying smaller cells, which can have a coverage area from tens to hundreds of metres, and establishing cooperation among those cells to adapt their control decisions is achievable. Also, using multiple input multiple output (MIMO) systems in LTE allows the antenna propagation to be beamed in a specific direction. As a matter of fact, providing backhaul link to an aircraft, managing interference from an onboard system to terrestrial systems and deploying multiple cells inside an aircraft are attainable for LTE systems. Accordingly, revising the imposed limitations on mobile connectivity for the passengers onboard is considered by the FCC [12, 13] and the Electronic Communications Committee (ECC) [2, 3, 14–17]. Based on the ECC reports and decisions, the in-cabin mobile system should only be operated when the altitude of the aircraft is 3000 m or more and the system should not be operated while the aircraft is on the ground or during take-off and landing [14].

Nowadays, satellite based systems are used to provide a backhaul link to aircraft onboard systems. However, due to the latency issue of the satellite based systems, an LTE based approach, which is called direct air-to-ground communication (DA2GC), is considered as a complementary technology to provide the backhaul link [7, 9]. Since in-flight connectivity is a newly proposed concept, many questions related to providing backhaul, designing in-cabin deployment and managing interference from the in-cabin system to terrestrial systems still remain open. Limitations of the satellite and LTE based techniques to provide the backhaul link are discussed in detail in [8, 9, 18]. This thesis focuses on the designing of an onboard communication system, which is motivated by the following considerations. On the one hand, in order to satisfy a quality of service (QoS) requirement for all passengers, a multi-cell network should be considered inside the aircraft. However, due to the channel conditions, weight and antenna mounting space constraints of an aircraft, deploying a multi-cell network inside is not as straightforward as it is in terrestrial systems. Therefore, the onboard system should be well investigated to provide the same performance for passengers irrespective of their seat location.

As noted, according to the current regulations, the onboard system can only be in operation when the altitude of the aircraft is above 3000 m. However, in order to provide seamless connectivity as a requirement for the new generation of communication system, the onboard system should be active in every phase of a flight. Therefore, the onboard system should be designed to avoid harmful interference to the terrestrial networks while the aircraft is on the ground.

An in-cabin communication system can be considered as a user dense and interference-limited environment due to the structure and construction materials of the aircraft. In a medium-sized commercial aircraft, the passenger capacity varies between 150 and 240, and the passenger seats are located very close to each other by means of rows and columns. Due to this tight structure and the metal hull of the aircraft, the radio frequency (RF) propagation characteristics inside the cabin severely limit the system capacity. It is important to note that the challenge is not in the selection of the best single link transmission technique, but in the design of the system as a whole, which is a challenging multi-user system with point-to-multipoint and multipoint-to-point transmission. Therefore, the in-cabin channel propagation characteristics should be well investigated to design such a multi-user system deployment. For these reasons, a series of measurement and modelling studies are conducted in this research.

It has been estimated that involvement of new technologies and applications such as cloud-based technologies, internet of things (IoT), machine-type communication (MTC) and virtual reality (VR) would see mobile data usage increasing at its current pace [19]. This increase is also foreseen for the in-flight connectivity where 15 Mbps per passenger[1] and 1.2 Gbps per aircraft downlink data rates are considered as 5G requirements for in-flight connectivity [20]. Such a performance can be achieved when more cells are deployed. However, the cable weight and wiring cost of a dense in-cabin deployment substantially increases the operational and manufacturing costs. In the designing of a multi-user system deployment, a number of system metrics such as system throughput, user throughput and deployment cost can be considered. In this thesis, the tradeoff between the overall system throughput and user data rate fairness is considered as the objective of the design. Therefore, techniques to improve the throughput performance of the users that are severely affected by interference and to improve the achievable peak data rate are investigated in the multi-cell, multi-user onboard system design in this research.

[1] It is assumed that 20% of the users are active in an aircraft which has a capacity of 400 passengers.

1.2 Contribution

This thesis focuses on investigating the characteristics of in-cabin communication systems. In a systematic approach, the following three research objectives are aimed to be addressed:

- Establishing a multi-cell system deployment model for in-cabin LTE-A communication systems.
- Evaluating and improving the downlink performance of the multi-cell, multi-user onboard LTE-A communication networks.
- Evaluating the compatibility between the in-cabin and already deployed terrestrial networks.

By following these objectives, several contributions have been established.

As the first contribution of this thesis, an optimum antenna deployment by means of minimizing the interference level among neighbour cells and maximizing the received signal level for the users is proposed. Due to the materials used to construct an aircraft, the in-cabin channel propagation has different characteristics than commonly considered indoor channel propagation. In the proposed deployment, measurement based channel propagation characteristics inside the aircraft are considered for an onboard multi-cell system deployment. A tilt angle which is optimum for deploying multiple evolved nodeBs (eNBs) inside the aircraft is obtained. The work conducted on antenna deployment and the measurement based channel propagation characteristics has led to the publication of [21, 22].

Following the second research objective leads to the second and main contribution of this thesis: the comprehensive performance evaluation of the multi-cell, multi-user onboard LTE-A system. A major concern in the multi-cell, multi-user systems is the user throughput fairness. Although deploying the multi-cell structure may improve the overall system throughput, it may cause performance outage for the users that are on the edge of the deployed cells and severely impacted by interference. A scheduling algorithm is proposed to provide a good tradeoff between the overall system throughput and fairness. In particular, the practical constraints that LTE-A systems have are considered in the formulation of the scheduling problem. The work conducted on the practical LTE-A scheduler has led to the publication of [23]. Furthermore, the performance of the techniques that are proposed to manage interference level in LTE-A systems is evaluated to recommend the system deployment for different QoS metrics. The research conducted on the system deployment recommendation has led to the submitted paper [24].

Regarding the third objective, an onboard mobile communication system can only be operated in certain phases of a flight. However, in order to provide seamless connectivity for aircraft passengers, the onboard communication system should be in operation in every phase of the flight. This leads to the third contribution of this thesis: compatibility of an onboard LTE-A system with the current terrestrial LTE-A systems when the aircraft is stationary on the ground. The signal-to-noise-plus-interference ratio (SINR) performance and interference level of the users, who are (1) inside the airport building; (2) waiting to board the aircraft; and (3) ground service employers, are investigated using computer simulations. To validate the simulation based analysis of the compatibility of both systems, a power leakage measurement from onboard to terrestrial and terrestrial to onboard systems has been conducted. Furthermore, how to handover the passengers to the in-cabin cells when the passenger steps on board the aircraft is studied. Different power levels for the terrestrial system are considered around the aircraft and the parameters that provide a smooth handover are obtained. The research conducted on the compatibility of the onboard and terrestrial systems when the aircraft is in the parked position on the apron has led to the submitted paper [25].

1.3 Thesis Outline

The remainder of this thesis is organised as follows. In Chapter 2, the evolution of the communication technologies is briefly introduced. Furthermore, the concept of the in-flight connectivity is introduced. For the investigation of an onboard LTE-A system, a number of basic procedures in LTE are provided.

In Chapter 3, the issue of deploying multiple cells inside the aircraft is introduced. Firstly, the aircraft geometry is presented. Then, a measurement and modelling procedure is proposed to characterize radio propagation inside an aircraft. The proposed procedure contains three phases in order to characterize (1) the propagation direction; (2) the reflections from the cockpit and tail ends of the cabin; and (3) the reflections from the sidewalls of the cabin. The first phase of the proposed measurement procedure is conducted in an Airbus A321 aircraft for the 1800 MHz frequency band. Based on the measured propagation characteristics, an optimum antenna tilt angle is found to deploy an onboard multi-cell system. Furthermore, a seat-by-seat measurement is conducted to investigate the received power level from the deployed cells inside the aircraft and validate the SINR performance of the found optimum tilt angle.

In Chapter 4, the downlink performance evaluation of the multi-cell, multi-user onboard LTE-A system is considered. The main objective of the downlink performance evaluation is to find an optimal system architecture which improves the tradeoff between the system throughput and user throughput fairness. Firstly, a resource scheduling problem is formulated to consider the LTE system constraints such as channel quality indicator (CQI) reporting, resource allocation (RA) type and single modulation and coding scheme (MCS) index assignment to the resources allocated to a user. Then, the scheduling problem is updated to consider interference coordination techniques. A proportional fair based coordinated scheduler (PCS) is proposed to improve the user data rate fairness to system throughput tradeoff. Accordingly, the performance of an onboard system with and without almost blank subframe (ABS) and reduced power-ABS (RP-ABS) techniques is analysed. Furthermore, effects of employing carrier aggregation (CA) and an enhanced modulation scheme, which is 256-quadrature amplitude modulation (QAM), are investigated. Finally, a recommended system decision diagram is provided.

In Chapter 5, compatibility of an onboard system and the already deployed terrestrial network is investigated while the aircraft is stationary and in the parked position on the apron. In order to understand how these two systems interact with each other, the downlink SINR and power leakage from onboard to terrestrial and terrestrial to onboard systems are analysed based on computer simulations. Then, the given simulation results are validated through on-site measurements. In the measurement setup, an A321 aircraft inside a hangar is covered by a terrestrial network provider. Transmission power level of the terrestrial and onboard systems is varied to investigate the power leakage from one system to another. Based on the measurement results, procedure and parameters on how to handover the passengers when they board the aircraft are provided. The results overwhelmingly demonstrate that the onboard system can be activated in every phase of a flight.

Chapter 6 summarises key findings of this thesis. Additionally, the limitations of the research presented in this thesis and future research directions are also discussed.

Chapter 2
Background

2.1 Introduction

In the early years of cellular communications systems, analogue technology was used to transmit voice signals. Service providers deployed cells with a range of up to 20 km in rural areas and up to 1 km in urban areas for mobile voice transmission. In the first generation (1G) systems, frequency division multiple access (FDMA), which divides the operated frequency band into multiple bands and assigns each band to a user, was used as the multiple access scheme. Along with enhancements in digital technology, multiplexing multiple users per channel was enabled in second generation (2G) digital systems. Moreover, text messaging was added to the already existing voice transmission as a mobile service. For these services, time division multiple access (TDMA) which uses operated frequency band for a user on a time basis, was used to serve multiple users. Today, many 2G systems are still in operation to deliver mobile voice services. When the number of mobile subscriptions increased and data transmission took place among the already available text and voice services, service providers had to shrink their deployed cells in order to improve their service quality in terms of connectivity and throughput. Also, another multiple access technique termed code division multiple access (CDMA), which spreads the user signal across the entire bandwidth at a transmission time period and uses a code for each user, was used in order to serve multiple users at the same time instance. However, mobile subscriptions and the demand for higher mobile data rates were increasing. Due to the used access technology, interference became a system limiting factor with an increased number of cells. Therefore, an enhanced access scheme was needed in order to deploy more, smaller cells.

Nowadays, the telecommunication industry is in its fourth generation (4G) and discussions on fifth generation (5G) technologies are ongoing. 4G is also known as Long Term Evolution (LTE) and designed to provide a smooth transition to 5G. The definition and key technologies of LTE are introduced for the first time in third generation partnership project (3GPP) Release 8. One of the most important technologies defined in LTE is orthogonal frequency division multiple access (OFDMA), which allows multiple users to share the same bandwidth at the same time by its orthogonality feature. Fig. 2.1 depicts the noted multi user access schemes.

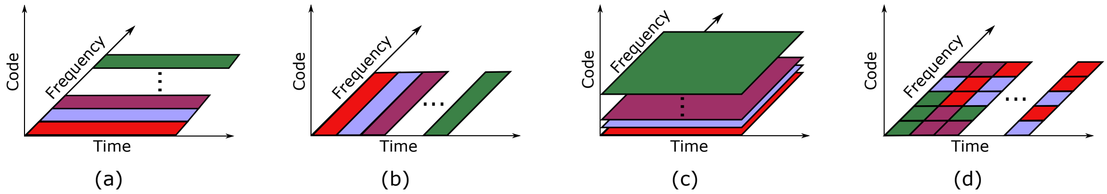

Figure 2.1: *Illustration of multi user access schemes where colors represent users. (a) FDMA. (b) TDMA. (c) CDMA. (d) OFDMA.*

However, due to the need to have high frequency reuse factors to satisfy capacity and coverage constraints, interference caused by nearby cell transmissions becomes a major factor that limits system and user capacity especially at the cell-edge. Thus, inter-cell interference coordination (ICIC) techniques are proposed in Release 8 to improve favorable channel conditions across subsets of users that are severely impacted by interference.

The evolution of LTE technology continues with 3GPP Release 9 which introduces LTE femtocells and several refinements to the techniques defined in Release 8. After the definition of LTE femtocells, the number of deployed small cells are free to increase in an unplanned manner. Thus, the performance of already planned cells (macrocells, microcells and picocells) by service providers is degraded for both centre and edge users. Therefore, better techniques are needed to simultaneously achieve the potential advantages of OFDMA as well as those granted by small cells. Accordingly, the enhanced inter-cell interference coordination (eICIC) techniques are proposed to improve small cell performance in 3GPP Release 10. One of the eICIC techniques used in time domain is almost blank subframe (ABS). ABS mitigates the interference on selected subframes by blanking data transmission at the interfering evolved nodeBs (eNBs)[1] in the system. However, blanking the data transmission at one of the eNBs means that resource blocks (RBs) of the muted eNB are unused during ABS. Thus, the throughput of the users attached to the muted eNB decreases.

Since Release 10, LTE is referred to as Long Term Evolution Advanced (LTE-A). The main reason behind the name change to LTE-A from LTE is due to two techniques introduced in Release 10: carrier aggregation (CA) and coordinated multi-point transmission (CoMP) [26]. CA is adopted to achieve wider deployment bandwidths by aggregating carrier components

[1] In LTE terminology, eNB is used to represent base station.

(CCs)[2]. Whereas, CoMP is adopted to efficiently manage the interference level between the deployed cells. Such a coordination between the geographically separated cells requires the sharing of data, which can be established by using the LTE X2 interface [27].

Beyond 3GPP Release 10, a number of refinements to existing capabilities are done to achieve a quality of service (QoS) threshold for all types of users. In 3GPP Release 11, an enhanced approach of ABS, reduced power-ABS (RP-ABS), is proposed to decrease the interference level, while providing throughput to interfering eNBs during the ABS subframe [28]. In Release 12 some new features such as 3D beamforming, dual connectivity, data offloading and LTE for unlicensed spectrum are proposed. Beyond Release 12, further enhancements have been done to the proposed features and new technologies such as software defined network (SDN) and network function virtualization (NFV) are introduced. Therefore, since Release 13 the term LTE-A is changed to LTE-A Pro. LTE-A Pro is the phase in which 4G systems pave their way to 5G systems.

2.2 Examination of Mobile Data Forecast

During the evolution of wireless communications, the way people use their mobile devices changed from voice-oriented to data-oriented services. The noted evolution in the communication technologies are involved with new applications such as cloud-based technologies, internet of things (IoT), machine-type communication (MTC), augmented and virtual reality lead to a data hungry ecosystem. Mobile data traffic and its 5 or 6 year based projection reports are released annually by several technology companies such as Cisco, Ericsson and Nokia. In these reports, the compound annual growth rate (CAGR) of mobile data usage, mobile subscriptions and the number of mobile handsets are obtained by using different methodologies[3]. The forecast methodology is based on historical data, internal and external measurements on mobile networks, advancement in the transceiver technologies and user-market trends.

In Fig. 2.2, the mobile data traffic forecast from 2011 to 2022 is given based on reports released

[2]The term CC is used in 3GPP terminology for CA to represent a channel, which is made up of several MHz of bandwidth at a time. In this study, phrases CC, channel and cell are used interchangeably.

[3]CAGR is calculated based on $(v_n/v_0)^{(1/(n-1))} - 1$ where v_0 and v_n are the initial and last values, respectively; and n is the considered time period.

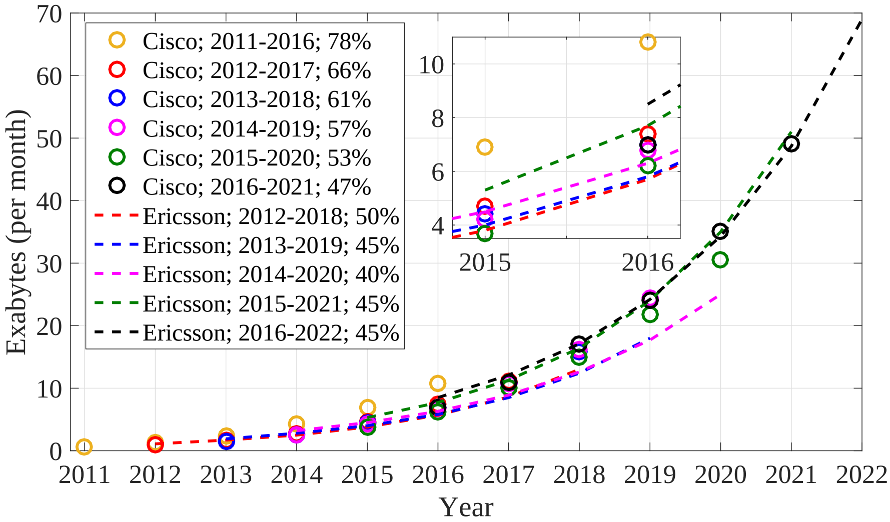

Figure 2.2: *Mobile data usage forecast. The graph label represents reporter company, forecast period and predicted CAGR for the given forecast period, respectively.*

by Cisco and Ericsson[4]. In general, although both the reporters accurately predict the mobile traffic of the following year, the long term predictions are either exaggerated or underestimated. The mobile traffic forecast report released in 2011 by Cisco predicts that the mobile traffic will grow at a CAGR of 78%, and will reach 10.8 exabytes in 2016. However, the recorded mobile data traffic in 2016 was 7.8 exabytes by Cisco and 8.5 exabytes by Ericsson[5]. According to the recently published forecast reports, the mobile data traffic from 2016 to 2021 is expected to rise at a CAGR of approximately 45% and reach 49 exabytes.

It is important to note that mobile data traffic dramatically increased from 2015 to 2016. In 2015, the mobile data usage was 3.7 exabytes. In 2016, the mobile data usage almost doubled and reached 7.2 exabytes. Based on the 2015 figures, both reporters were not expecting such growth in 2016. The main underlying driver for this increase is the advanced technologies used in mobile networks and user equipment (UE) handsets, such as CA, employing multiple input multiple output (MIMO), data offloading to hotspots and network densification[6]. Network densification arguably has been the main contributing factor for the increase in achieved user data rates and consequently for the total mobile data traffic. As noted in [29], of the six orders

[4] '*Cisco Visual Networking Index: Global Mobile Data Forecast*' reports published by Cisco for the years 2011-2016, 2012-2017, 2013-2018, 2014-2019, 2015-2020, and 2016-2021; and '*Ericsson Mobility Report*' reports published by Ericsson for the years 2012-2018, 2013-2019, 2014-2020, 2015-2021, and 2016-2022 are analysed.

[5] The reason of having different recorded mobile data for 2016 is that both the reporters have different collaborators and customers to perform the mobile traffic measurements.

[6] Increasing the spatial density of cell sites in order to improve achievable data rate in terms of per unit area is termed as network densification.

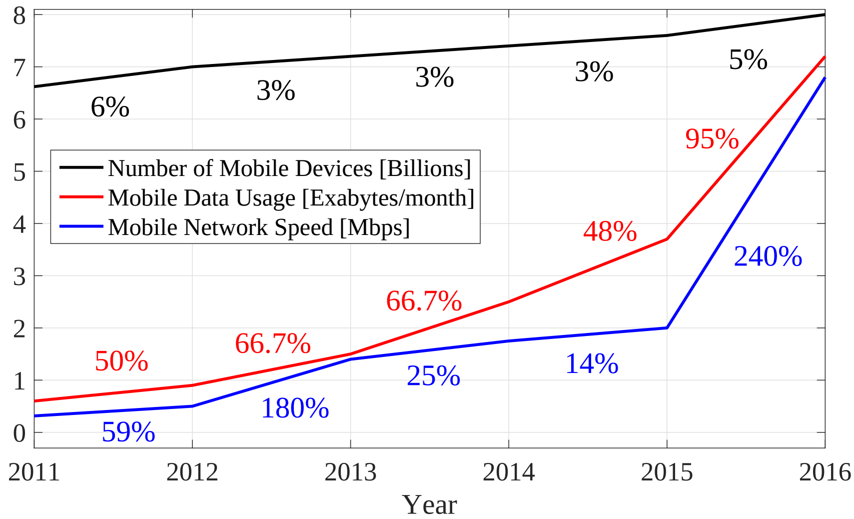

Figure 2.3: *Mobile devices, traffic and network speed.*

of magnitude improvements in data rates on our mobile devices during the last decades, the small cell concept contributed by a staggering factor of 1600, and this is in stark contrast to a factor of 25 attributed to the allocation of new spectrum.

In Fig. 2.3, the recorded data for mobile network speed, mobile data traffic and number of mobile devices from 2011 to 2016 are shown based on Cisco reports. The increase in the number of mobile devices has a linear trend. The recorded number of mobile devices has increased by 1.38 billion from 2011 to 2016 where 30% of the increase is seen from 2015 to 2016. For the mobile network speed, an increase from 315 kbps to 2 Mbps is recorded from 2011 to 2015 whereas from 2015 to 2016, a significant increase to 6.8 Mbps, which is a 240% improvement in the mobile network speed, is seen.

In order to understand how both the reports could not predict the mobile traffic increase from 2015 to 2016, the recorded and predicted overall mobile network rate, 4G network rate, and hotspot rate as well as the number of 4G capable devices from 2011 to 2016 are analysed in more detail. The most accurate prediction for the speed of the mobile network is made for the hotspots, as shown in Fig. 2.4. From 2011 to 2015, the hotspots' speed increased linearly, and it was predicted to be around 30 Mbps in 2016. The recorded hotspot rate was 32 Mbps in 2016 which is slightly above the prediction given in 2015. The prediction given in the forecast reports from 2011 to 2015 for overall mobile data rate varies from 2.1 Mbps to 2.9 Mbps. However, the achieved overall mobile data rate was 6.8 Mbps in 2016. This increase can be explained by considering mobile data offloading to the hotspots. Offloading the third generation (3G) and

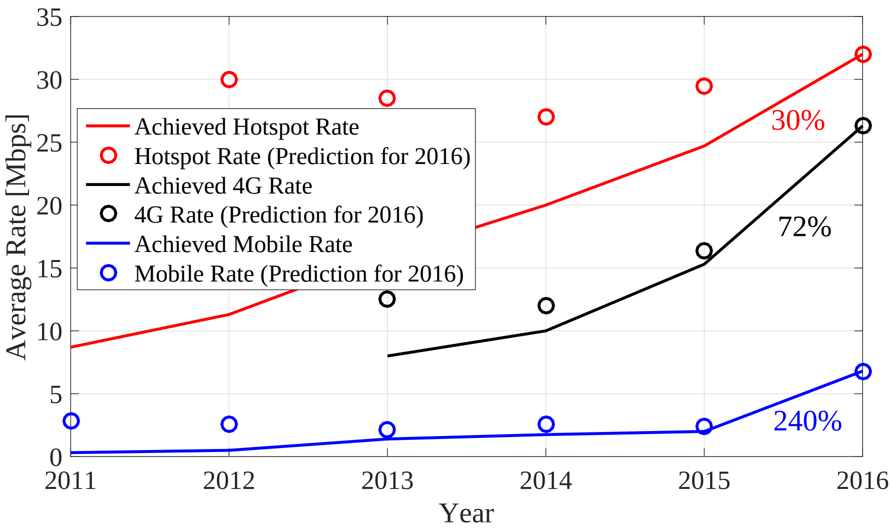

Figure 2.4: *Achieved and predicted rates.*

4G mobile traffic to the hotspots increased the achieved overall mobile data rate. The same underestimation is seen for the 4G network speed in 2016 as well. The latest prediction given in 2015 was 16.4 Mbps which is 10 Mbps lower than the actually recorded rate in 2016.

As shown in Fig. 2.3, there is a correlation between the trends of mobile traffic and overall network speed. Also it is shown that the number of newly added mobile devices notably affects the mobile traffic trend. In other words, 7.6 billion mobile devices generated 3.7 exabytes mobile traffic in 2015, whereas in 2016, 400 million newly added mobile devices generated almost the same amount of mobile traffic. Therefore, although there was no significant increase in the number of mobile devices from 2015 to 2016, the capability of the recently added 400 million devices in 2016 affected the mobile data traffic. In Fig. 2.5, the amount of 3G and 4G devices from 2012 to 2016 as well as the prediction on the number of 4G devices in 2016 are shown. Overall, from 2012 to 2016, the number of 3G and 4G mobile devices increased by 800 million and 1.9 billion, and reached to 2.4 billion and 2 billion, respectively. From 2015 to 2016, the number of 4G mobile devices increased from 1 billion to 2 billion, and the number of 3G mobile devices increased by several million. However, the number of 4G mobile devices in 2016 was underestimated. The amount of 4G devices in 2016 is predicted as 0.6 billion, 0.8 billion, 1 billion and 1.5 billion in the reports relased in 2012, 2013, 2014 and 2015, respectively.

The huge rise seen in the number of 4G devices led to increase in the overall percentage for 4G devices, which increased from 14% to 26% between 2015 and 2016. In the forecast reports

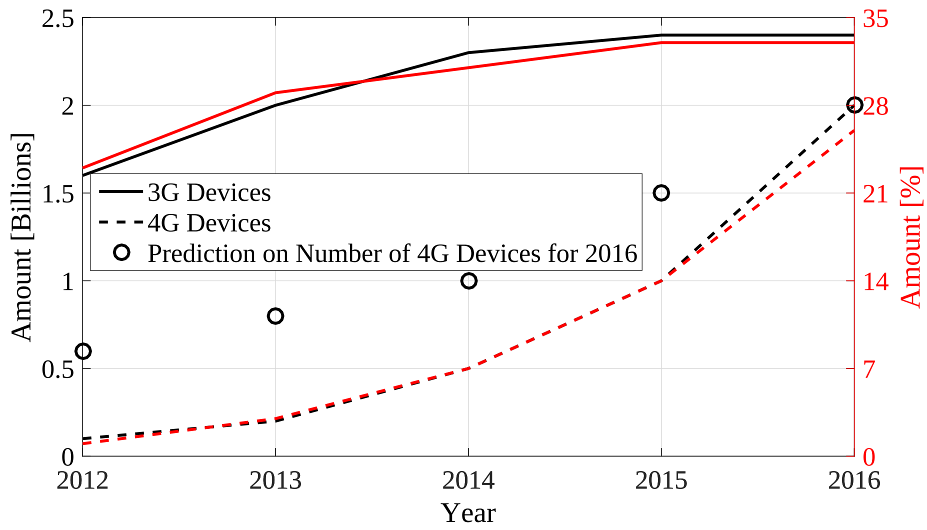

Figure 2.5: *Amount of 3G and 4G devices. On the left axis of the figure, black graphs shows the amount of devices in billion, and on the right axis of the figure, red graphs shows the amount of devices as percentage.*

released in 2012, 2013 and 2014, it is not expected that the number of 4G devices would reach the number of 3G devices. However, the report released in 2015 predicted that the number of 4G devices would overlap with the number of 3G devices by 2020. In the recent report in 2016, the overlap is expected by 2017. Due to such increases in 4G devices, a drop in the percentage for 3G devices is expected. However, the percentage of 3G devices remained the same at 33% in 2016. Although it is not shown in Fig. 2.5, the reason for having the same percentage for 3G devices is due to the decrease in the amount of 2G devices. In fact, it can be concluded that the 4G devices have taken the place of the 2G devices.

Consequently, this analysis has shown one very important fact: whatever the amount of wireless network capacity provided, it will be utilized by the mobile users. This is shown by the unforeseen 240% increase in average mobile data speeds enabled by offloading from cellular.

2.3 In-Flight Connectivity

The desire of mobile users to be connected to online services at anytime leads the in-flight connectivity market, of which the share is expected to be around $15.9 Billion by 2028 [30]. According to a survey based study given in [31], 83% of passengers would prefer to have in-flight connectivity during their flight. In fact, applications that are proposed to enhance passenger

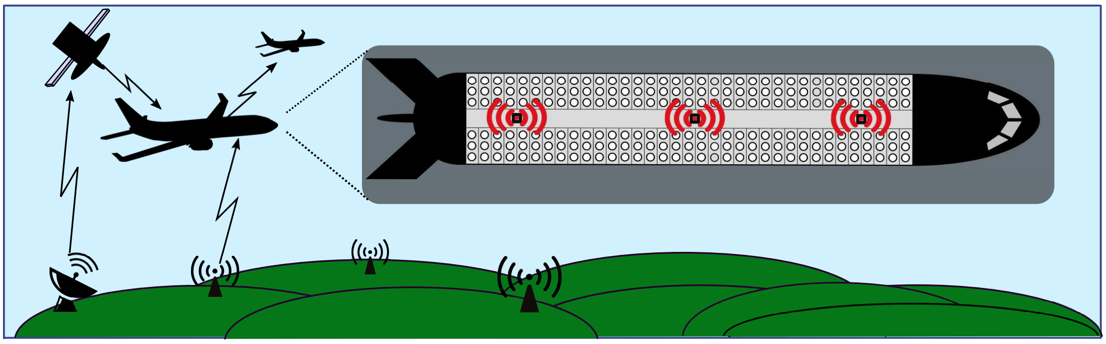

Figure 2.6: *An in-flight connectivity scenario.*

experience such as augmented reality (AR) and virtual reality (VR) require an onboard system that provides high data rates. Therefore, an aircraft is an environment where connectivity is of primary importance.

2.3.1 Regulations

Deployment and compatibility of mobile communication services on board aircraft and ground-based systems have been studied for the Global System for Mobile Communications (GSM) and Universal Mobile Telecommunications System (UMTS) in [14–16]; and for LTE in [2, 3, 17]. Based on the Electronic Communications Committee (ECC) reports and decisions, the in-cabin mobile system should only be operated when the altitude of the aircraft is 3000 m or more, and the system should not be operated while the aircraft is on the ground or during take-off and landing [14].

For in-flight connectivity, a backhaul link, which is the connection link between the core network and small networks that are close to the end-user, to the aircraft can be provided by using satellite based or LTE based direct air-to-ground communication (DA2GC) technologies [7–9, 32]. Although satellite and LTE based DA2GC technologies can be used independently, a hybrid solution, which allows both of technologies to be used complementary to each other, is achievable [8]. In Fig. 2.6, an in-flight connectivity scenario with satellite and DA2GC backhaul links is depicted.

Nowadays, satellite based systems operating at L-band (in between 1 GHz and 2 GHz), Ku-band (in between 12 GHz and 14.5 GHz) and Ka-band (in between 26.5 GHz and 40 GHz) are the widely used solutions to provide a backhaul link to the aircraft [33]. However, the main drawback of the satellite links is latency [32, 33]. Latency is the round trip time for a data package between the transmit and receive nodes. It is foreseen that the latency between two nodes connected via a satellite can exceed 400ms [9, 32]. With such a high latency, it is not possible to provide real-time services such as video conferencing in an onboard aircraft. Moreover, the peak rate performance of the noted satellite technologies are ranging between 30 Mbps and 70 Mbps [33].

Whereas, in LTE based DA2GC systems, terrestrial base stations are used to provide the backhaul link to the aircraft. In order to establish a link between the terrestrial stations and aircraft, some modifications are needed on both sides. Terrestrial base stations are designed to provide a coverage on the ground. Therefore, most of the terrestrial base station antennas are pointed toward the ground. In order to provide an aerial coverage area, an antenna should be placed and pointed upwards on the already deployed terrestrial base stations. On the aircraft side, an antenna should be placed below the aircraft to receive the link from the ground station. Both of the antennas dedicated for DA2GC should be able to dynamically shape and steer beams in order to mutually track each other [34]. Additionally, in order to serve multiple aircraft at the same time, the antenna placed at the terrestrial stations should produce multiple beams.

Performance of a 60 ms latency and a downlink rate of 26 Mbps is achieved in a test flight [7]. Along with the noted enhancements in LTE, it is expected that the latency and achievable rates will be improved. Current industrial and commission studies are aiming to have a latency of less than 10 ms and peak data rate of 75 Mbps per cell [8]. For the DA2GC systems, frequencies at 1900-1920 MHz and 5855-5875 MHz are considered as a short term solution. For the next generation DA2GC systems, the required data rate is provisioned as 1.2 Gbps per aircraft [20]. Therefore, in order to provide such a high data rate backhaul link, frequencies above 6 GHz are subject to investigation for the next generation DA2GC systems [7].

Furthermore, in Fig. 2.6, an aircraft-to-aircraft link is also shown. Although such a network structure is not considered by ECC, Federal Communications Commission (FCC) has recently released an agreement to test an aircraft-to-aircraft mesh network structure, which is patented back in 2001 [35]. Based on [35], 30 GHz frequency band is considered to provide aircraft-to-aircraft link.

Once the backhaul link is provided to the aircraft, an onboard communication system should be used to distribute the traffic inside the aircraft. In ECC reports and decisions [2, 3, 14–17], it is suggested that a network control unit (NCU) should be operated in order to prevent in-cabin UE sets trying to access the terrestrial networks. The NCU is used to raise the noise floor inside the cabin. Therefore, the quality of the signal received from the in-cabin eNBs will become higher than the terrestrial eNBs and the in-cabin UE sets will not attempt to access the terrestrial network. The same goal can be achieved through radio frequency (RF) shielding of the aircraft. The RF shielding of the aircraft increases the signal attenuation of the aircraft fuselage. Thus, the quality of the signal received from the terrestrial eNBs will be much lower than the signal received from the in-cabin eNBs. Therefore, the in-cabin UE sets will try to access the in-cabin network, not the terrestrial network.

The limitations of activating the onboard communication system are firstly investigated for GSM 1800 MHz in [15]. Then, in [2, 3], the frequency bands given in Table 2.1 are analysed for UMTS and LTE technologies. In Table 2.1, connectivity bands represent the frequencies used inside the aircraft and controlled bands represent the frequencies that are currently being used by the terrestrial networks.

<table>
<tr><th rowspan="2">Band Type</th><th rowspan="2">Technology</th><th colspan="2">Frequency</th></tr>
<tr><th>Uplink</th><th>Downlink</th></tr>
<tr><td rowspan="3">Connectivity</td><td>LTE 1800</td><td>1710-1785 MHz</td><td>1805-1880 MHz</td></tr>
<tr><td>UMTS 2100</td><td>1920-1980 MHz</td><td>2110-2170 MHz</td></tr>
<tr><td>LTE 2600</td><td>2500-2570 MHz</td><td>2620-2690 MHz</td></tr>
<tr><td rowspan="4">Controlled</td><td>LTE 800</td><td colspan="2">791-821 MHz</td></tr>
<tr><td>LTE 900</td><td colspan="2">925-960 MHz</td></tr>
<tr><td>LTE 1800</td><td colspan="2">1805-1880 MHz</td></tr>
<tr><td>LTE 2600</td><td colspan="2">2500-2690 MHz</td></tr>
</table>

Table 2.1: *Analysed frequency bands in [2]*

According to [2, 17], when the altitude of the aircraft is 3000 m, the maximum effective isotropic radiated power (EIRP) from the in-cabin station to outside the aircraft must not exceed 1 dBm for 5 MHz (or -13 dBm for 200 kHz) of a LTE 1800 MHz system to prevent service degradation at the ground-based systems. This limit represents a 1 dB increase of the noise figure of the system. For a UMTS 2100 MHz system, this limit is given as 1 dBm for 3.84 MHz channel. In Table 2.2, the limitations on the UE and base station inside the aircraft are given for both the UMTS and LTE systems when the altitude of the aircraft is higher than 3000 m. It is important to note, in [2], due to the radar services in the band adjacent to 2600 MHz, LTE 2600 MHz system is found incompatible and it is not considered for the onboard communication systems.

For an onboard LTE system, the only option is to use 1800 MHz frequency band. Although

Aircraft Altitude [km]	UMTS 2100 MHz		LTE 1800 MHz	
	UE inside the aircraft [dBm/3.84 MHz]	Onboard Station [dBm/3.84 MHz]	UE inside the aircraft [dBm/5 MHz]	Onboard Station [dBm/5 MHz]
3	3.1	1.0	1.7	1.0
4	5.6	3.5	3.9	3.5
5	7	5.4	5	5.5
6	7	7.0	5	7.1
7	7	8.3	5	8.4
8	7	9.5	5	9.6

Table 2.2: *Maximum EIRP, which is defined as outside the aircraft, limitations [2, 3]*

there are other bands available for LTE such as 800 MHz and 900 MHz, interference to the terrestrial networks will be less in 1800 MHz systems due to its wavelength. From GSM to LTE, low frequency bands are used to provide a wide coverage area and high frequency bands are used to provide high data rate. Moreover, the total downlink bandwidth is 30 MHz in LTE 800 MHz whereas, it is 75 MHz in LTE 1800 MHz [36].

2.3.2 Aircraft Cabin Geometry

In this research, an Airbus A321 aircraft, which is a commercial 38 m long medium sized aircraft with a seating capacity of 210 passengers in economy class, is considered. The passenger seat layout of the aircraft is configured with a single aisle and 35 rows of seats, as shown in Fig. 2.7. In addition to the seating plan shown in the figure, five points, from A to E, are shown. These points are placed on the ceiling of the cabin (close to overhead storage) and provisioned for an antenna placement inside the cabin. The approximated A321 cabin interior dimensions are given in Table 2.3.

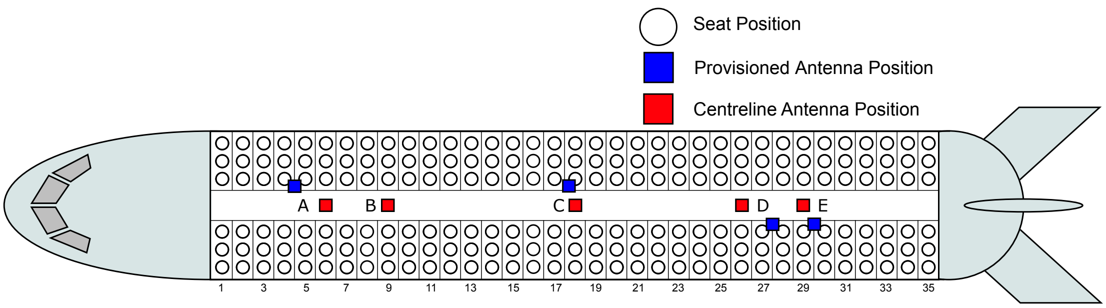

Figure 2.7: *Cabin layout of Airbus A321 - Points represents the antenna mounting locations. Provisioned positions means the positions designed by the aircraft manufacturer which provide pre-configured power supply. Centreline positions are used to ensure that the antennas are uniformly distributed in the cabin. There is no power supply provided by the aircraft manufacturer for the centreline positions.*

Number of Rows	35	Aisle width	50 cm
Number of Seats	210	Row width	80 cm
Seat width	60 cm	Cabin width	395 cm
Seat height	110 cm	Cabin height	249 cm

Table 2.3: *Dimensions of Aircraft*

In this study, deployment of the systems with 2 eNBs and 3 eNBs are considered. For the considered deployments, each eNB is operated within LTE band 3 (1800 MHz - 3×20 MHz channels and 1×15 MHz channel). The channel index, bandwidth, number of RBs and the frequency range information used are given in Table 2.4.

For 3 eNBs deployment, the points A, C and E are used to mount the antennas for both provisioned and centreline antenna positions. However, if a deployment of 2 eNBs is considered, eNB antennas are placed on the points A and D for provisioned antenna positions and placed on points B and D for centreline antenna positions, as shown in Fig. 2.7. In order to decrease interference among the eNBs, cell sectorization is employed. In cell sectorization, directional antennas are used to direct the propagation to a specific point. By doing that, while the frequency reuse factor of the eNB is not changed, a minimum distance between a user and an interfering eNB is enforced. Therefore, each eNB is equipped with two 2×1 directional patch antennas in the considered in-cabin LTE system model. For each antenna mounting point, which is an eNB location for the considered system, two antennas are deployed and directed in opposite directions along the aisle, as in [21]. In other words, according to the employed cell sectorization, each eNB has two channels pointed towards the cockpit of the aircraft and two channels pointed towards the tail of the aircraft. Channels with indexes 3 and 4 are used in the cockpit direction and channels with indexes 1 and 2 are used in the tail direction of the aircraft.

2.4 LTE System Basics

LTE is proposed to achieve a higher data rate and lower latency on the user and control planes

Channel Index	Bandwidth	Number of RBs	Frequency Range
CH 1	20 MHz	100	1805 - 1825 MHz
CH 2	20 MHz	100	1825 - 1845 MHz
CH 3	15 MHz	75	1845 - 1860 MHz
CH 4	20 MHz	100	1860 - 1880 MHz

Table 2.4: *Channel information*

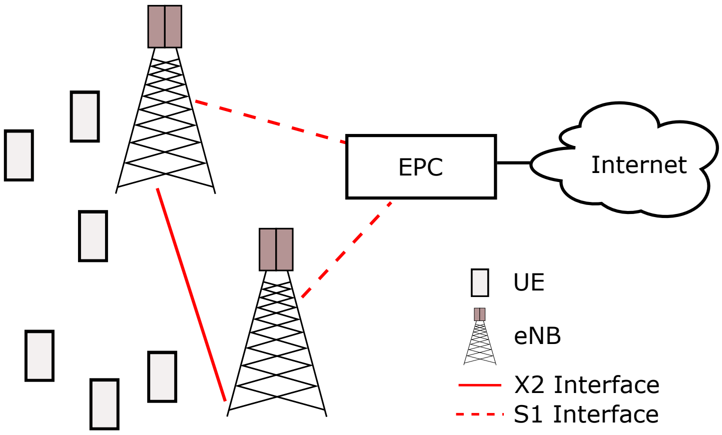

Figure 2.8: *Overall LTE network architecture.*

by introducing a packet-optimized radio access technology. Therefore, there are several modifications on the existing UMTS network architecture. In Fig. 2.8, an overall LTE network architecture is illustrated. Accordingly, the network has four main components namely UE, evolved universal terrestrial radio access network (E-UTRAN) which consists of eNBs, evolved packet core (EPC) and service domains. UE is typically a handset and E-UTRAN eNB is the base station that controls all radio related functions of the network. The E-UTRAN provides physical layer (PHY), medium access control (MAC), radio link control (RLC), packet data convergence protocol (PDCP) and radio resource control (RRC) protocols for user and control planes. Accordingly, packet compression, modulation/demodulation, coding/decoding, UE radio signal measurement control and resource allocation are done in the eNB. Signalling within the E-UTRAN eNBs is carried out via the X2 interface whereas each eNB is connected to the EPC via the S1 interface. EPC consists of three main units namely mobility management entity (MME) which handles signalling and controlling of UE network connection, serving gateway (SGW) which transports all internet protocol (IP) data traffic between the UE and network, and packet data network gateway (PGW) which provides IP address allocation to UE to communicate with external networks.

2.4.1 Frame Structure

In LTE, two types of frame structure are defined for different duplexing methods, namely frequency division duplex (FDD) and time division duplex (TDD). In FDD, simultaneous uplink and downlink transmissions are allowed on different portions of a band. For example, as shown in Table 2.1, for LTE 1800 MHz, uplink and downlink transmissions take place on different bands where there is a 20 MHz gap between these bands. Whereas, in TDD, uplink and downlink transmissions are allocated to the same frequency portion but transmission takes place on different time instances.

In Europe, FDD is used as the duplexing method for LTE. An FDD frame has 10 ms duration and consists of subframes and slots. Each subframe has 1 ms interval and consists of two equally sized slots with 0.5 ms, as shown in Fig. 2.9. In each slot, there are 6 (extendend cyclic

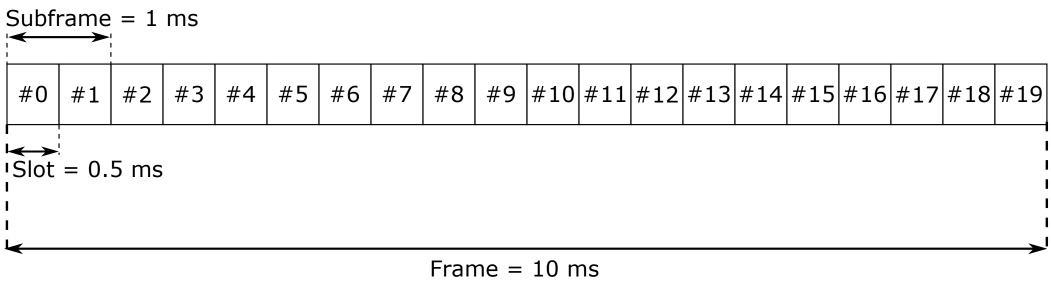

Figure 2.9: *LTE FDD frame structure [1].*

prefix) or 7 (normal cyclic prefix) orthogonal frequency division multiplexing (OFDM) symbols based on the used cyclic prefix type. In each OFDM symbol, the subcarriers are located with 15 kHz spacing. During one slot, 12 consecutive subcarriers (180 kHz) correspond a RB. The number of RBs, N_{RB}, spans between 6 and 110 depending on the transmission bandwidth, as given in Table 2.5.

Bandwidth	$N_{\mathbf{RB}}$
1.4 MHz	6
3 MHz	15
5 MHz	25
10 MHz	50
15 MHz	75
20 MHz	100

Table 2.5: *Number of RBs for different transmission bandwidths*

In LTE, each element in a RB is called a resource element (RE). REs are uniquely defined to represent a time and frequency domain pair in a RB. As it will be shown in the next section, each RE is used to carry specific information.

2.4.2 Power Allocation

In LTE, there is no power control for the data part of the signaling. Most hardware allows for a static transmission power to be set as a configuration parameter i.e. the total transmission power of the eNB can be constrained [37]. The downlink power allocation algorithm in the LTE eNBs is based on UE-specific parameter P_A, cell-specific parameter P_B and cell-specific reference signal (CRS) power.

In the reference signaling power control algorithm, the parameter *referenceSignalPower* provided by higher layers is used to derive the downlink reference signal (RS) energy per resource element (EPRE) [4]. Then, the ratio of the physical downlink shared channel (PDSCH) EPRE to CRS EPRE among PDSCH REs is derived for each OFDM symbol. This ratio is denoted by either ρ_A or ρ_B based on OFDM symbol index. Fig. 2.10 shows LTE RB structure when a single antenna port and normal cyclic prefix is considered. The ratio of the PDSCH EPRE

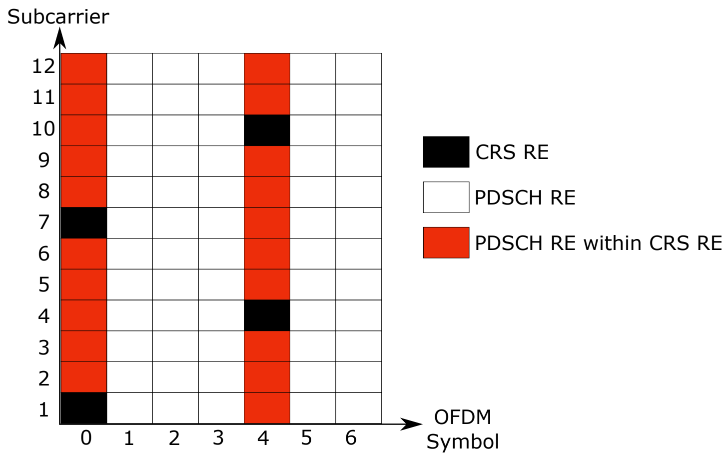

Figure 2.10: *LTE RB structure - single antenna port.*

to the CRS EPRE is denoted by ρ_A for OFDM symbol indices 1, 2, 3, 5, 6 where the ratio is denoted by ρ_B for OFDM symbol indices 0 and 4 within a slot [4, Table 5.2-2 and Table 5.2-3]. The ratio ρ_A is calculated as follows:

$$\rho_A[\mathrm{dB}] = \begin{cases} \delta_{\text{power-offset}} + P_A + 10\log_{10} 2, & \text{precoding with 4 cell-specific antenna ports,} \\ \delta_{\text{power-offset}} + P_A, & \text{otherwise,} \end{cases} \tag{2.1}$$

where $\delta_{\text{power-offset}}$ is 0 dB for all PDSCH transmission schemes except multi-user MIMO [4]. According to the cell-specific parameter P_B and number of configured eNB cell-specific antenna ports signalled by higher layers, a cell-specific power ratio ρ_B/ρ_A is determined. The

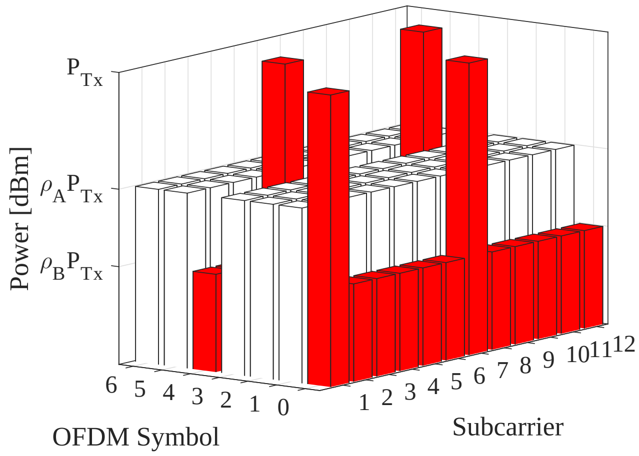

Figure 2.11: *Power level of REs in a RB.*

cell-specific power ratio values based on parameter P_B and number of antenna ports are given in Table 2.6.

P_B	ρ_B / ρ_A	
	One Antenna Port	**Two and Four Antenna Ports**
0	1	5/4
1	4/5	1
2	3/5	3/4
3	2/5	1/2

Table 2.6: *LTE cell-specific ratio [4, Table 5.2-1]*

When there is no RS present in the OFDM symbol, the power of the PDSCH RE is configured as a multiplication of the CRS EPRE, *referenceSignalPower*, and UE-specific parameter, ρ_A. However, when there is a RS in the OFDM symbol, then the power of the PDSCH RE is equal to the multiplication of *referenceSignalPower* and the cell-specific parameter, ρ_B. In Fig. 2.11, a single antenna port is considered with CRS EPRE of P_{tx}. Accordingly, power of the PDSCH REs of the OFDM symbol without RS is $\rho_A P_{\text{tx}}$ W. When P_B is configured as an integer from 0 to 3, the cell-specific power ratio for a single antenna port system can be found from Table 2.6. As noted, the power of the PDSCH RE of the OFDM symbol with RS will be multiplied with ρ_B.

2.4.3 Received Power Level Determination

In LTE, a UE measures the received power level from its connected and neighbour cells, determines its channel quality and reports it back to its connected cell. There are two different received power levels measurements in LTE, namely reference signal received power (RSRP) and received signal strength indicator (RSSI). Based on the definition given in [38], RSRP is the linear average of the RS within the used channel bandwidth. It provides information on the signal strength of the connected cell. Whereas, RSSI is the linear average of the total received power observed in the OFDM symbols that carry RS within the used channel bandwidth. It is representative of the wideband power level, which includes co-channel serving and non-serving (interfering) cells, adjacent channels and noise, and is used to determine interference and noise information. In other words, RSRP is the average power level of the CRS REs, which are shown black in Fig. 2.10, and RSSI is the total power level of all the REs given in red and black in Fig. 2.10, which is averaged over the two OFDM symbols. Once a UE measures the RSRP and RSSI levels, it can determine the quality of the received signal, which is represented by reference signal received quality (RSRQ). RSRQ is determined by multiplying the number of RBs in the used channel bandwidth and the ratio of RSRP and RSSI, $\text{RSRQ} = N_{\text{RB}} \times (\text{RSRP}/\text{RSSI})$.

It is worthwhile to note that a UE does not report its RSSI measurements. RSSI measurements are only used to determine RSRQ level. A UE reports the RSRP and RSRQ measurements which can be used to trigger cell re-selection or handover events, which will be described later. The reporting range for RSRP is defined from -140 dBm to -44 dBm with 1 dB resolution [39, Table 9.1.4-1] and for RSRQ is defined from -34 dB to 2.5 dB with 0.5 dB resolution [39, Table 9.1.7-1].

2.4.4 Channel State Reporting

In LTE systems, the modulation order to be used on a RB is represented by a modulation and coding scheme (MCS) index, and it is chosen by the adaptive modulation and coding (AMC) functions. As noted, adaptive downlink power allocation to the available RBs is not supported in LTE. This implies that the power amplifier is always transmitting at full power and the downlink-rate adaptation is controlled by adjusting the MCS indexes using AMC functions [37]. The AMC functions use channel quality indicator (CQI) reports to decide on the MCS indexes. In LTE, CQI reporting and MCS index assignments are based on a set of defined structures. Due to extensive signaling overhead, CQI reporting with per RB granularity and using different MCS indexes across scheduled RBs for a user are not supported [40]. Thus, subband and wideband based CQI reporting modes and single MCS assignment to all RBs allocated to a user are currently used in LTE systems [5, 37, 40].

Based on LTE specification [5], CQI reports can be sent periodically or aperiodically. In the periodic reporting, UE reports its CQI based on a fixed period. In the aperiodic reporting, UE reports its CQI based on a request from the eNB. Moreover, the CQI reporting is classified into modes as wideband (Mode 1-0), UE-selected subband (Mode 2-0) and higher layer configured subband (Mode 3-0). In wideband CQI reporting Mode 1-0, the UE reports a single CQI for the whole bandwidth. However, in periodic CQI feedback in Mode 2-0 and aperiodic Mode 3-0, the UE reports a CQI for a portion of the bandwidth. The difference between Mode 2-0 and Mode 3-0 is how the reported subband is chosen. In Mode 2-0, the UE selects the best M subbands and reports the averaged CQI value of the selected M bands. However, in Mode 3-0, the eNB decides which subband will be reported by the UE.

The number of RBs in a subband depends on the available bandwidth. As shown in Table 2.5, for 15 MHz and 20 MHz bandwidths, there are 75 and 100 RBs, respectively. Based on [5], if the number of available RBs is in between 64 and 110, the subband size is equal to 8 RBs and the subband index starts from the lowest frequency. Therefore, the last subband may have fewer RBs than 8 RBs. For example, as shown in Table 2.7, the last subband has 3 RBs and 4 RBs when the channel bandwidth is 15 MHz and 20 MHz, respectively.

Bandwidth	Subband size	Size of the last subband
1.4 MHz	NA	NA
3 MHz	4	3
5 MHz	4	1
10 MHz	6	2
15 MHz	8	3
20 MHz	8	4

Table 2.7: *Size of subband for different transmission bandwidths*

2.4.5 Allocation Types

OFDMA allows multiple users to access the frequency resources at the same time. In LTE, the smallest unit that can be assigned to users is the RB. The way to assign the available RBs is called resource allocation (RA) and it is also based on a defined structure. In LTE, RA is divided in three different types, Type 0, Type 1 and Type 2 [5].

In Type 0, contiguous RBs are grouped and RB groups (RBGs) are allocated to users based on a bitmap. When a value is '1' in the bitmap, it means the RBG is allocated to a user, and '0' otherwise. As in the subband CQI reporting, the size of a RBG depends on the available bandwidth. Based on [5], if the number of available RBs is between 64 and 110, the RBG size is equal to 4 RBs. As in the subband CQI reporting, the number of RBs in the last RBG may have fewer RBs. The size of a RBG and the size of the last RBG are given for different transmission bandwidths in Table 2.8.

Bandwidth	Size of RBG	Size of the last RBG
1.4 MHz	1	1
3 MHz	2	1
5 MHz	2	1
10 MHz	3	2
15 MHz	4	3
20 MHz	4	4

Table 2.8: *Size of RBG for different transmission bandwidths*

The granularity of the allocation in Type 0 is a RBG where the number of RBGs is 19 for 15 MHz and 25 for 20 MHz. Type 0 RB indexing, RBG mapping and their allocation based on a bitmap are shown in Fig. 2.12 when 20 MHz bandwidth is considered (100 RBs) in the system.

In Type 1, RBs are grouped as in Type 0. However, in Type 1, an additional grouping is also used to group RBGs. In LTE specification [5], the grouped RBGs are termed 'subset' and number of subsets are defined as 4 for 15 MHz and 20 MHz channel bandwidths. Same as in Type 0, the bitmap approach is used to indicate which resources are allocated to users. As noted, in Type 0, the bitmap indicates RBGs. However, in Type 1, the bitmap indicates a selected subset and allocated RBs in this subset. Accordingly, the granularity of the allocation is a RB in Type 1, where in Type 0, RA is in terms of RBG and the granularity is 4 RBs (for 15 MHz and 20 MHz). In Fig. 2.14, the subset mapping for the 20 MHz (100 RBs) channel is shown. Based on this shown subset mapping, in Fig. 2.15, the bitmap reading and resource allocation are shown. It is important to note that non-contiguous RB allocation in a subset is possible by using Type 1. However, in Type 0, the non-contiguity is based on RBG. Also, for both of the allocation types Type 0 and Type 1, the size of the bitmap is the same, and equals the number of RBGs (25 bits for 20 MHz and 19 bits for 15 MHz) [5].

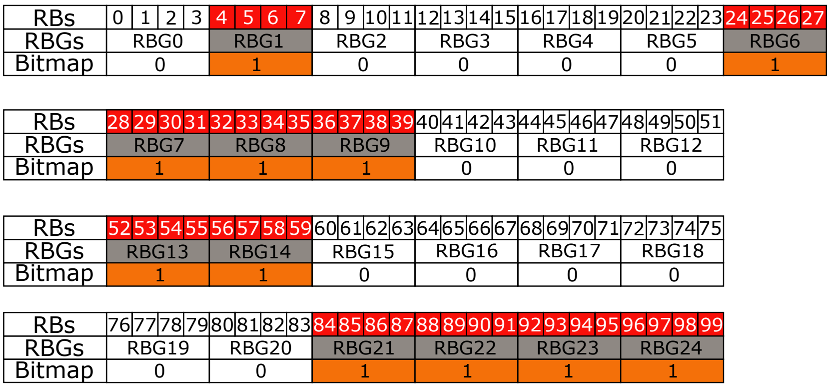

Figure 2.12: *RA Type 0 for bitmap '1 1110 0000 0110 0011 1100 0010' where RB group indexing starts from the least significant bit (LSB) to most significant bit (MSB) in the bitmap. When a value is '1' in the bitmap, it means the RB group is allocated to user, otherwise, the RB group is not allocated. Value '1' in the bitmap is shown by amber, allocated RB groups and RBs are shown by grey and red, respectively, and unallocated RB groups and RBs are shown by white color.*

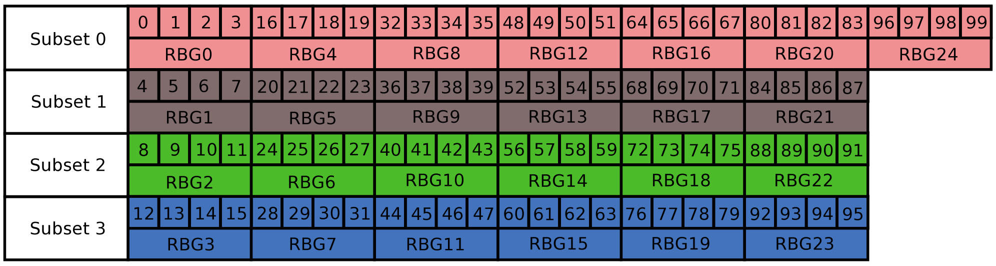

Figure 2.13: *RA Type 1 - Subset mapping for 20 MHz*

In Type 2, the allocation does not rely on a bitmap. A resource indication value (RIV) is used to indicate the start position and length of the RA. Therefore, signaling overhead is reduced with Type 2. Based on the indicated RIV information, Type 2 supports contiguous RB allocation whereas non-contiguous RB allocation can be supported by using virtualized resource blocks (VRBs). In LTE, two types of VRBs are defined as localized VRB and distributed VRB [1]. In the localized VRB, RBs are directly mapped to VRBs. However, in distributed VRB, RBs are mapped to VRB based on a principle [1]. According to this principle, even VRBs are contiguous, RBs in the frequency domain can be non-contiguous. Also, the granularity of Type 2 is 1 RB. An example of Type 2 allocation based on distributed VRBs with 48 RBs gap rule is given in Fig. 2.15.

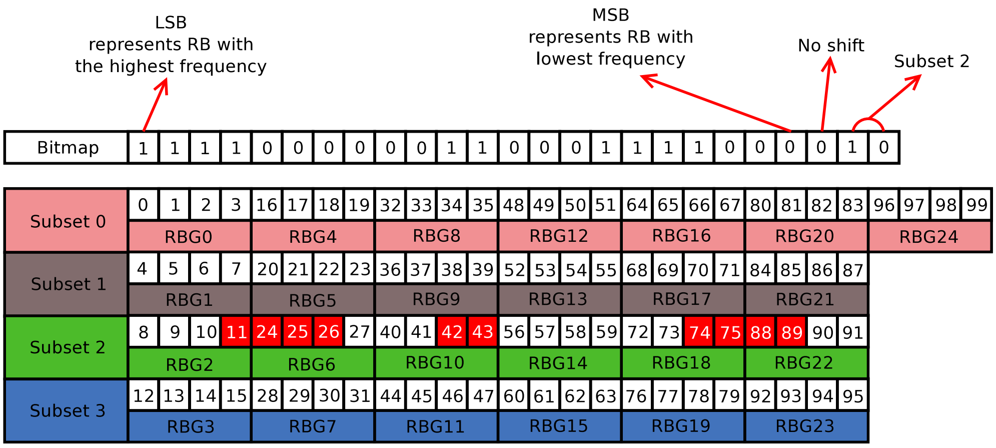

Figure 2.14: *RA Type 1 for bitmap '1 1110 0000 0110 0011 1100 0010' where starting from MSB (right-hand side) the first 2 bits represents selected subset, following 1 bit represents shifting RBs is used or not. From the fourth bit to last, allocation bitmap per RB granularity is used where as same in Type 0 RBs are in decreasing order of frequency from LSB to MSB in the bitmap. When a value is '1' in the bitmap, it means the RB in the subset is allocated to user, otherwise, the RB in the subset is not allocated. Subsets and RB groups belongs to subsets are shown by different colors, allocated RBs in the subset are shown by red and unallocated RBs are shown by white color.*

2.4.6 Handover

When a UE is turned on, it starts to look for cells that provide an acceptable level of signal power to attach to. When the UE is attached to one of the cells, it becomes a part of the network and periodically measures the RSRP and RSRQ levels based on the RS received from the connected and neighbour cells, which are the cells adjacent to the connected cell. In case the UE moves out[7] of the coverage area of its connected cell, it starts to look for another cell that provides a better signal power level. When a neighbouring cell provides better signal quality than the connected cell, the UE will connect to the neighbouring cell. When the UE has no dedicated resources for transmission, this is called idle mode and means that the UE just transmits and receives control messages. Connecting to the neighbour cell in the idle mode is called cell re-selection. However, when the UE is in the connected mode, where it transmits and receives data messages, connecting to the neighbor cell is called handover. In LTE, these processes are triggered by the eNB based on measurement reports sent by UE. Therefore, cell re-selection and handover are a UE assisted, the eNB triggered processes in LTE.

[7] In some cases, due to the load level of the cell or channel quality degradation due to fading or interference, UE can look for other cells to connect.

VRBs	48	49	50	51	52	53	54	55	56	57	58	59	60	61	62	63	64	65	66	67	68	69	70	71	72	73	74	75
RBs	0	1	2	3	4	5	6	7	8	9	10	11	12	13	14	15	16	17	18	19	20	21	22	23	24	25	26	27
RBGs	RBG0				RBG1				RBG2				RBG3				RBG4				RBG5				RBG6			

VRBs	76	77	78	79	80	81	82	83	84	85	86	87	88	89	90	91	92	93	94	95	0	1	2	3
RBs	28	29	30	31	32	33	34	35	36	37	38	39	40	41	42	43	44	45	46	47	48	49	50	51
RBGs	RBG7				RBG8				RBG9				RBG10				RBG11				RBG12			

VRBs	4	5	6	7	8	9	10	11	12	13	14	15	16	17	18	19	20	21	22	23	24	25	26	27
RBs	52	53	54	55	56	57	58	59	60	61	62	63	64	65	66	67	68	69	70	71	72	73	74	75
RBGs	RBG13				RBG14				RBG15				RBG16				RBG17				RBG18			

VRBs	28	29	30	31	32	33	34	35	36	37	38	39	40	41	42	43	44	45	46	47	48	49	50	51
RBs	76	77	78	79	80	81	82	83	84	85	86	87	88	89	90	91	92	93	94	95	96	97	98	99
RBGs	RBG19				RBG20				RBG21				RBG22				RBG23				RBG24			

Figure 2.15: *RA Type 2 for RB gap equals to 48 and RIV equals to 924. Allocated RBs are shown by red and unallocated RBs are shown by white color.*

In LTE, system information and configuration messages are sent by the eNB to the UE via system information blocks (SIBs). Each SIB carries specific configuration messages which are dedicated to specific cases. For instance, cell re-selection and handover configuration messages are carried by SIB 3. As noted, cell re-selection and handover are based on measurement reports sent by the UE. Before the UE conducts any measurement, the eNB specifies the type of measurement through *RRCConnectionReconfiguration* message. The type of measurement is called an "event" in LTE. In Table 2.9, event types and their descriptions as well as the information element (IE) that conveys the event types are given.

Based on the measurement reports sent by the UE, the eNB decides to trigger cell re-selection or the handover process. Triggering these processes can be based on the RSRP level, RSRQ level or both of them. The triggering quantity depends on the eNB configuration and is sent to UE via SIB messages. When the trigger quantity is achieved by a neighbouring cell, the serving eNB decides whether to handover the UE or not. In Fig. 2.16, the measurement event A3 is depicted. As shown in Fig. 2.16, RSRP is chosen as the trigger quantity and there are offset and hysteresis parameters added to the serving cell RSRP. The offset parameter is used to make the serving cell attractive in order to decrease the number of handovers. The hysteresis parameter is used to discard small fluctuations and make sure that the UE has a stronger signal from a neighbouring cell. Moreover, there is another offset value used for the neighbouring cell, called *cellIndividualOffset*. This parameter is used to extend the range of a cell, termed

[8] Primary cell is the cell operating on the frequency that user established the initial connection procedure or initiated the connection re-establishment.

[9] Primary secondary cell is a subset of cells that are used when a user is configured with dual-connectivity.

[10] Secondary cell is a cell that operates on a secondary frequency.

Event Type	**Description**	**Information Element**
A1	Serving becomes better than threshold	ReportConfigEUTRA
A2	Serving becomes worse than threshold	
A3	Neighbour becomes offset better than primary cell[8] / primary secondary cell[9]	
A4	Neighbour becomes better than threshold	
A5	Primary cell / primary secondary cell becomes worse than threshold1 and neighbour becomes better than threshold2	
A6	Neighbour becomes offset better than secondary cell[10]	
C1	CRS resource becomes better than threshold	
C2	CRS resource becomes offset better than reference CRS resource	
B1	Neighbour becomes better than absolute threshold	ReportConfigInterRAT
B2	Primary cell becomes worse than absolute threshold1 AND Neighbour becomes better than another absolute threshold2	

Table 2.9: *LTE measurement reporting events*

cell range extension (CRE) in LTE. CRE method is used in heterogeneous networks to force a user, which is connected to a highly loaded macrocell, to connect a lightly loaded small (pico or femto) cell. Therefore, the *cellIndividualOffset* parameter artificially increases the received signal quality of a cell in order to offload the highly loaded cells.

As shown in Fig. 2.16, when the artificial RSRP of the neighbouring cell exceeds the triggering threshold of the serving cell, event A3 is triggered. At this point, the cell handover has not happened yet. The event A3 is triggered with a *time-to-trigger* parameter. The *time-to-trigger* is a duration that UE performs frequent measurements of the signal quality of the serving and neighbouring cells. The purpose of using such a time interval before handover the UE is to avoid a ping-pong effect[11]. Therefore, when the *time-to-trigger* duration is finished and the filtered[12] signal quality measurement of the neighbouring cell is better than the serving cell, then the eNB decides to handover the UE to the cell which provides better signal quality.

[11] A ping-pong effect is the term used to describe a situation that a UE is continuously handedover between the same two cells.

[12] In LTE, UE applies a filtering (averaging) for all measurements (except for UE transmitter-receiver time difference, RSSI and channel occupancy measurements) before evaluating or reporting the measurement result [41].

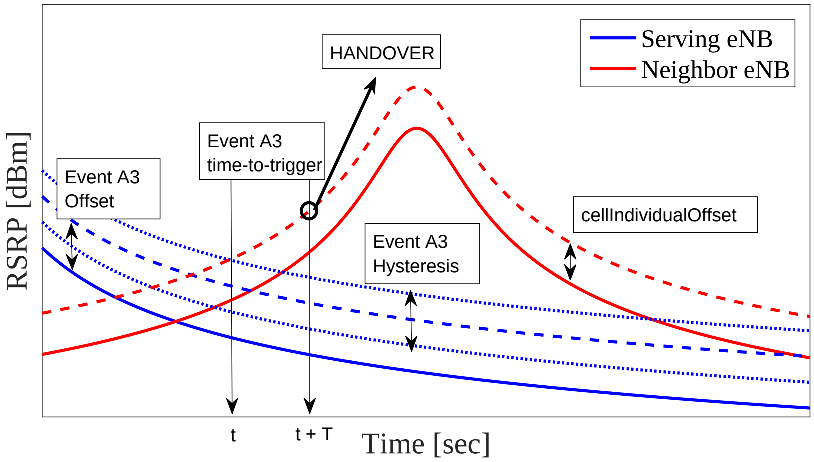

Figure 2.16: *Handover in event A3.*

2.4.7 Interference Mitigation

In cellular networks, different frequencies are used in adjacent base stations based on a specific pattern in order to decrease the co-channel interference level. This is called frequency reuse. However, in LTE networks, the same frequencies are used in each eNB. Therefore, for LTE systems, the frequency reuse factor is equal to 1. In other words, LTE uses full frequency reuse to achieve high spectral efficiency. In virtue of OFDM, intra-cell interference is eliminated. However, due to using the same frequency in adjacent eNBs, inter-cell interference becomes a major factor that limits system throughput performance. In order to address the inter-cell interference problem, different techniques such as ICIC, eICIC and CoMP are proposed in LTE.

2.4.7.1 ICIC Techniques

A potential technique to control and suppress the level of downlink interference is ICIC. The ICIC techniques are employed to reduce the impact of interference in the network planning stage by an operator or during transmission at an eNB or after the reception of the signal at UE by sharing the current or prospective status of the interference among cells. Those techniques can be classified into two groups: interference mitigation and interference avoidance [42]. The interference mitigation techniques are also classified into three categories of techniques. The first one is interference randomization where users have allocated resources spread over the available bandwidth based on cell-specific scrambling, interleaving or frequency hopping, instead of having adjacent resources. The goal of the interference randomization techniques is to spread out the interference, instead of cancelling it. However, in the second category of interference mitigation techniques, interference is cancelled by detecting and subtracting or selecting the best quality signal at the receiver, when the receiver has more than one antenna. Adaptive beamforming is the third technique to mitigate interference by changing the radiation pattern of the antenna based on the location and desired data of users[13].

2.4.7.2 eICIC Techniques

In LTE specifications, the ABS technique is proposed to mitigate interference on selected subframes by blanking data transmission at one of the eNBs in the system. However, ABS still uses normal transmission power on control channels on the selected subframes. Thus, a high level of interference on control channels is inherent when the ABS technique is used. In addition to that, blanking data transmission at one of the eNBs on the selected subframes means that RBs of the muted eNB are unused. Therefore, there will be no throughput for the users attached to the muted eNB during the ABS subframe. Accordingly, an enhanced approach, RP-ABS, is proposed to decrease interference on control channels, as well as provide throughput to victim eNB during the ABS subframe [28, 43–46].

The difference between the RP-ABS and ABS is data transmission in the blanked subframe. As noted, in ABS, although there is no data transmission at all in the subframe which is selected to be blank, the control channel is transmitted with normal transmission power. However, in RP-ABS, there is control and data transmission in the subframe with a reduced level of transmission power, as illustrated in Fig. 2.17. Thus, the additional data transmission on the RP-ABS subframes increases the achieved total capacity compared to ABS and the number of served users at any given time instant in the system [43]. However, when RP-ABS is used at one of the eNBs, a lower modulation order should be used in the AMC function to conserve modulation accuracy, which is measured by the error vector magnitude (EVM) [28, 47].

2.4.7.3 CoMP Techniques

A transmission based on the coordination between geographically separated cells is termed CoMP [26, 27, 48–50]. In CoMP, multiple cells cooperate to determine scheduling decisions,

[13]The beamforming technique needs multiple antennas at the transmitter side.

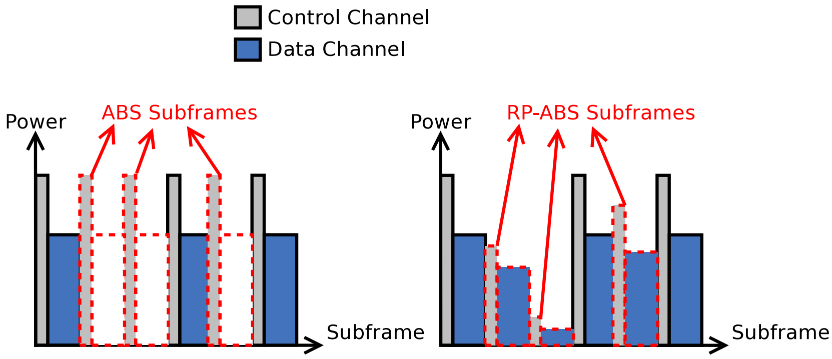

Figure 2.17: *Illustration of ABS and RP-ABS.*

transmission parameters and transmit antenna weights for a particular user in order to decrease interference levels or convert interfering signals to useful signals for cell-edge users. This cooperation can be established on an intra-site basis where deployed cells in an eNB cooperate without the need for an external connection. The technique can also be employed on an inter-site basis where an external connection is needed between the cooperating cells. Such a connection can be established by the LTE X2 interface [26].

Based on the complexity level of the data transmission and scheduling, CoMP techniques can be classified into two groups: joint processing (JP), which includes joint transmission (JT) and dynamic point selection (DPS), and coordinated scheduler (CS)/coordinated beamforming (CB). In JP techniques, channel state information (CSI) and transmission data for multiple users are available at each coordinated cell. The available data is transmitted from every coordinated cell by using jointly (coherent) or individually (non-coherent) decided precoding matrices in JT. However, in DPS, even the transmission data is simultaneously available at each coordinated cell, one of the coordinated cells is selected as the transmission cell and only this cell transmits data at each time instance. On the contrary, in CS/CB, coordinated cells share only CSI for multiple users and only one cell has transmission data [27]. Thus, with regard to complexity and overhead, implementation of the CS/CB is easier than the JP techniques.

In published research and 3GPP meetings, several scenarios and techniques are proposed for CS/CB and JT [51, 52]. Since several eNBs are coordinated to perform CS/CB and JT, connection delay among those eNBs is also considered in the proposed techniques as ideal backhaul (IB) without delay and non-ideal backhaul (NIB) with delay. In [51, 52], detailed analysis and performance evaluations of Release 12 inter-eNB CoMP with a dynamic coordinated muting algorithm based on NIB is proposed for both distributed and centralized architecture options by Nokia. The basic function of the coordinated muting is to jointly decide the resource allocation/muting pattern for multiple eNBs in a coordination area. For a decentralized inter-eNB coordination, every eNB can decide the muting pattern for its own cells. Updating the muting pattern can happen (1) every transmission time interval (TTI) when instant CSI and buffer status are available; or (2) periodically when delayed CSI and buffer status are available. Then, the muting pattern is shared through the LTE X2 interface. However, in a centralized deployment, there is a need for a new backhaul interface for the coordination information as outlined in [52].

An algorithm based on a master/slave relation is considered for the coordinated muting in a decentralized CoMP with NIB in [53]. In the considered master/slave relation, one of the eNBs, which can be the eNB with the highest or lowest traffic, becomes master eNB and informs the remaining coordinated eNBs as its slaves to mute indicated RBs. In [54], another approach for a decentralized scheduling algorithm is proposed by sharing information of semi-static power allocation and scheduling for users through the LTE X2 interface in the NIB connection. In the proposed semi-static power allocation algorithm, firstly, users are classified into different groups based on their received signal power levels as cell-centre, cell-middle and cell-edge. Then, the downlink transmission power for cell-centre and cell-middle users is set to quarter of the allowed maximum transmission power, and the maximum transmission power is set for cell-edge users. Afterwards, a CS is proposed to be used in conjunction with fractional frequency reuse (FFR) which is an ICIC based resource management technique [42].

Field trial results for a centralized CS by Deutsche Telekom AG (DTAG) and Samsung, and for non-coherent JT by Zhong Xing Telecommunication Equipment (ZTE) and China Mobile Communications Cooperation (CMCC) companies are given in [55]. An LTE network consisting of 12 macro and 3 small sites was tested for a centralized CS. When the full buffer traffic model with insensitive latency and a single cell-edge user are considered, gains of 120% and 30% are observed in the throughput performance of cell-edge users and overall cell capacity, respectively. Another LTE network with 18 cells was also tested for a non-coherent JT in [55]. In the test setup, non-coherent JT technique was applied to 3 out of 18 cells, and the remaining 15 cells provided load and interference to those 3 cells. Results of the non-coherent JT test show that the cell-average throughput is improved by about 40% when a 30% of traffic load was considered. Also, the probability of UE sets having throughput below 4 Mbps decreased to 2% from 15% when JT was employed in the system.

2.4.8 Carrier Aggregation

CA is proposed to improve the achievable peak data rate and system throughput by combining several channel bandwidths, CCs. The aggregated CCs can be in the same band and adjacent to each other or in the same band but separated along the band. These types of aggregations are called intra-band contiguous CA and intra-band non-contiguous CA, respectively. The aggregated CCs can also be in different bands. This is called inter-band non-contiguous aggregation [56]. An illustration of the CA types are given in Fig. 2.18.

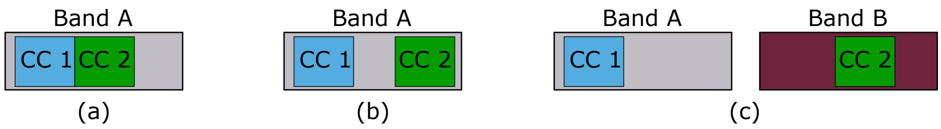

Figure 2.18: *Aggregation types. (a) Intra-band contiguous. (b) Intra-band non-contiguous. (c) Inter-band non-contiguous.*

In Release 10, a maximum 2 downlink CCs can be aggregated. Also in Release 11, a maximum number of downlink CC aggregation is limited to 2. However, aggregating 3 CCs, 4 CCs and 5 CCs in the downlink direction is supported in 3GPP standards Release 12, Release 13 and Release 14, respectively.

Several field test reports are published to show the performance of CA. In a collaboration between Huawei, Qualcomm and EE, LTE-A CA was tested at Wembley Stadium. A data rate of 400 Mbps was achieved from a single UE by aggregating a CC with 20 MHz of 1.8 GHz spectrum and CCs with 15 MHz and 20 MHz bandwidth in the 2.6 GHz spectrum [57]. StarHub and Nokia have successfully demonstrated 600 Mbps data transmission speed by using 4×4 MIMO technology with 3 aggregated CCs in different bands [58].

2.5 Summary

In this chapter, the evolution of LTE has been introduced. Predictions on mobile data traffic, number of mobile devices and mobile network speed have been compared with achieved values in order to understand how mobile data usage correlates with the number of devices and network capability. Then, the in-flight connectivity and its regulations have been described. Finally, the basic description of LTE systems has been introduced.

Chapter 3
In-Cabin Antenna Deployment

3.1 Introduction

Due to the construction materials and shape of the cabin, electro-magnetic (EM) propagation inside the aircraft is not similar to commonly considered indoor channel propagation models. In particular, the metal hull of the aircraft is an excellent reflector of radio frequency (RF) waves. Moreover, the high density of passenger seating and the tunnel shape structure of the cabin make the environment highly reflective. A medium-sized aircraft is approximately 30 m long and has a capacity of 150-240 passengers. Therefore, covering such a user dense environment with one cell will not be sufficient to satisfy the required high data rates. Thus, deploying more than one cell is needed in order to satisfy high data rates [21]. As a result of this, interference is the system throughput limiting factor for a multi-cell in-cabin system. To optimize such an interference limited system deployment, the radio propagation characteristics in that specific environment should be well identified.

Channel characterization of an aircraft cabin environment has been performed in different aircraft models and frequency bands [59–61]. In [59], the ultra wideband channel over the frequency range of 3.1 to 10.6 GHz is characterized for a Boeing B737-200 aircraft. In [61], radio propagation measurements are taken at 2.45 GHz and 5.8 GHz bands in a Bombardier CRJ700 jet aircraft, and channel characterization is obtained. In [60], the objective was to develop a propagation model at 1.8 GHz, 2.1 GHz and 2.45 GHz bands inside a Boeing B737-400. By using the measurement data on in-cabin propagation: path loss exponent, free-space loss, slow fading and frequency-selective fading distribution functions are determined.

In the noted studies [59–61], the transmit antenna position in the measurements is fixed at the front of the cabin and placed in the middle of the aisle. Only in [61] another transmit antenna position is considered where it is again fixed at the front of the cabin but placed at slightly right of the middle of the aisle. For this type of measurement setup, the modelled propagation is only valid for the given particular location and given particular propagation direction. Therefore, considering another antenna location with the radio propagation model given in [59–61] will not be valid and realistic for an in-cabin multi-cell deployment. A passenger seat has two parts, i) the seat front which consists of foam and fabric, and ii) the seat back which consists of aluminum and plastic. Due to the differences between the used materials in the front and back, and since the radio propagation depends on the media, reflections from both parts will be different. In order to propose and design a multi-cell in-cabin deployment, a more general channel propagation model which addresses the effects of propagation direction inside the cabin is required.

In this research, a measurement and modelling procedure is proposed to accurately characterize channel propagation inside an aircraft. In general, conducting a channel propagation measurement campaign takes a substantial amount of time. When the measurement campaign is scheduled to be conducted in an aircraft, in addition to a substantial amount of time, the campaign can also cost a considerable amount of money. Therefore, the proposed measurement and modelling procedure is divided into three phases: (1) characterization of the direction of propagation; (2) characterization of the reflection from the cockpit and tail ends of the cabin; and (3) characterization of the reflection from the sidewalls of the cabin. In order to prove that the proposed measurement and modelling procedure is worthwhile to employ and follow, the obtained results of the first phase are given in this chapter. In the first phase, in order to investigate how the channel propagation changes based on the direction of the propagation inside the cabin, three different transmit antenna locations are considered. For each transmit antenna location, the receive antenna is located in different passenger seats. Each receive antenna location is classified with respect to the transmit antenna location to identify the propagation direction.

The proposed measurement procedure is conducted in the Airbus A321 aircraft described in Section 2.3.2. The Airbus A321 is a medium-sized, medium range aircraft and is one of the most commonly used models by flight operators. In the measurements, the propagation characteristics of the 1800 MHz frequency band are obtained. As explained in Section 2.3, Long Term Evolution (LTE) 1800 MHz is the preferred option for the onboard communication system. Also, the 1800 MHz band is one of the most commonly used LTE bands in Europe.

As described in Section 2.3.2, cell sectorization is employed by using directional antennas in order to decrease interference among neighbouring evolved nodeBs (eNBs). Therefore, it is important to find an optimum tilt angle that minimizes interference among eNBs. For the considered in-cabin system model, besides minimizing the interference, finding the optimum tilt angle is crucial in order to provide a better desired signal quality for the users[1]. Thus, the obtained tilt angle should be optimum by means of minimizing the interference among neighbour eNBs and minimizing the path loss for the users. The former is the objective of cell sectorization and the latter is the condition to further improve the users' desired signal quality.

The optimum tilt angle that improves the throughput of the users at the cell-edge is found by using Taguchi's method in [21]. The tilt angle of each antenna is considered as a parameter to optimize the throughput when a proportional fair (PF) scheduler is used in an onboard system in [21]. Taguchi's method is an experiment-based searching algorithm that uses orthogonal arrays to reduce the number of parameter combinations [62]. It has been shown in [62] that Taguchi's method performs better than simulated annealing, which is one of the common optimization methods used by the network operators. Therefore, Taguchi's method is used to reach the near-optimal results in [21]. As a result of considering each antenna tilt angle as a parameter, different tilt angles have been found for different objectives such as improving throughput of users at the cell-edge, cell-middle and cell-centre. Also, finding the optimum tilt angle based on the achieved throughput highly depends on the considered scheduling algorithm. Therefore, in this study, finding the optimum angle is based on achieved path loss, not the achieved throughput as in [21]. Improving the throughput performance will be considered as another optimization criteria of the in-cabin system design in combination with enhanced inter-cell interference coordination (eICIC) techniques, carrier aggregation (CA) and a scheduler. When the tilt angle of each antenna is considered as a parameter in the optimization problem as in [21], there will be several combinations of optimum tilt angle for antennas due to symmetry in the system. Thus, in this study, in order to find only one optimum tilt angle for all deployed antennas, it is assumed that each antenna has the same tilt angle.

The remainder of this chapter is arranged as follows. The proposed channel characterization measurement procedure and an in-cabin measurement based channel model are given in Section 3.2. Based on the proposed in-cabin channel model, the optimum tilt angle is found in Section 3.3. The validation of the modelled channel propagation characteristics inside the aircraft is presented in Section 3.4. This chapter is summarised in Section 3.5.

[1] Desired signal means the signal that a user gets from its connected cell.

3.2 In-Cabin Channel Propagation Characterization

3.2.1 Proposed Measurement and Modelling Procedure

3.2.1.1 Characterizing the Propagation Direction

To perform the first phase, several transmit antenna mounting locations, such as locations close to the cockpit, in the middle of the cabin and near the tail, should be considered to understand how the channel propagation behaves in different propagation directions. As noted, different materials are used in the passenger seat front and seat back, and therefore, reflection from the different parts will be different. In order to identify the change in the propagation characteristics based on the reflectivity of the passenger seat back and seat front, the measured seat locations are classified with respect to each transmit antenna location. The passenger seats located in the direction of flight with respect to the transmit antenna position are mainly affected by reflections from the seat back and labeled *seats in the in-flight direction*, and the seats located in the opposite direction are mainly affected by reflections from the seat front and labeled *seats in the in-rear direction*. Fig. 3.1 illustrates dominant reflection points. According to the given labeling description, seats in rows X, Y and Z in Fig. 3.1 can be labeled as *seats in the in-flight direction*, and seats in rows Q, P and R can be labeled as *seats in the in-rear direction*. Once the received power is measured, based on the given procedure, the distance dependent

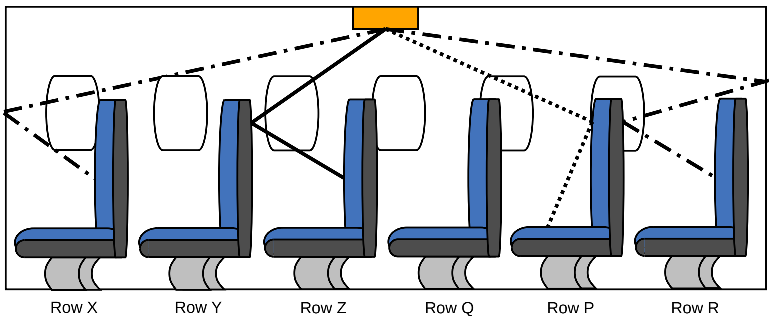

Figure 3.1: *Propagation reflection - solid line represents reflection from seat back; dotted line represents reflection from seat front; dashed-dotted line represents reflection from top and end walls of the cabin (cockpit and tail).*

path loss should be modelled for each propagation direction separately. Therefore, the channel propagation in the in-flight direction and in the in-rear direction should be analysed individually in order to investigate how the channel propagation in the aircraft cabin changes according to the propagation direction.

3.2.1.2 Characterizing the Reflection From the Cabin Ends

The second phase of the proposed measurement and modelling procedure is to characterize the radio wave reflection from the cockpit and tail ends of the aircraft cabin. In a commercial aircraft, the passenger seating area is divided from the cockpit and tail ends of the aircraft by plastic walls filled with flame resistant foam. In general, storage units (for food and first aid materials) and in-flight control units used by the cabin crew are placed on a metal profile at the cockpit and tail ends of the cabin. Therefore, due to the plastic walls used to divide the seating area and the metal profile used in the galley and in-flight control units, there should be reflections from both the ends of the aircraft cabin. In order to understand the characteristics of the reflection from the cabin end, the cockpit and tail ends of the cabin should be covered by a RF absorbing material, and the same measurement procedure described in the first phase should be conducted. Then, the measured values obtained with (the second phase) and without (the first phase) the RF absorbing material should be compared to understand the contribution of the reflected power from the cockpit and tail ends of the cabin. As described in the first phase, the direction of the propagation should be taken into account in the characterization of the reflection from both the ends of the cabin.

3.2.1.3 Characterizing the Reflection From the Cabin Sidewalls

In general, a commercial aircraft has several passenger seats in a row, and the seats in a seat row are labeled from one sidewall to the other as columns, such as column A, column B, etc. The third phase of the proposed measurement and modelling procedure is to investigate how the received power level changes from seat to seat in the same row. Due to the concave structure of the aircraft fuselage, reflections from the sidewalls may differ for seats at different columns in the same row. In order to characterize the reflections from the aircraft sidewalls, all the passenger seats in a seat row should be measured as described in the first phase. Based on the measurement results, the distance dependent path loss should be modelled for each seat column.

3.2.2 Measurement Environment

The Airbus A321 aircraft cabin is configured with 35 rows of seats and a single aisle. It has a seating capacity of 210 passengers (all in economy class). The approximated cabin interior dimensions are given in Table 2.3.

In the A321 aircraft interior design, three positions are already designated in the ceiling of the cabin for antenna placement. Accordingly, the first provisioned antenna location is close to the cockpit and close to seat 5D, the second antenna location is in the middle of the cabin, close to seat 18D, and the third location is close to the tail, next to seat 29C on the aisle side. The cabin layout and already provisioned antenna locations can be found in Fig. 2.7.

3.2.3 Measurement Setup

In the given measurement procedure, a 75 MHz wide channel in the 1.8 GHz band was measured for each of the given provisioned antenna positions. In order to represent the LTE structure, the 75 MHz channel is divided into four channels as given in Table 2.4. A continuous wave (CW) signal with 1 MHz bandwidth was generated by an Agilent E4438C signal generator and transmitted via a directional 2×1 patch antenna. The directional antenna has 12 dBi antenna gain, 10 dB front-to-back attenuation, 80° azimuth half power beamwidth (HPBW) and 45° elevation HPBW. The transmit antenna is mounted to the ceiling of the aircraft at the three different locations shown as provisioned in Fig. 2.7 and directed to the floor of the cabin. On the receiver side, an omnidirectional probe antenna was used to capture the transmitted signal over the air by an Agilent E4440A spectrum analyser. The omnidirectional probe antenna has 2 dBi antenna gain. Both the signal generation and capture were controlled by Matlab code executed on a laptop. In each measurement point, the measurements are repeated 10 times and the average received power level is used in the path loss modelling. The measurement steps can be ordered as follows:

- Establish a connection between the signal generator and spectrum analyser;
- Set measurement parameters in order to test the desired transmitter position;
- Set the position of the intended measurement seat;
- Set the span of the spectrum analyser based on the considered channel bandwidth;
- Set the centre frequency of the transmitted signal;
- Run measurements to capture the received power of the transmitted CW signal with 1 MHz bandwidth at the spectrum analyser.

The given measurement steps will be repeated 10 times. The centre frequency of the transmitted signal is varied from 1805 MHz to 1880 MHz to obtain the channel frequency response and the given steps will be repeated for each centre frequency. An example of the user interface of the Matlab code is shown in Fig. 3.2. An observation of the frequency response of a receiver

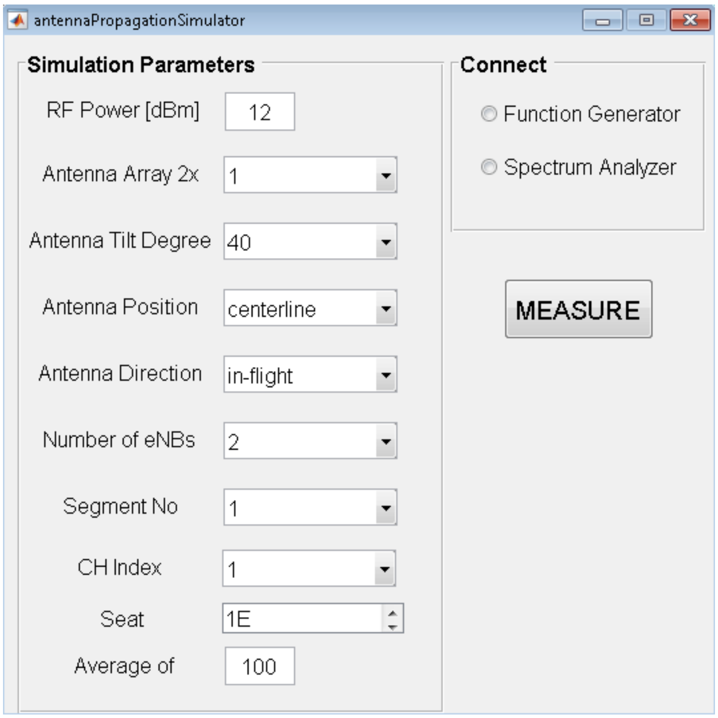

Figure 3.2: *User interface of Matlab code used in the measurements.*

location is shown in Fig. 3.3.

In terms of the measurement testbed, the signal generator and spectrum analyser were controlled from the same laptop to mitigate any possible problems with synchronization. Thus, a trolley to carry the spectrum analyser and an Ethernet cable which was long enough to connect the laptop and the signal generator (which was located below the antenna position) were used. The transmit and receive antennas were connected to the function generator and spectrum analyser, respectively, by 5 metres long RF cables which had 2.5 dB loss. According to the operation limit of the function generator, antenna gain and the used RF cable loss, the output power level of the function generator was set to 20.5 dBm (for a radiated power of 20.5 dBm + 12 dBi - 2.5 dB = 30 dBm). An illustration for the measurement setup is shown in Fig. 3.4.

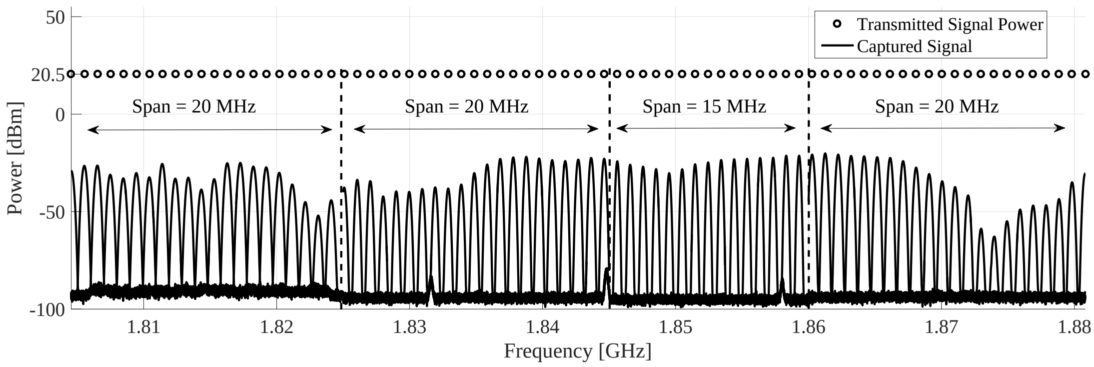

Figure 3.3: *Captured signal - noise level is around -100 dBm, and some peaks around the noise level represent the received power from the terrestrial cells.*

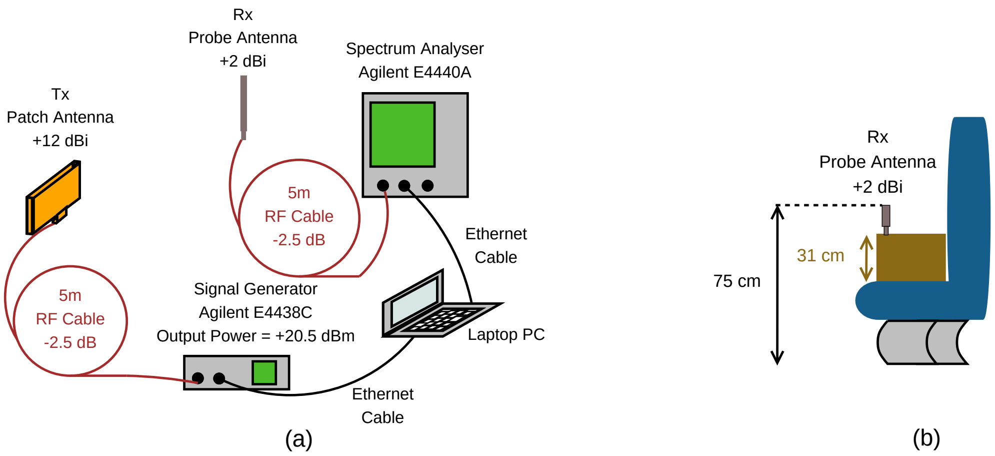

Figure 3.4: *Measurement setup. (a) Link budget. (b) Receive antenna position.*

3.2.4 Large-Scale Propagation Path Loss Model

To obtain generalized propagation path loss characteristics, any antenna related gain should be suppressed to make the model independent from the used antenna characteristics. The used transmit antenna has directionality along both its elevation and azimuth planes, as shown in Fig. 3.5. Hence, the antenna pattern gain is mitigated in the measured path loss calculation. The 3-D antenna pattern gain, $B\left(\Phi, \phi, \Theta, \theta\right)$, is calculated according to [63] and is equal to:

$$B\left(\Phi, \phi, \Theta, \theta\right) = -\min\left\{-\left(B_{\phi}(\Phi, \phi) + B_{\theta}(\Theta, \theta)\right), B_0\right\} \tag{3.1}$$

where B_0 is the maximum antenna front-to-back attenuation in decibels; and $B_{\phi}(\Phi, \phi)$ and $B_{\theta}(\Theta, \theta)$ are the azimuth and elevation pattern gains of the antenna. The calculation of the azimuth and elevation patterns of the antenna according to [63] are given in (3.2) and (3.3) as

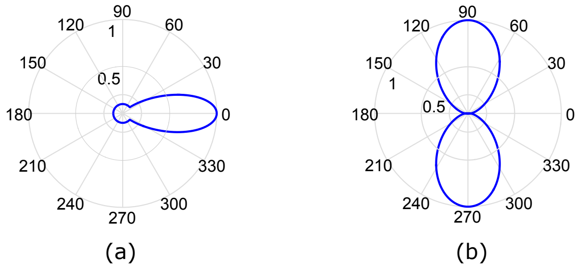

Figure 3.5: *Antenna pattern. (a) Elevation plane. (b) Azimuth plane.*

follows:

$$B_\phi\left(\Phi,\phi\right) = -\min\left\{B_0, 12\left(\frac{\phi-\Phi}{\Delta_\phi}\right)^2\right\} \tag{3.2}$$

$$B_\theta\left(\Theta,\theta\right) = -\min\left\{B_0, 12\left(\frac{\theta-\Theta}{\Delta_\theta}\right)^2\right\} \tag{3.3}$$

where Φ and Θ are azimuth and elevation orientations of the antenna; ϕ and θ parameters are angles between transmitter and receiver in azimuth and elevation planes as shown in Fig. 3.6; and Δ_ϕ and Δ_θ are the azimuth and elevation HPBWs, respectively.

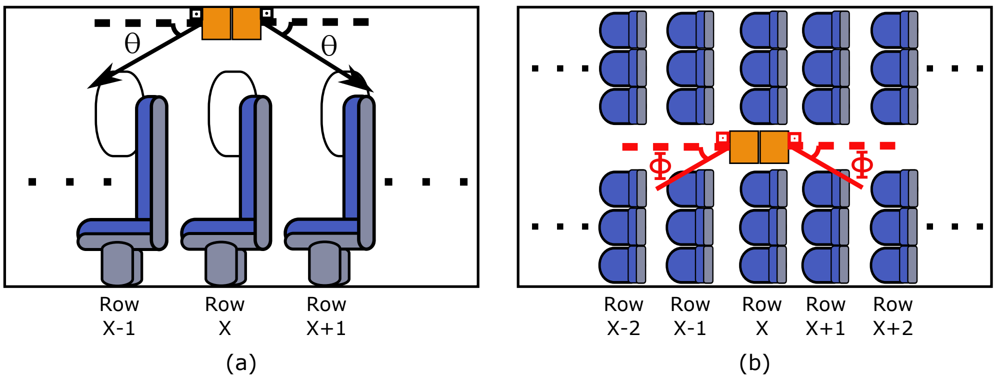

Figure 3.6: *Illustration of azimuth and elevation orientation of the antenna. (a) Elevation orientation. (b) Azimuth orientation.*

Consequently, the measured path loss is calculated as follows:

$$\mathrm{PL}_{\mathrm{aircraft}}(d,\Theta) = P_{\mathrm{tx}} + G_{\mathrm{tx}} + G_{\mathrm{rx}} + B\left(\Phi,\phi,\Theta,\theta\right) - L_{\mathrm{cable}} - \left(P_{\mathrm{rx}} + 0.5\right) \tag{3.4}$$

where d is the 3-D transmitter and receiver separation distance in metres; $\mathrm{PL}_{\mathrm{aircraft}}(d,\Theta)$ is the measured path loss for antenna tilt angle Θ at distance d in decibels; P_{tx} and P_{rx} are the transmit and received power levels in decibels referenced to milliwatt (dBm); G_{tx} and G_{rx} are the transmit and receive antenna gains; L_{cable} is the total RF cable loss at transmitter and receiver sides (2.5 dB $+$ 2.5 dB $=$ 5 dB in total). In the equation, the received power, P_{rx} is normalized by adding 0.5 dB which is the amount of loss when the receiver gain and RF cable loss at the receiver side are taken into account (2 dBi - 2.5 dB = -0.5 dB).

Once the measured path loss is obtained, the in-cabin large-scale distance dependent propagation path loss is modelled by the standard log-distance path loss law which is:

$$\mathrm{PL}_{\mathrm{model}}\,(d) = F_{\mathrm{PL}}(d_0) + 10n\log_{10}\left(\frac{d}{d_0}\right) + \chi_{\sigma_L} \tag{3.5}$$

where $\mathrm{PL}_{\text{model}}(d)$ is the modelled path loss at distance d in decibels; $F_{\mathrm{PL}}(d_0)$ is the free-space path loss in decibels at reference distance d_0; n is the path loss exponent; and χ_{σ_L} is the large-scale signal fluctuations (shadowing) term which is a zero-mean Gaussian random variable with a standard deviation σ_L in decibels.

In Fig. 3.7, the measured received power at the seats labeled as in-flight and in-rear is shown. There is a 6 dB difference between the seats in the in-flight and in-rear directions when the transmitter-receiver separation is between 5 and 14 metres. However, when distances that are shorter than 5 metres and longer than 14 metres are considered, the received power level is approximately the same for both directions. Accordingly, the path loss exponent n and standard deviation of the large-scale signal fluctuations σ_L, are obtained for three different distance ranges as illustrated in Fig. 3.7: (1) distances shorter than 5 metres; (2) distances between 5 and 14 metres; and (3) distances longer than 14 metres.

In Fig. 3.8(a), the path loss models for the measurement results of seats in the in-flight and in-rear directions are given for distances shorter than 5 metres. The path loss exponent of 1.5 is used for the path loss model for both seats in the in-flight and in-rear directions with a standard deviation of 1.81 dB and 2.55 dB, respectively. For such short distances, there is a direct link between transmitter and receiver. Thus, line of sight (LoS) path dominates the measured received power level, and the same path loss exponent is found for both the propagation directions.

In Fig. 3.8(b), the path loss models for the seats in the in-flight and in-rear directions are given for distances between 5 and 14 metres. When the seats in the in-flight direction are considered,

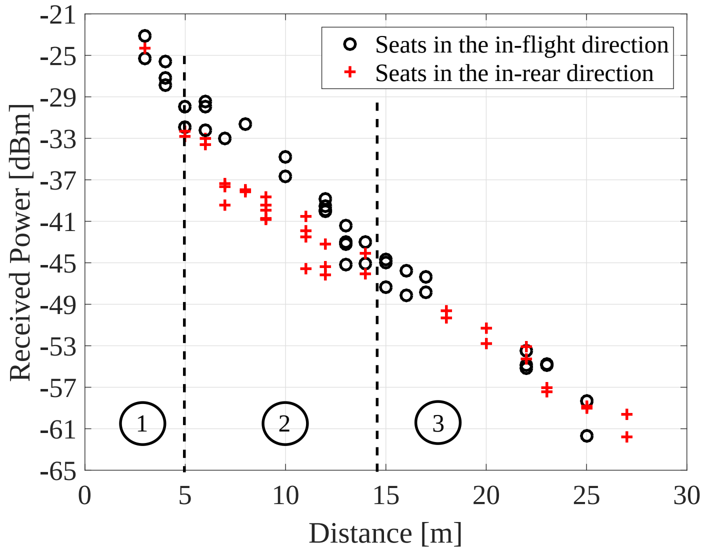

Figure 3.7: *Average received power for seats in the in-flight and in-rear directions - three distance based regions are considered.*

the path loss is well modelled with a path loss exponent of 2 which is considered as a free-space path loss exponent, and standard deviation of the log-normal shadowing component of 2.49 dB. However, when the seats in the in-rear direction are considered, the path loss exponent is increased to 2.3 and the standard deviation is reduced to 1.84 dB. Based on the given path loss model parameters, it can be said that the propagation loss for seats in the in-rear direction is larger than the in-flight direction. As depicted in Fig. 3.1, when the seats in the in-flight direction are considered, the radio wave first hits the seat back, which consists of aluminum and plastic, and bounces back to the receiver. When the seats in the in-rear direction are considered, the radio wave first hits the seat front, which consists of foam an fabric. Due to the materials used in the seat front, the radio wave does not bounce back to the receiver located on the seat as it does in the seat back case. Therefore, the received power level is decreased, and accordingly, the path loss is increased in the in-rear propagation direction.

Measurement results and modelled path loss of seats in the in-flight and in-rear directions for distances longer than 14 metres are given in Fig. 3.8(c). As shown in Fig. 3.7, the received power level in both propagation directions follow the same decay trend when the distance between transmitter and receiver is longer than 14 metres. Accordingly, the same path loss exponent, which is 2.6, is found for both seats in the in-flight and in-rear directions. For such distances, there is no LoS link between the transmitter and receiver due to the cabin geometry

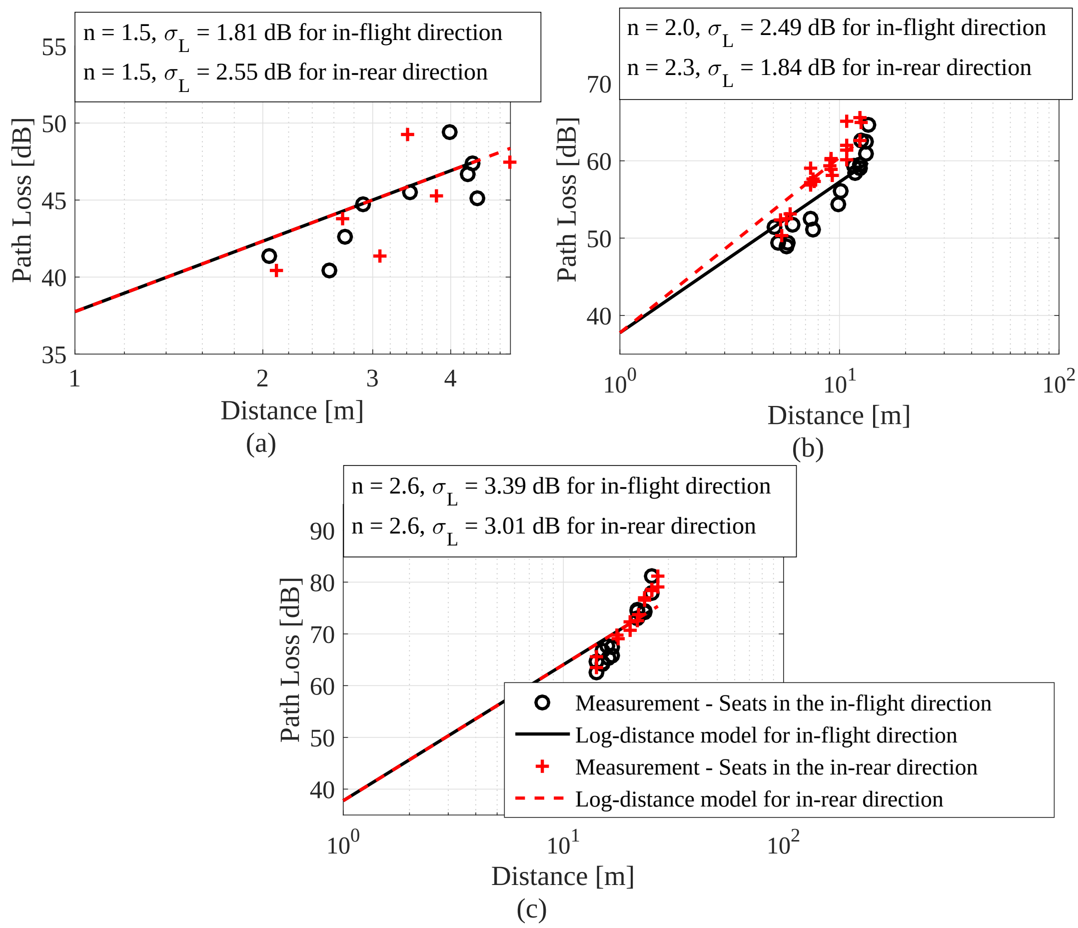

Figure 3.8: *Path loss model based on seats in the in-flight and in-rear directions. (a) For distances shorter than 5 metres. (b) For distances between 5 and 14 metres. (c) For distances longer than 14 metres. Path loss model parameters n and σ_L are given for each region and propagation direction.*

where the link is blocked by passenger seats[2]. Although this is the case for distances between 5 and 14 metres, the number of blockage points is higher for distances longer than 14 metres. It can be found that once the received power decreases to a particular level and the blockage points are increased to a particular number, the reflected power from the seat back does not contribute to the received power level in the in-flight direction.

[2]When the cabin height, seat height and row width given in Table 2.3, and the receiver height shown in Fig. 3.4(b) are considered, a direct link between the transmitter and receiver occurs for the first few metres.

3.2.5 Frequency Response Characteristics

As described in Section 3.2.3, the transmitted CW signal has a bandwidth of 1 MHz and the centre frequency of the transmitted signal is varied from 1805 MHz to 1880 MHz in order to obtain the frequency response of a receiver location. An observation on the spectrum analyser screen is shown in Fig. 3.3 and the measured frequency response of different receiver positions is given in Fig. 3.9.

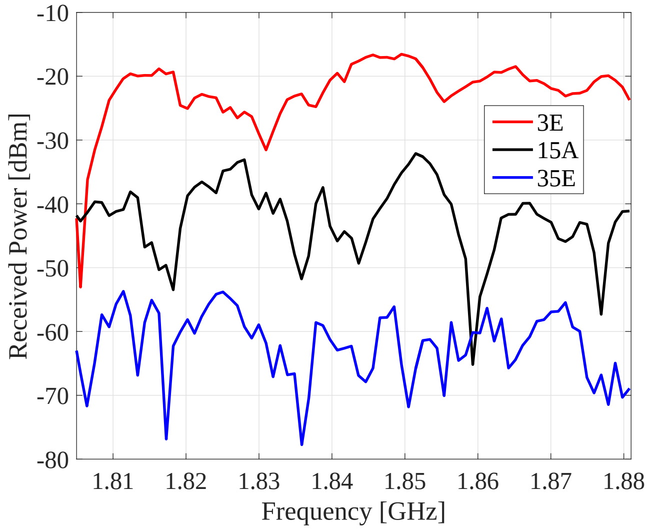

Figure 3.9: *Snapshot of the measured channel frequency response at different seats when the antenna is mounted on the point A given in Fig. 2.7.*

To obtain the characteristics of the frequency response of the channel, the measured power level is normalized by subtracting the distance-dependent path loss characteristic as follows:

$$\Delta P_{\text{rx}} = 10^{(P_{\text{rx}} - \overline{P_{\text{rx}}})/10}, \tag{3.6}$$

where ΔP_{rx} represents the ratio of the received power variation through the channel frequency; and $\overline{P_{\text{rx}}}$ is the average measured power level. Once the received power variations are obtained, the probability distribution function (PDF) of the ratio of the variations are modelled by using Nakagami-m, Rayleigh, exponential and Weibull distribution functions. It is assumed that ΔP_{rx} has L elements, where each element $\Delta P_{\text{rx},l}$ $(l = \{1, \ldots, L\})$, is identical and independently distributed (i.i.d.), and its probability depends on a set of unknown parameters. In order to find the set of distribution parameters that represents the statistics of the obtained power level variation ratio, maximum likelihood estimation (MLE) is used. Log-likelihood of the obtained power level ratio, $\ell(\mathcal{D}_x)$, for a given PDF x, f_x^{PDF}, and its distribution parameters set $\mathcal{D}_x$ are obtained by (3.7). In f_x^{PDF}, x represents the considered distribution function such as $f_{\text{nakagami}}^{\text{PDF}}$, $f_{\text{weibull}}^{\text{PDF}}$, $f_{\text{exponential}}^{\text{PDF}}$ and $f_{\text{rayleigh}}^{\text{PDF}}$[3]. When x represents Nakagami-m distribution, $\mathcal{D}_x$ has two elements, namely the shape parameter m, which ranges from 0.5 to ∞, and spread controlling parameter ω, which is the mean-square value. In the Rayleigh and exponential distributions, the parameter σ_{ray} and λ_{exp} are used as a scaling parameter and are the only parameter of set $\mathcal{D}_x$, respectively. In the Weibull distribution, parameters λ_{wei} and k_{wei} are used as scale and shape parameters of the distribution, respectively. The parameters of the distribution x that fits the empirical data, $\hat{\mathcal{D}}_x$, can be estimated by (3.8).

$$\ell(\mathcal{D}_x) = \sum_{l=1}^{L} \log f_x^{\text{PDF}} \left(\Delta P_{\text{rx},l} | \mathcal{D}_x \right) \tag{3.7}$$

$$\hat{\mathcal{D}}_x = \underset{\mathcal{D}_x}{\arg\min} \quad -\ell(\mathcal{D}_x) \tag{3.8}$$

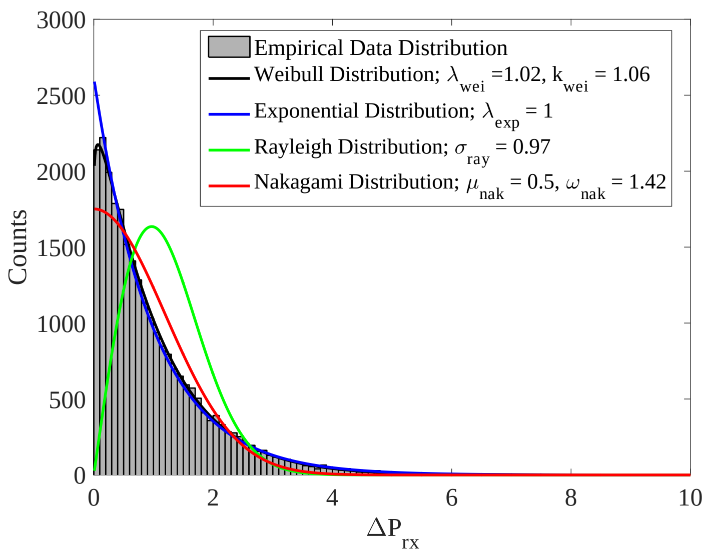

Figure 3.10: *Distribution of the fade depth.*

In Table 3.1, the output of (3.8) and the set of distibution parameters are given. According to the table, the Weibull distribution with parameters $\lambda_{\text{wei}} = 1.02$ and $k_{\text{wei}} = 1.06$ has the minimum negative log-likelihood result. Also, as shown in Fig. 3.10, distribution of the empirical data

[3]PDF of the Nakagami-m, Rayleigh, exponential and Weibull distributions are given in Appendix A.

closely matches the Weibull PDF[4].

Distribution:	Weibull	Exponential	Rayleigh	Nakagami-m
$\hat{\mathcal{D}}_x$	$\lambda_{\text{wei}} = 1.02$ $k_{\text{wei}} = 1.06$	$\lambda_{\text{exp}} = 1$	$\sigma_{\text{ray}} = 0.97$	$\mu_{\text{nak}} = 0.5$ $\omega_{\text{nak}} = 1.42$
$-\ell(\hat{\mathcal{D}}_x)$	26083	26154	38189	27826

Table 3.1: *Log-likelihood performance of the considered distributions*

3.2.6 Overall In-Cabin Channel Model

The path loss model with varying path loss exponent according to the direction of propagation and distance, the path loss characteristics are obtained for the Airbus A321 aircraft model. The path loss exponent n is obtained by (3.9).

$$(n, \sigma_L) = \begin{cases} (1.5, 1.81) & d \leq 5 \text{ m}, & \text{in-flight direction;} \\ (1.5, 2.55) & d \leq 5 \text{ m}, & \text{in-rear direction;} \\ (2.0, 2.49) & 5 \text{ m} < d \leq 14 \text{ m}, & \text{in-flight direction;} \\ (2.3, 1.84) & 5 \text{ m} < d \leq 14 \text{ m}, & \text{in-rear direction;} \\ (2.6, 3.39) & 14 \text{ m} < d, & \text{in-flight directions;} \\ (2.6, 3.01) & 14 \text{ m} < d, & \text{in-rear directions.} \end{cases} \tag{3.9}$$

Once the overall signal attenuation is obtained, the channel response of each resource block (RB) is generated by:

$$H_{\text{RB}}^{\text{A}}(d, \Theta) = \sqrt{10^{\frac{-(\text{PL}_{\text{model}}(d) + B(\Phi, \phi, \Theta, \theta))}{10}}} \kappa_{\text{RB}}, \tag{3.10}$$

where $H_{\text{RB}}^{\text{A}}(d, \Theta)$ is the channel frequency response of the RB for a given distance d and antenna tilt angle Θ; and κ_{RB} is the Weibull distributed power variation term of the RB with the parameters $\lambda_{\text{wei}} = 1.02$ and $k_{\text{wei}} = 1.06$.

[4]The accuracy of the given model will be discussed in Section 3.4.

3.3 Antenna Orientation

3.3.1 Antenna Tilt Optimization

In order to find the optimum tilt angle of an eNB that minimizes interference at a neighbouring eNB and provides minimum path loss for its connected users, the following optimization problem is considered:

$$\underset{\Theta}{\text{maximize}} \quad Z(\Theta), \tag{3.11}$$

where $Z(\Theta)$ is the utility function that an angle Θ achieves. The utility function consists of harmonic means of the path loss difference between two antennas at the deployed eNB locations and observed path loss for users connected to each eNB[5]. In this study, user-eNB/channel association is considered as the maximum-power based association. In maximum-power based user-eNB/channel association, a user will connect to the eNB/channel that provides the maximum signal power. In other words, minimum path loss will be the criterion for a user to pick an eNB/channel to connect.

Accordingly, the utility function $Z(\Theta)$ can be written as follows:

$$Z(\Theta) = \overline{T}_{\text{PL}}(\Theta) - \overline{Z}_{\text{PL}}(\Theta), \tag{3.12}$$

where $\overline{T}_{\text{PL}}(\Theta)$ is the harmonic mean of the absolute value of the path loss difference seen at each antenna location; and $\overline{Z}_{\text{PL}}(\Theta)$ is the harmonic mean of the path loss of each user. The $\overline{T}_{\text{PL}}(\Theta)$ is obtained by (3.13) and can be considered as achievable signal-to-interference ratio (SIR) when the same transmission power is considered for each antenna. In (3.13), PL_X represents the path loss of the antenna located at point X, where X can be any antenna location point given in Fig. 2.7. $d_A \to d_u$ represents the absolute distance between point A and the location of user u where $u = a$ and $u = x$ represent users a and x which are located just below the antenna at point A and X, respectively. The harmonic mean of the path loss of each user, $\overline{Z}_{\text{PL}}(\Theta)$, is calculated by (3.14) where N_U is the number of users between point A and point X; and Y_u is the eNB that user u is connected to. As noted, the optimum tilt angle should minimize both the interference and path loss for users. Therefore, based on the maximization problem

[5] Harmonic mean is calculated by dividing the number of data points by the summation of the reciprocal of values of data points. For example, harmonic mean of a data set $X \in x_1, x_2, \ldots, x_N$ is calculated by $N / \sum_i^N 1/x_i$. The reason for using the harmonic mean instead of the arithmetic mean to average the performance is that the harmonic mean does not alleviate the effect of small values and over emphasize the effect of large values, which is not the case in the arithmetic mean [62].

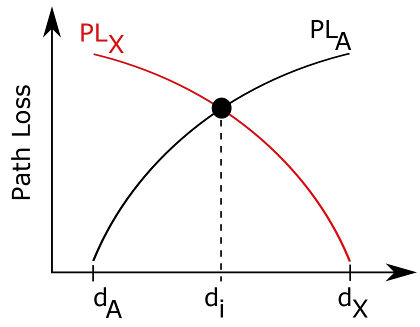

Figure 3.11: *Illustration for path loss - d_X is the location of the second eNB point X, which depends on the considered number of eNBs as shown in Fig. 2.7; d_i is the intersection point, which can be considered as the cell border; and PL$_X$ represents the path loss of the antenna located at point X.*

given in (3.11), the achieved SIR is maximized and observed path loss for users is minimized by using subtraction in (3.12).

$$\overline{T}_{\text{PL}}(\Theta) = \frac{2}{\frac{1}{|\text{PL}_A(d_A \to d_{u=x},\Theta) - \text{PL}_X(d_X \to d_{u=x},\Theta)|} + \frac{1}{|\text{PL}_A(d_A \to d_{u=a},\Theta) - \text{PL}_X(d_X \to d_{u=a},\Theta)|}} \tag{3.13}$$

$$\overline{Z}_{\text{PL}}(\Theta) = \frac{N_U}{\sum_u^{N_U} \frac{1}{\text{PL}_{Y_u}(d_{Y_u} \to d_u,\Theta)}} \tag{3.14}$$

In order to comply with third generation partnership project (3GPP) descriptions [63], the antenna tilt angle is obtained based on consideration of the horizontal plane as the antenna main lobe, as shown with dashed lines in Fig. 3.6(a). The considered optimization criteria are obtained for users between the two eNBs, which are the users from row A to row $X = D$ for 2 eNBs and to row $X = C$ for 3 eNBs deployments for the provisioned antenna positions shown in Fig. 2.7. In order to clarify how to obtain the utility function, Fig. 3.11 illustrates the path loss of different antennas located at distance d_A and d_X, namely PL$_A$ and PL$_X$, respectively. The harmonic mean of the path loss difference at deployed eNB locations d_A and d_X can be obtained by (3.13). The intersection point of the path loss of the antennas, d_i, can be described as the cell border. Therefore, based on the considered user-eNB/channel attachment, it can be said that users between d_A and d_i are connected to the eNB/channel located at point A and users located from d_i to d_X are connected to the eNB/channel located at point X. Then, the harmonic mean of the observed path loss of each considered user can be obtained by (3.14).

The antenna tilt optimization problem given in (3.11) is solved with fixed and propagation direction dependent path loss parameters. The idea is to investigate the robustness of the found optimum tilt angle to the different propagation parameters.

3.3.2 Effects of Path Loss Model Parameters

3.3.2.1 Fix Path Loss Parameters

For the fix path loss parameter case, the average of the path loss exponents and standard deviation of the large-scale signal fluctuations given in (3.9) are used. Accordingly, the path loss exponent and standard deviation are considered as $n = 2.1$ and $\sigma_L = 2.5$, respectively.

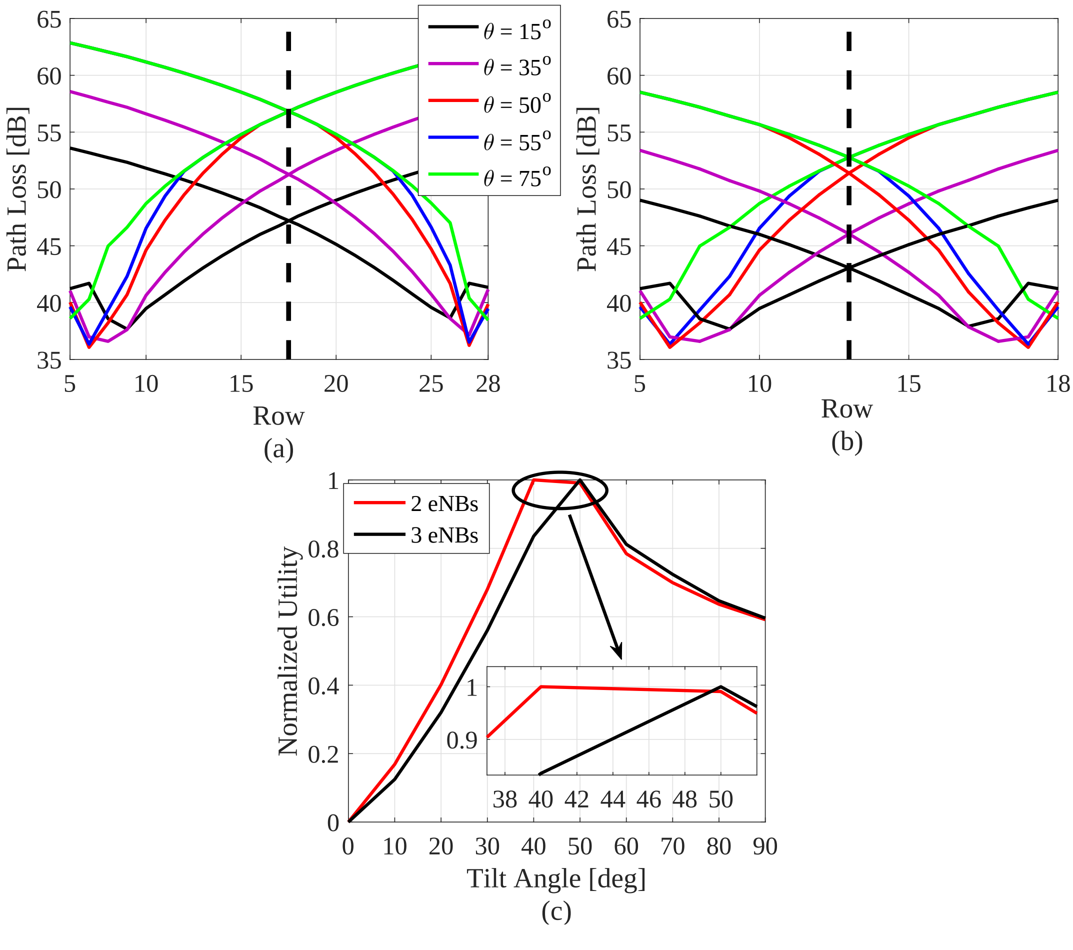

Figure 3.12: *Path loss of different antenna tilt angles. (a) 2 eNBs deployment. (b) 3 eNBs deployment. (c) Utility for different tilt angles.*

In Fig. 3.12(c), the normalized utility and the average path loss per row are shown for 2 eNBs and 3 eNBs deployments. The average path loss per row is obtained by averaging the path loss values seen for users in a row. Intuitively, when the antenna is oriented to its cell border, the path loss for the cell-edge users will be minimal. However, such antenna orientation will also cause the highest possible interference at its neighbour eNBs. As noted, the main purpose of using directional antennas to employ cell sectorization is to decrease the interference level at the neighbour eNBs. Based on Fig. 3.12(a) and Fig. 3.12(b), the maximum path loss at the cell border is 57 dB for 2 eNBs and 53 dB for 3 eNBs deployments when the antenna tilt angle is greater than $50°$. The reason for having 4 dB lower maximum path loss at the cell border for 3 eNBs is related to the distance from the antenna location to the cell border, as can be seen in Fig. 2.7. For the antenna tilt angles greater than $50°$, the lowest possible interference at the neighbour eNB is achieved.

Although the antenna tilt angles smaller than $50°$ achieved lower path loss for the cell-edge users, one of the antenna tilt angles greater than or equal to $50°$ will be the optimum tilt angle based on the main purpose of cell sectorization. When the Fig. 3.12(a) is considered, $50°$ can be seen as one of the optimum tilt angles for 2 eNBs deployment by means of minimizing the interference at the neighbour eNB and providing the possible minimum path loss[6]. For 3 eNBs deployment, as shown in Fig. 3.12(b), $50°$ tilt angle would be the optimum tilt angle. To propose a single tilt angle independent from the number of eNBs used in the system, $50°$ is chosen as the tilt angle for the sectorized in-cabin deployment.

3.3.2.2 Propagation Direction Dependent Path Loss Parameters

When the fixed path loss parameters are considered for different propagation directions, $50°$ is found as one of the optimum tilt angles that minimizes the interference level at the neighbour eNB and minimizes the path loss of the desired signal. In this section, the propagation direction dependent path loss parameters given in (3.9) are used. When the distance and antenna propagation direction dependent path loss model given in (3.9) is used, the $50°$ tilt angle is still one of the optimum tilt angles by means of minimizing the interference level at the neighbour eNB and minimizing the path loss of the desired signal, as shown in Fig. 3.13. However, for the considered realistic path loss model, considering the same tilt angle for all antennas does not provide an equal share of the number of users per cell. As can be seen from Fig. 3.13(a) and Fig. 3.13(b), the intersection of the path loss level of two antenna locations are shifted to the left of the cell border that equally shares the number of users. Therefore, it can be expected

[6]The interference level can be obtained by considering the level of the path loss of the neighbour eNB.

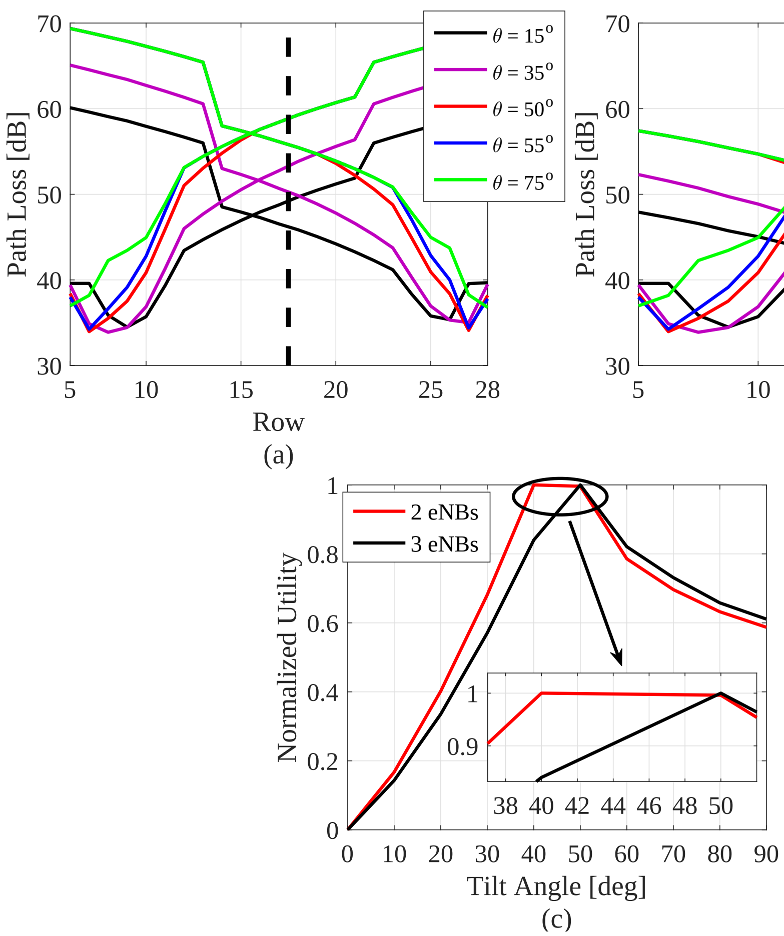

Figure 3.13: *Effects of path loss model parameters. (a) 2 eNBs deployment. (b) 3 eNBs deployment. (c) Utility for different tilt angles.*

that the number of users connected to the cell propagated to the in-rear direction is less than the cell propagated to the in-flight direction. The unequal distribution of the users per cell and its effects on the user throughput fairness will be considered in the resource scheduling problem in the next chapter.

3.4 Propagation Modelling Accuracy

In order to validate the modelled propagation characteristics inside the aircraft, a set of received power level measurements has been conducted. As noted, in LTE, reference signal received power (RSRP) and received signal strength indicator (RSSI) values are used to determine the signal-to-noise-plus-interference ratio (SINR) performance of a user. Therefore, the RSRP and RSSI measurements are taken inside the aircraft seat-by-seat. Then, the in-cabin propagation

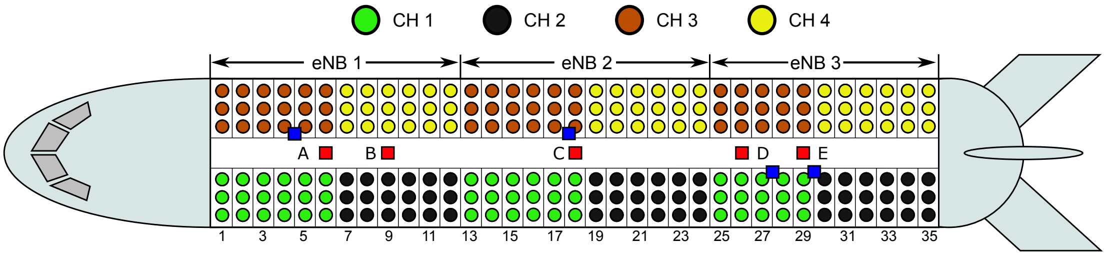

Figure 3.14: *Considered user-channel assignment for measurements.*

model is used to generate channel coefficients by computer simulations. The distribution of the measured and simulated RSRP and RSSI values are compared to understand the accuracy of the modelled propagation characteristics.

In the measurement, a pre-planned seat map shown in Fig. 3.14 is used to assign the users to specific eNB-channel pairs in order to track measurements. The 3 eNBs deployment in the provisioned antenna positions is considered where the antennas are tilted with a 50° angle to employ cell sectorization. The RSRP and RSSI values are measured using 6 QualiPoc Android handsets which have a special software that collects and reports the RF network parameters. The QualiPoc Android handsets were Samsung S5 model. During the measurements, 6 QualiPoc handsets are placed on the seats in a row with a cardboard box[7] in order to mimic a standing passenger holding a handset. Once the handsets are placed on the seats, they are forced to connect to the channels based on the pre-planned seat map given in Fig. 3.14. Then, the RSRP and RSSI values are measured for 30 seconds in each location.

Also, in the measurements, two different transmission power levels are considered. In order to have the similar power level on all available RBs in the 1800 MHz band, the transmission power of the 15 MHz channel is adjusted based on the power of the 20 MHz. Accordingly, when a 14 dBm transmission power is used for the channels with 20 MHz bandwidth, the transmission power of the 15 MHz channel is set to 12 dBm. The same is applied for the 8 dBm transmission power for 20 MHz channel where 6 dBm is used for the 15 MHz bandwidth.

As explained in Section 2.4.3, RSRP is the linear average of the reference signal (RS) within the used channel bandwidth. Therefore, in order to obtain the RSRP level of the simulated channel model, firstly, the transmission power is equally shared among all available RBs in the channel bandwidth. Then, the received power level is divided into the number of resource

[7]For illustration of the used cardboard box, please see Fig. 3.4(b).

elements (REs) in a RB, which is 84 as shown in Fig. 2.10, to find the received power of a RE. Afterwards, the RSRP value can be obtained by averaging the received power level of the cell-specific reference signal (CRS) REs in orthogonal frequency division multiplexing (OFDM) symbols 0 and 4. The same steps can be followed to determine the RSSI value where as noted, it is the averaged total power of the all REs in OFDM symbols 0 and 4. Accordingly, for the simulated channel model, RSSI values can be obtained by dividing the received power level of a RB to 7.

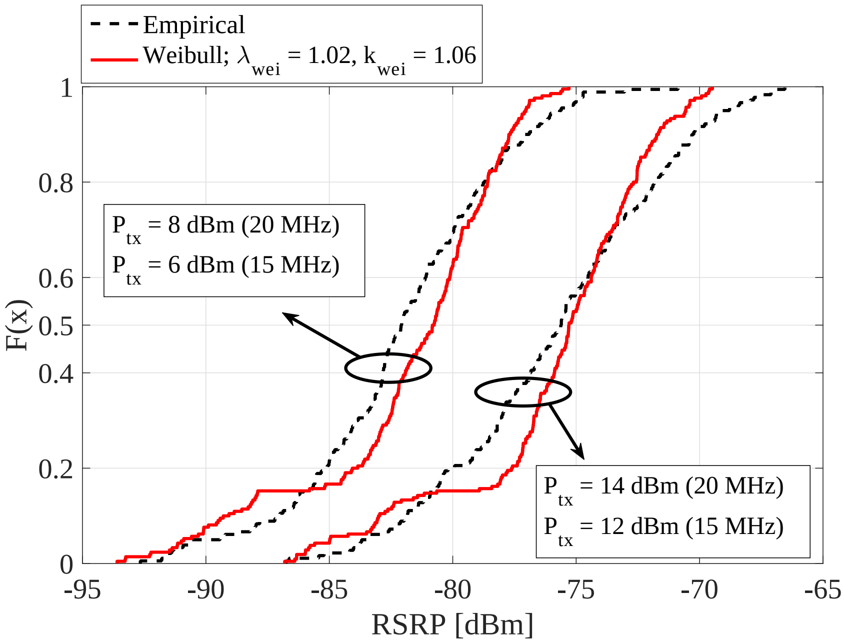

Figure 3.15: *Comparison of the measured and simulated RSRP distributions for different transmission power levels.*

The cumulative distribution function (CDF) of the measured and simulated values are given for RSRP in Fig. 3.15 and for RSSI in Fig. 3.16. As it can be seen from Fig. 3.15, for the considered transmission power levels, the cumulative distribution of the measured and modelled RSRP values are closely matched. The same observation can be seen for the CDF of the RSSI of the measured and simulated models. In order to understand the difference between the measured and simulated model, the Kolmogorov-Smirnov test is applied. In the Kolmogorov-Smirnov test, the output of two different CDFs for each sample value is compared. The maximum difference between the output of the CDFs can be found by (3.15) where $F(.)$ is the empirical CDF; $\mathrm{RSRP}_{\mathrm{measured}}$ and $\mathrm{RSRP}_{\mathrm{modelled}}$ are measured and modelled RSRP values, respectively. The maximum difference represents the result of the Kolmogorov-Smirnov test which determines how different the two distributions are. In Table 3.2, the results of the Kolmogorov-Smirnov test are given. According to the table, it can be said that the modelled in-cabin channel propagation characteristics are representative of the real-world measurements. The reason for having a relatively higher difference in RSSI than RSRP can be explained when the interference from the terrestrial network is considered during the measurements.

$$d_{\mathrm{K-S}} = \max\left(\left|F(\mathrm{RSRP}_{\mathrm{measured}}) - F(\mathrm{RSRP}_{\mathrm{modelled}})\right|\right) \tag{3.15}$$

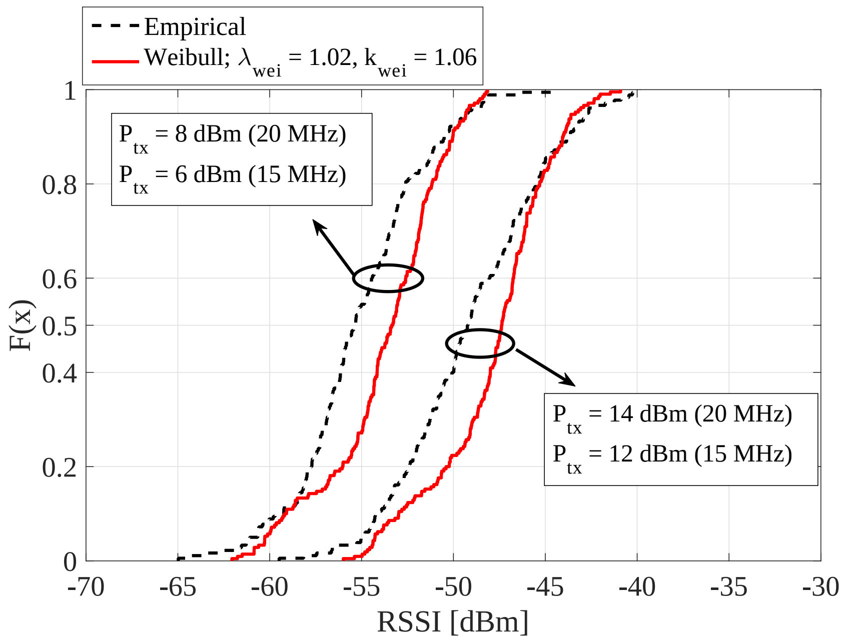

Figure 3.16: *Comparison of the measured and simulated RSSI distributions for different transmission power levels.*

	14 dBm (20 MHz) 12 dBm (15 MHz)		8 dBm (20 MHz) 6 dBm (15 MHz)	
	RSRP	RSSI	RSRP	RSSI
$d_{\mathrm{K-S}}$	0.158	0.258	0.154	0.273

Table 3.2: *Kolmogorov-Smirnov test results*

3.5 Summary

In this chapter, the channel propagation characteristics of an aircraft in-cabin environment are investigated based on the proposed measurement and modelling procedure conducted inside an Airbus A321 aircraft for 1.8 GHz frequency band. Based on the measurement results, it is shown that the path loss model has different path loss exponents according to the distance between transmitter and receiver, and the considered propagation direction. Also, it is shown that the frequency response characteristics inside the aircraft follow a Weibull distribution. The Weibull distribution parameters that fit with the measured power variations are obtained and an in-cabin channel propagation model is proposed. Based on the proposed channel model, a tilt angle, which minimizes the interference at a neighbour cell and provides the minimum path loss for its connected user for deployments of 2 eNBs and 3 eNBs, is obtained. It is shown that the found tilt angle is the same for the fixed and propagation direction dependent path loss parameters.

Furthermore, another set of measurements has been conducted to verify the RSRP and RSSI values generated by the proposed in-cabin channel model. Accordingly, the RSRP and RSSI values are measured inside the aircraft by a special handset that uses a software to collect and report RF network parameters. The distribution of the measured RSRP and RSSI values are compared with the ones generated by the proposed channel model. A Kolmogorov-Smirnov test is applied to the CDF of the measured and model values. It is shown that the RSRP and RSSI values generated by the proposed channel model closely match the measured values.

To sum up, this chapter verifies that the proposed measurement and modelling procedure can be considered for the in-cabin radio propagation characterization. Based on the given results, co-channel interference can be more realistically modelled for a multi-cell in-cabin communications system.

Chapter 4
In-Cabin LTE-A System Design

4.1 Introduction

In Long Term Evolution (LTE) and Long Term Evolution Advanced (LTE-A) systems, a resource allocation (RA) algorithm should comply with the specified channel quality indicator (CQI) reporting, modulation and coding scheme (MCS) assignment and RA types. However, in literature, most of the studies where RA/scheduling schemes are proposed assume that the transmitter has a CQI report for each resource block (RB) and/or assigns different MCS as well as power to each RB. For example, in [64], a multi-cell RA problem is considered to maximize the tradeoff between user data rate fairness and system throughput by using almost blank subframe (ABS) at the most interfering evolved nodeB (eNB). However, it is assumed that the CQI of each RB is known at the transmitter and individual MCS indexes are assigned to allocated RBs for a user. Using the same MCS index across the allocated RBs to a user is considered as a constraint in the multi-user scheduling problem in [65] for a single-cell, and in [66] for multi-cell deployments. However, the assumption of having a CQI report with RB granularity still exists in [65, 66], where in [66], allocating different power levels to RBs also exists. Besides that, in [67], different CQI reporting modes are considered. However, assigning different MCS indexes to the allocated RBs to a user is assumed. In addition, any of the LTE RA types are not considered in the noted studies [64–67]. In [68], although LTE RA Type 0 and subband CQI feedback mode are considered, the single MCS index constraint per user is not taken into account.

Consequently, practical LTE system constraints such as the common MCS index assignment to all allocated RBs for a user, the CQI reporting modes and the RA types are not combined and considered in a single scheduling optimization problem. In this research, the user data rate fairness, which is defined as the lowest variation in user data rates across a large user population, to system throughput tradeoff is investigated for a multi-cell multi-user in-cabin communication system inside the Airbus A321 aircraft. A proportional fair (PF) based downlink coordinated scheduler is proposed. The goal of the proposed scheduler is to improve the user rate fairness to system throughput tradeoff with a given quality of service (QoS) target by using enhanced inter-cell interference coordination (eICIC) techniques, namely ABS and reduced power-ABS (RP-ABS), and/or carrier aggregation (CA) under practical system constraints. It is shown that such a scheduling problem is a NP-hard [69] problem. In particular, the proposed solutions given in [64] and [65] are adapted to approximate and solve the considered NP-hard problem as a linear programming problem. It is assumed that users report their CQI based on higher layer configured subband reporting, Mode 3-0. The scheduler allocates RBs based on RA Type 0 and assigns single MCS index to the allocated RBs.

The remainder of this chapter is arranged as follows. In Section 4.2, the resource scheduling problem, which takes into account the LTE system constraints, is described. The considered scheduling policies, which include the proposed scheduler, are introduced in Section 4.3. The downlink performance of the in-cabin LTE-A network with various schedulers, interference management techniques and system parameters is evaluated in Section 4.4. A recommended system decision diagram for a given QoS metric is provided in Section 4.5. Finally, this chapter is summarised in Section 4.6.

4.2 Resource Scheduling Problem

In orthogonal frequency division multiple access (OFDMA), users communicate via orthogonal RBs so that downlink intra-cell interference is completely avoided. However, inter-cell interference can be potentially experienced by users due to spectrum reuse in the nearby cells in a multi-cell deployment. Thus, when the full transmission power is used by every cell, which is referred to normal subframes (NSF) transmission, the signal-to-noise-plus-interference ratio (SINR) of a user $u \in \mathcal{U}^{(c)} \triangleq \{1, \dots, U^{(c)}\}$ in a cell $c \in \mathcal{C} \triangleq \{1, \dots, C\}$ on a RB $r \in \mathcal{R} \triangleq \{1, \dots, R^c\}$ in the downlink transmission direction, $\gamma_{u,r}^c$, is:

$$\gamma_{u,r}^c = \frac{P_r^c H_{u,r}^c}{\sum\limits_{\hat{c}=1, \hat{c} \neq c}^{C} P_r^{\hat{c}} H_{u,r}^{\hat{c}} + N_r}, \tag{4.1}$$

where P_r^c is the transmitted power of cell c on RB r; $H_{u,r}^c$ represents the channel gain, which includes fading components, path loss and antenna gain, from cell c to user u on RB r; and N_r is the noise power on RB r. The channel gain $H_{u,r}^c$ is obtained by (3.10) where the cell index c and the user index u can be used to obtain the distance d in (4.1). The noise power N_r is computed by utilizing the well known thermal noise power equation $N_r = kTB_r$, where k is Boltzmann's constant; T is the temperature in Kelvin; and B_r is the bandwidth of a RB.

In this study, higher layer configured subband CQI reporting, which is called CQI feedback in Mode 3-0 [5], is considered. Accordingly, a user reports one CQI value for each subband set $s \in \mathcal{S} \triangleq \{1, \ldots, S\}$, where the size of each set is 8 RBs. In addition to that, RA Type 0 is considered in this study. In Type 0, contiguous RBs are grouped to form a RB group (RBG) $g \in \mathcal{G}^{(c)} \triangleq \{1, \ldots, G^{(c)}\}$, where the size of a RBG is given in Table 2.8.

In order to satisfy the block error ratio (BLER) condition, which is 10% in LTE [70, 71], an effective SINR value of a RB, $\Gamma^c_{u,r}$, is determined by an effective SINR mapping function, f_{eff}, as given in (4.2).

$$\Gamma^c_{u,r} = f_{\text{eff}}\left(\gamma^c_{u,r}\right), \tag{4.2}$$

Then, the effective SINR of a RBG, $\Gamma^c_{u,g}$, is obtained by $f_{\text{CQI,RA}}$ in (4.3), which determines the effective SINR of subbands and maps them to RBGs.

$$\Gamma^c_{u,g} = f_{\text{CQI,RA}}\left(\Gamma^c_{u,r}\right). \tag{4.3}$$

In LTE, data rate calculation is based on the number of allocated RBs, CQI, MCS and transport block size (TBS) indexes [5]. According to LTE standards, once the CQI report of a user is received at the eNB, it is mapped to a MCS index and then mapped to a TBS index based on [5, Tables 7.1.7.1-1, 7.1.7.2.1-1 and 7.2.3-1]. In [5, Table 7.1.7.2.1-1], TBS is determined according to its index mapped from the MCS index and number of allocated RBs. The TBS represents the number of bits that can be transmitted per transmission time interval (TTI). Although mapping the CQI index to achievable spectral efficiency and mapping the MCS index to TBS index are defined in LTE, there is no specific mapping between the CQI index to MCS index. It is considered as vendor/operator specific. In this research, achievable rates are determined based on the reported SINR values and corresponding MCS indexes of the RBGs by using an adaptive modulation and coding (AMC) function f_{AMC}. Accordingly, the reported SINR, $\Gamma^c_{u,g}$, the achievable rate, $\xi^c_{u,g}$, and the MCS index, $Q^c_{u,g}$, on a RBG g for a user u in a cell c are given by

$$\left(\xi^c_{u,g}, Q^c_{u,g}\right) = f_{\text{AMC}}\left(\Gamma^c_{u,g}\right). \tag{4.4}$$

CQI Index	Γ [dB]	MCS Index	f_{AMC}	
			$M_{f_{\text{AMC}}}$	k_j
0	-	-	-	0
1	-6	0	QPSK	0.1523
2	-5	1		0.2344
3	-3	3		0.3770
4	-1	5		0.6016
5	1	7		0.8770
6	3	9		1.1758
7	5	12	16QAM	1.4766
8	8	14		1.9141
9	9	16		2.4063
10	11	19	64QAM	2.7305
11	12	22		3.3223
12	14	24		3.9023
13	16	26		4.5234
14	18	28		5.1152
15	20	28		5.5547

Table 4.1: *Modulation order and spectral efficiency in bits/symbol for NSF based on [5, Tables 7.1.7.1-1 and 7.2.3-1]*

The considered AMC function f_{AMC}, which maps the CQI index, SINR Γ, MCS index, modulation order $M_{f_{\text{AMC}}}$ and spectral efficiency k_j, is given in Table 4.1. Once the MCS index of a RBG and its corresponding spectral efficiency k_j is determined, the achievable rate for user u on RBG g at cell c is obtained as follows:

$$Q^c_{u,g} = j^*, \tag{4.5}$$

$$\xi^c_{u,g} = k_{j^*} C^{\text{RB}}_{\text{RE}}, \tag{4.6}$$

where j^* is the chosen MCS index; and $C^{\text{RB}}_{\text{RE}}$ is the constant that represents the number of physical downlink shared channel (PDSCH) subcarriers per RB in a subframe. $C^{\text{RB}}_{\text{RE}}$ depends on the considered control format indicator (CFI) [72]. The CFI can be 1, 2 or 3 and it represents the number of symbols that are going to be used for the physical downlink control channel (PDCCH)[1]. Therefore, the subcarriers in the PDCCH symbols are not considered as PDSCH subcarriers and they are neglected in the user data rate calculation. In this study, CFI

[1]Based on [72], when the number of RBs of a channel is less than 10, CFI should be 2 or 3. However, for the channel that has more than 10 RBs, CFI can be set to 1, 2 or 3.

is considered as 1. Accordingly, the number of PDSCH subcarriers can be obtained as follows:

$$C_{\mathrm{RE}}^{\mathrm{RB}} = \frac{N_{\mathrm{RE}}^{\mathrm{symbol}} \left(N_{\mathrm{symbol}}^{\mathrm{subframe}} - N_{\mathrm{symbol}}^{\mathrm{PDCCH}} \right) - N_{\mathrm{CRS,RE}}^{\mathrm{PDSCH}}}{2T_{\mathrm{slot}}}, \tag{4.7}$$

where $N_{\mathrm{RE}}^{\mathrm{symbol}}$ is the number of resource elements (REs) in a symbol; $N_{\mathrm{symbol}}^{\mathrm{subframe}}$ is the number of symbols in a subframe; $N_{\mathrm{symbol}}^{\mathrm{PDCCH}}$ is the number of the symbols that are used for PDCCH based on the considered CFI; $N_{\mathrm{CRS,RE}}^{\mathrm{PDSCH}}$ is the number of cell-specific reference signal (CRS) REs except that are used in PDCCH[2] and T_{slot} is the slot duration. According to the parameter values given in Table 4.2, the $C_{\mathrm{RE}}^{\mathrm{RB}}$ is equal to 150000.

$N_{\mathrm{RE}}^{\mathrm{symbol}}$	$N_{\mathrm{symbol}}^{\mathrm{subframe}}$	$N_{\mathrm{symbol}}^{\mathrm{PDCCH}}$	$N_{\mathrm{CRS,RE}}^{\mathrm{PDSCH}}$	T_{slot}
12	14	1	6	0.5 ms

Table 4.2: *Parameters to obtain* $C_{\mathrm{RE}}^{\mathrm{RB}}$

Fig. 4.1 shows the data rate performance of the MCS-TBS index mapping used in [5] and the described CQI-MCS based AMC function, f_{AMC}, given in Table 4.1. It is shown that the performance of the described CQI-MCS based data rate calculation is representative of what is achieved in LTE standards using the MCS-TBS index mapping. The only exception to this is the maximum index used in the MCS-TBS index mapping where its performance is in between CQI indexes 14 and 15. Thus, the same MCS index is used for CQI indexes 14 and 15 in Table 4.1.

4.2.1 Scheduling with NSF

Most of the existing studies assume that the CQI is known for each RB and RBs are assigned to users with different MCS indexes. However, in practice, due to the defined CQI reporting schemes, there may be different CQI values for the available RBGs for the users. Therefore, the CQI reporting scheme, common MCS assignment for all RBs allocated for a user and RA types should be considered in a scheduling optimization problem. As noted, common MCS assignment for all allocated RBs to a user in the scheduling problem under the assumption of having the CQI report with RB granularity is considered in [65]. In this study, the proposed solution in [65] is adopted to consider not only the common MCS assignment but also LTE CQI

[2]As shown in Fig. 2.10, there are 4 CRS REs in a slot and 8 in a subframe. However, 2 of them are inside the PDCCH for the considered CFI configuration and they are already neglected in (4.7).

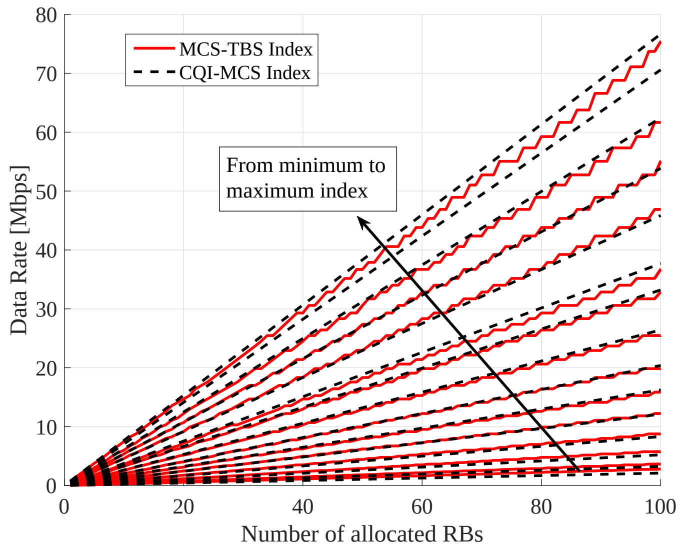

Figure 4.1: *Achievable rate comparison for the specified MCS-TBS mapping and the considered AMC function that maps CQI-MCS.*

reporting, and RA schemes in the scheduling problem.

The scheduling problem for NSF under the LTE constraints can be written as in (4.8) where $x^c_{u,g}$ is a binary decision variable that is equal to 1 if user u in cell c uses the RBG g; $b^c_{u,j}$ is a binary decision variable that is equal to 1 if user u in cell c uses the MCS index j; k_j represents spectral efficiency of the MCS index j based on Table 4.1; K_g represents the number of RBs in a RBG g; and w^c_u is the scheduling metric of user u in cell c, which is described in Section 4.3. Constraint (4.8b) ensures that the RBG g is assigned to a single user; constraint (4.8c) ensures that a common MCS index is used for all the allocated RBGs to user u. In (4.8c), Q^c_{u*} represents the maximum MCS index among all RBGs for user u.

$$\underset{x^c_{u,g}, b^c_{u,j}}{\text{maximize}} \quad \sum_{u=1}^{U^{(c)}} \sum_{g \in \mathcal{G}^{(c)}} w^c_u x^c_{u,g} K_g \sum_{j=1}^{Q^c_{u,g}} b^c_{u,j} k_j C^{\text{RB}}_{\text{RE}} \tag{4.8a}$$

$$\text{subject to} \quad \sum_{u=1}^{U^{(c)}} x^c_{u,g} = 1, \tag{4.8b}$$

$$\sum_{j=1}^{Q^c_{u*}} b^c_{u,j} = 1, \qquad \forall c, u, \tag{4.8c}$$

$$x^c_{u,g}, b^c_{u,j} \in \{0, 1\}, \quad \forall c, u, g, j. \tag{4.8d}$$

Due to the multiplication of two binary decision variables, the given scheduling problem (4.8) is a nonlinear optimization problem. Therefore, an auxiliary variable $t_{u,g,j}^{c} = x_{u,g}^{c} b_{u,j}^{c}$ is considered to transform (4.8) to a linear problem [65] as follows:

$$\underset{x_{u,g}^{c}, b_{u,j}^{c}, t_{u,g,j}^{c}}{\text{maximize}} \quad \sum_{u=1}^{U^{(c)}} \sum_{g \in \mathcal{G}^{(c)}} \sum_{j=1}^{Q_{u,g}^{c}} w_u^c K_g t_{u,g,j}^{c} k_j C_{\text{RE}}^{\text{RB}} \tag{4.9}$$

subject to (4.8b), (4.8c), (4.8d) and

$$t_{u,g,j}^{c} \leq b_{u,j}^{c}, \tag{4.10a}$$

$$t_{u,g,j}^{c} \leq x_{u,g}^{c} V, \tag{4.10b}$$

$$t_{u,g,j}^{c} \geq b_{u,j}^{c} - \left(1 - x_{u,g}^{c}\right) V, \tag{4.10c}$$

where V is a large positive real valued constant. As noted in [65], the transformed problem (4.9) can be solved by integer linear programming tools.

4.2.2 Scheduling with eICIC Techniques

In light of the higher layer configured subband CQI reporting scheme, common MCS assignment and RA Type 0, the multi-cell multi-user scheduling problem with ABS is given in this section. Before stating the scheduling problem, some modifications in the SINR calculation given in (4.1) and in the achievable rate determination given in (4.4) are needed to take into account the use of ABS in the system.

The SINR expression given in (4.1) represents the full transmission power being used by every cell. This is referred to as NSF transmission. However, when ABS (or RP-ABS) is used on a specific subframe, some of the cells use zero (or reduced) transmission power. Assume that cell c is the cell with full transmission power and cell $\acute{c}$ is the most dominant interfering cell to cell c. Accordingly, cell $\acute{c}$ is chosen to transmit with zero or reduced transmission power in the specific subframe. Thus, due to the differences in transmission power, the SINR level for all the users will change. The SINR expression for RB r for user u in cell c, $\tilde{\gamma}_{u,r}^{c}$, and user $\acute{u}$ in cell

$\acute{c}$, $\tilde{\gamma}_{\acute{u},r}^{\acute{c}}$ during the blanked or reduced power subframe can be written as follows, respectively:

$$\tilde{\gamma}_{u,r}^{c} = \frac{P_r^c H_{u,r}^c}{\sum\limits_{\hat{c}=1, \hat{c}\neq c}^{C} P_r^{\hat{c}} H_{u,r}^{\hat{c}} - \left(1 - p_{\text{offset}}^{\acute{c}}\right) P_r^{\acute{c}} H_{u,r}^{\acute{c}} + N_r}, \tag{4.11}$$

$$\tilde{\gamma}_{\acute{u},r}^{\acute{c}} = \frac{p_{\text{offset}}^{\acute{c}} P_r^{\acute{c}} H_{\acute{u},r}^{\acute{c}}}{\sum\limits_{\hat{c}=1, \hat{c}\neq \acute{c}}^{C} P_r^{\hat{c}} H_{\acute{u},r}^{\hat{c}} + N_r}, \tag{4.12}$$

where $p_{\text{offset}}^{\acute{c}}$ is the used power offset in the cell $\acute{c}$ in ABS (or RP-ABS) subframe. The $p_{\text{offset}}^{\acute{c}}$ is zero when ABS is considered, and is $10^{-p/10}$ where p is the level of reduction in transmission power for RP-ABS in dB. Thus, the term $\left(1 - p_{\text{offset}}^{\acute{c}}\right)$ is used to neglect the blanked cell or to consider the interference level of the cell with reduced transmission power when ABS or RP-ABS is considered in the system, respectively.

In LTE, the level of reduction in transmission power for RP-ABS is limited to 0 dB, 3 dB and 6 dB ($p \in \{0, 3, 6\}$) [28]. In order to conserve the modulation accuracy determined by error vector magnitude (EVM) in LTE, the used modulation order is limited to the quadrature phase shift keying (QPSK), 16-quadrature amplitude modulation (QAM) and 64-QAM, for 6 dB, 3 dB and 0 dB power reduction levels, respectively [28, 47]. However, it is also stated in [28] that power reduction can be considered as a vendor specific parameter.

In this research, the above noted power reduction levels and modulation order limits are considered. Thus, the supported modulation order of AMC $M_{f_{\text{AMC}}}$ should be modified for a RP-ABS subframe as $M_{f_{\text{AMC}}^p}$ based on the used power reduction level p as given in (4.13). In the case of using 0 dB power reduction, $M_{f_{\text{AMC}}^{p=0}}$ is equal to $M_{f_{\text{AMC}}}$.

$$M_{f_{\text{AMC}}^p} \in \begin{cases} \{\text{QPSK}, \text{16-QAM}\}, & p = 3 \quad \text{dB} \\ \{\text{QPSK}\}, & p = 6 \quad \text{dB}, \end{cases} \tag{4.13}$$

According to the updated SINR values for the specific subframe, the input of functions given in (4.2) and (4.3) will be different for the users u and $\acute{u}$. Also, due to modulation order limitation during RP-ABS, the achievable rate and MCS index of the users u and $\acute{u}$ will be obtained by different AMC functions. Accordingly, the CQI value, reported SINR, achievable rate and MCS index of a RBG are rewritten for the user u with normal AMC function f_{AMC} and for the user $\acute{u}$ with power reduction level based limited AMC function $\tilde{f}_{\mathrm{AMC}}(\Gamma, p)$ as given in (4.14)[3].

$$
\begin{aligned}
\tilde{\Gamma}^{c}_{u,r} &= f_{\mathrm{eff}}\left(\tilde{\gamma}^{c}_{u,r}\right), && (4.14a)\\
\tilde{\Gamma}^{\acute{c}}_{\acute{u},r} &= f_{\mathrm{eff}}\left(\tilde{\gamma}^{\acute{c}}_{\acute{u},r}\right), && (4.14b)\\
\tilde{\Gamma}^{c}_{u,g} &= f_{\mathrm{CQI,RA}}\left(\tilde{\Gamma}^{c}_{u,r}\right), && (4.14c)\\
\tilde{\Gamma}^{\acute{c}}_{\acute{u},g} &= f_{\mathrm{CQI,RA}}\left(\tilde{\Gamma}^{\acute{c}}_{\acute{u},r}\right), && (4.14d)\\
\left(\tilde{\xi}^{c}_{u,g}, \tilde{Q}^{c}_{u,g}\right) &= f_{\mathrm{AMC}}\left(\tilde{\Gamma}^{c}_{u,g}\right), && (4.14e)\\
\left(\tilde{\xi}^{\acute{c}}_{\acute{u},g}, \tilde{Q}^{\acute{c}}_{\acute{u},g}\right) &= \tilde{f}_{\mathrm{AMC}}\left(\tilde{\Gamma}^{\acute{c}}_{\acute{u},g}, p\right). && (4.14f)
\end{aligned}
$$

<table>
<tr><th rowspan="3">CQI Index</th><th rowspan="3">Γ [dB]</th><th rowspan="3">MCS Index</th><th colspan="6">$\tilde{f}_{\mathrm{AMC}}$</th></tr>
<tr><th colspan="2">$p = 0$ [dB]</th><th colspan="2">$p = 3$ [dB]</th><th colspan="2">$p = 6$ [dB]</th></tr>
<tr><th>$M_{f^{p}_{\mathrm{AMC}}}$</th><th>k_j</th><th>$M_{f^{p}_{\mathrm{AMC}}}$</th><th>k_j</th><th>$M_{f^{p}_{\mathrm{AMC}}}$</th><th>k_j</th></tr>
<tr><td>0</td><td>-</td><td>-</td><td>-</td><td>0</td><td>-</td><td>0</td><td>-</td><td>0</td></tr>
<tr><td>1</td><td>-6</td><td>0</td><td rowspan="6">QPSK</td><td>0.1523</td><td rowspan="6">QPSK</td><td>0.1523</td><td rowspan="15">QPSK</td><td>0.1523</td></tr>
<tr><td>2</td><td>-5</td><td>1</td><td>0.2344</td><td>0.2344</td><td>0.2344</td></tr>
<tr><td>3</td><td>-3</td><td>3</td><td>0.3770</td><td>0.3770</td><td>0.3770</td></tr>
<tr><td>4</td><td>-1</td><td>5</td><td>0.6016</td><td>0.6016</td><td>0.6016</td></tr>
<tr><td>5</td><td>1</td><td>7</td><td>0.8770</td><td>0.8770</td><td>0.8770</td></tr>
<tr><td>6</td><td>3</td><td>9</td><td>1.1758</td><td>1.1758</td><td rowspan="10">1.1758</td></tr>
<tr><td>7</td><td>5</td><td>12</td><td rowspan="3">16QAM</td><td>1.4766</td><td rowspan="9">16QAM</td><td>1.4766</td></tr>
<tr><td>8</td><td>8</td><td>14</td><td>1.9141</td><td>1.9141</td></tr>
<tr><td>9</td><td>9</td><td>16</td><td>2.4063</td><td rowspan="7">2.4063</td></tr>
<tr><td>10</td><td>11</td><td>19</td><td rowspan="6">64QAM</td><td>2.7305</td></tr>
<tr><td>11</td><td>12</td><td>22</td><td>3.3223</td></tr>
<tr><td>12</td><td>14</td><td>24</td><td>3.9023</td></tr>
<tr><td>13</td><td>16</td><td>26</td><td>4.5234</td></tr>
<tr><td>14</td><td>18</td><td>28</td><td>5.1152</td></tr>
<tr><td>15</td><td>20</td><td>28</td><td>5.5547</td></tr>
</table>

Table 4.3: *Modulation order and spectral efficiency in bits/symbol for normal and RP-ABS subframes based on [5, Tables 7.1.7.1-1 and 7.2.3-1]*

As given in Table 4.1, in the AMC function f_{AMC}, the MCS index j represents different achievable spectral efficiency k_j based on the reported effective SINR values. However, this is not the case for the AMC function $\tilde{f}_{\mathrm{AMC}}(\Gamma, p)$ due to limitations on the supported modulation order $M_{f^{p}_{\mathrm{AMC}}}$. The MCS indexes that have a modulation order smaller or equal to the limited

[3]The parameters used in NSF transmission are updated and given with $(\tilde{\cdot})$ in (4.14) when RP-ABS is considered.

modulation order $M_{f^p_{\mathrm{AMC}}}$ have different achievable spectral efficiencies. Although the reported effective SINR may support more than the limited modulation order, the achievable spectral efficiency will be fixed to k_{j_p}, where j_p is the MCS index that represents the index of the limited modulation order with the highest efficiency as shown in Table 4.3. For example, when the level of reduction in transmission power is set to 6 dB, $p = 6$, the MCS index $j \leq 6$ has different achievable spectral efficiencies and the MCS index $j > 6$ will have the efficiency of index $j_p = 6$.

4.2.2.1 Cell Indexing

The optimization problem given in (4.9) is used to allocate RBGs to users with a single MCS index. When eICIC techniques ABS and RP-ABS are employed in the system, there is a need to decide on which cell(s) should be blanked or used at a reduced transmission power level during the specific subframe. To this end, the level of additional rate that can be gained by reducing the transmission power of a cell $\acute{c}$ should be taken into account. The additional rate is equal to the difference between the rate per RBG with NSF, $\xi^c_{u,g}$, and the rate in the reduced power subframe, $\tilde{\xi}^c_{u,g}$. Obtaining the additional rate by reducing the transmission power of an interfering cell with the common MCS assignment constraint will make the problem more difficult. Therefore, firstly, the interfering cells are indexed without taking into account the common MCS assignment constraint. Then, RBG allocation is carried out using (4.9) for all active cells.

Accordingly, the interfering cell indexing problem can be written according to [64] as follows:

$$\underset{x^c_{u,g}, I^c}{\text{maximize}} \quad \sum_{c=1}^{C} \sum_{u=1}^{U^{(c)}} w^c_u x^c_{u,g} K_g \left(\xi^c_{u,g} + \max_{\acute{c}} I^{\acute{c}} \left(\tilde{\xi}^c_{u,g} - \xi^c_{u,g} \right) \right) \tag{4.15a}$$

$$\text{subject to} \quad \sum_{u=1}^{U^{(c)}} x^c_{u,g} = 1 - I^c, \qquad \forall c, \tag{4.15b}$$

$$x^c_{u,g}, I^c \in \{0, 1\}, \qquad \forall u, \tag{4.15c}$$

where I^c is the binary decision variable to indicate that cell c is blanked (or forced to use RP-ABS), $I^c = 1$, or not, $I^c = 0$. It is important to note that the RA decision variable $x^c_{u,g}$ in (4.15) does not represent the actual RA. As noted, the actual RA will be done using (4.9) when the interfering cells are indexed. The reason for using $x^c_{u,g}$ in the interfering cell indexing problem is to ensure that a RBG can only be assigned to a user in cell c as long as cell c is not blanked, as given in (4.15b). Also, in [64], the blanking decision is taken based on a RB level. However, in practice, if the ABS or RP-ABS decision is taken for a subframe, the interfering cell should set its transmission power for all RBs.

It is also important to note the given problem in (4.15) is for a dominant interference environment where only the most interfering cell is chosen to be blanked. When the employed cell sectorization for the described multi-cell in-cabin system is considered, there is only one dominant interfering cell in the system independent from the number of deployed eNBs. Therefore, the term $\max_{\acute{c}} I^{\acute{c}}\left(\tilde{\xi}^{c}_{u,g} - \xi^{c}_{u,g}\right)$ in (4.15a) is representative of a single blanked cell and does not allow combination of different cells, which are operating at the same frequency band, to be blanked. Blanking cells irrespective of their interference dominance will degrade the total system throughput due to wasting the available resource in the less interfering cells.

The expression $\left(\tilde{\xi}^{c}_{u,g} - \xi^{c}_{u,g}\right)$ in (4.15a) presents how much additional rate will be gained on RBG g for user u at cell c by reducing the transmission power of the interfering cell $\acute{c}$. Due to point-wise maximum operation and multiplication in the term $x^{c}_{u,g}\max_{\acute{c}} I^{\acute{c}}\left(\tilde{\xi}^{c}_{u,g} - \xi^{c}_{u,g}\right)$, the given problem is a binary non-linear optimization problem. It can be converted to a binary linear optimization problem by introducing an auxiliary variable $y^{c,\acute{c}}_{u,g}$ [64] as follows:

$$x^{c}_{u,g}\max_{\acute{c}} I^{\acute{c}}\left(\tilde{\xi}^{c}_{u,g} - \xi^{c}_{u,g}\right) = \max \sum_{\acute{c}} y^{c,\acute{c}}_{u,g}\left(\tilde{\xi}^{c}_{u,g} - \xi^{c}_{u,g}\right), \tag{4.16}$$

where $y^{c,\acute{c}}_{u,g}$ is defined as follows:

$$\sum_{\acute{c}} y^{c,\acute{c}}_{u,g} \leq x^{c}_{u,g}, \quad \forall u, g, \tag{4.17a}$$

$$\sum_{U^{\acute{c}}} y^{c,\acute{c}}_{u,g} \leq I^{\acute{c}}, \quad \forall c, \acute{c}, \tag{4.17b}$$

$$y^{c,\acute{c}}_{u,g} \in \{0, 1\}, \quad \forall c, \acute{c}, u. \tag{4.17c}$$

Accordingly, the problem in (4.15) can be written in linear form as follows:

$$
\begin{aligned}
\underset{x_{u,g}^{c}, y_{u,g}^{c,\acute{c}}, I^{c}}{\text{maximize}} \quad & \sum_{c=1}^{C} \sum_{u=1}^{U^{(c)}} w_u^c \left(x_{u,g}^c \xi_{u,g}^c + \sum_{\acute{c}} y_{u,g}^{c,\acute{c}} \left(\tilde{\xi}_{u,g}^c - \xi_{u,g}^c \right) \right) && \text{(4.18a)} \\
\text{subject to} \quad & \sum_{u=1}^{U^{(c)}} x_{u,g}^c = 1 - I^c, \qquad \forall c, && \text{(4.18b)} \\
& \sum_{\acute{c}} y_{u,g}^{c,\acute{c}} \leq x_{u,g}^c, && \text{(4.18c)} \\
& \sum_{u=1}^{U^{(c)}} y_{u,g}^{c,\acute{c}} \leq I^{\acute{c}}, && \text{(4.18d)} \\
& x_{u,g}^c, y_{u,g}^{c,\acute{c}}, I^c \in \{0,1\}, \quad \forall c, \acute{c}, u. && \text{(4.18e)}
\end{aligned}
$$

The binary linear optimization problem given in (4.18) can be solved by relaxing the constraint given in (4.18e) to non-integer values in $[0, 1]$. When the solution of the relaxed problem is rounded to the closest binary feasible solution, it becomes a near-optimal solution of (4.15) [64].

4.2.2.2 Scheduling for eICIC

Once the cells are indexed, LTE constraint based RBG allocation can be carried out by modifying (4.9) and the constraint given in (4.8c). For the cells that use full transmission power ($I^c = 0$), the MCS index of a RBG will be updated with $\tilde{Q}_{u,g}^c$ in (4.9) and the maximum MCS index among RBGs for user u will be changed to $\tilde{Q}_{u^*}^c$ in (4.8c).

Inherently, if ABS is used in the indexed cells ($I^c = 1$), there will be no allocation. However, if RP-ABS is used, the indexed cells do transmission with the constrained AMC function given in (4.14f) and Table 4.3. Accordingly, the MCS index of a RBG will be updated with $\tilde{Q}_{\acute{u},g}^{\acute{c}}$ in (4.9) and the maximum MCS index among RBGs for user u will be changed to $\tilde{Q}_{\acute{u^*}}^{\acute{c}}$ in (4.8c) to allocate RBGs to users during the RP-ABS subframe.

4.2.3 Carrier Aggregation

As noted, in LTE, CA is adopted to achieve wider deployment bandwidths by aggregating carrier components (CCs). Based on [36], the maximum aggregated bandwidth can be 40 MHz for the LTE 1800 MHz, irrespective of the contiguous or non-contiguous aggregation type.

Lemma 1. *In each eNB, aggregating the CCs that are pointed in opposite directions would improve the fair distribution of resources in the system.*

Proof. According to the employed cell sectorization, each eNB has two channels pointed towards the cockpit of the aircraft and two channels pointed towards the tail of the aircraft. Also, it is noted that the maximum received signal power based user-channel association is considered in this study. Therefore, due to the provisioned antenna mounting locations and different propagation characteristics based on antenna direction, this type of user-channel association causes uneven user-channel bandwidth distribution, which leads to an unfair user data rate performance, please see Fig. 3.13[4]. Lets α^* be the user-resource ratio, which is obtained as

$$\alpha^* = \frac{\sum_{c=1}^{C} U^c}{\sum_{c=1}^{C} R^c}, \tag{4.19}$$

where R^c is the number of RBs in the considered channel as given in Table 2.5. The numerator represents the total number of users in the system and the denominator is the total number of RBs in the system. For an even user-channel bandwidth distribution, the ideal number of users per channel, U^{c^*}, can be determined based on the channel bandwidth as

$$U^{c^*} = \lceil \alpha^* \times R^c \rceil, \tag{4.20}$$

where $\lceil x \rceil$ is the ceiling function which maps the smallest integer greater than or equal to x. Accordingly, U^{c^*} is 19 for a 20 MHz channel and 14 for a 15 MHz channel for the 3 eNBs deployment. Fig. 4.2 shows the ideal number of users and user distribution per channel when the eNB antennas are mounted on the provisioned positions shown in Fig. 2.7. The maximum received power based user-channel association is considered and the received power is averaged over 1000 realizations. Due to the channel characteristics inside the aircraft and the mounting location of the first eNB, there is a significant gap between the number of connected users at the channels pointed to the cockpit of the aircraft. Inherently, there will be a significant difference in the distribution of resources, hence, there will also be a significant difference in the achieved

[4] In Fig. 3.13(a) and (b), the dashed line represents a virtual cell border where each cell has an equal number of users. However, when the antenna direction based propagation characteristics are taken into account, the actual cell border, which is the intersection point of the propagation of different cells, is observed at a few rows left of the virtual cell border. This means that the number of users connected to the cell on the left will be less than the one on the right.

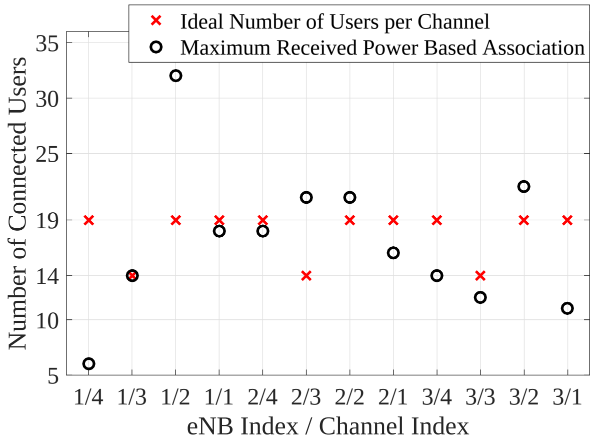

Figure 4.2: *Number of users per channel distribution.*

data rate performance of these channels. At one side, the 20 MHz bandwidth is used to serve around 6 users and on the other side, there are approximately 30 users which will be served by the same amount of bandwidth. However, when the channels that are pointed in opposite directions are aggregated, the total number of connected users per aggregated channel become close to each other. Therefore, an ideal number of users per channel bandwidth distribution will be achieved. $\square$

Accordingly, the channels with indexes 4 and 2 are aggregated to compose a 40 MHz bandwidth in one hand, and on the other hand, the channels with indexes 3 and 1 are aggregated to compose a 35 MHz bandwidth. The given aggregation is the intra-band non-contiguous CA. The cell that a user is connected to based on its received signal strength is considered as the primary cell and the cell that aggregated with the connected cell is considered as the secondary cell. The users sent their CQI reports for both the primary and secondary cells. In the described CA, the aggregated CCs are in the same eNB. Thus, the scheduling decision is taken centrally for the two aggregated CCs. Accordingly, when there is no eICIC techniques employed, for an aggregated channel $c_n \in \mathcal{C}^n \triangleq \{1, \ldots, C^n\}$, which is composed by aggregating two CCs, the user set is defined as $\mathcal{U}^{(c_n^{i,j})} \triangleq \mathcal{U}^{(c=i)} \cup \mathcal{U}^{(c=l)}$; and the resource set is defined as $\mathcal{R}^{(c_n^{i,j})} \triangleq \mathcal{R}^{(c=i)} \cup \mathcal{R}^{(c=l)}$, where i and l, $i \neq l$, represents the aggregated CCs. When ABS or RP-ABS is employed along with CA, firstly the cells to be blanked or forced to reduce transmission power level, $I^c = 1$, are determined by (4.18). Then the aggregation takes place for the non-indexed channels, $I^c = 0$ and modification is carried out for the user and resource sets. Once the modified sets are obtained, the LTE constraints based scheduling decision is taken as described in Section 4.2.1 and Section 4.2.2.2 for normal and blanked subframes, respectively.

4.3 Scheduling Policies

In LTE systems, scheduling policies are not specified in the standards and are based on vendor/operator preferences. However, in the literature, several well-known scheduling policies exist [37]. In this research, different scheduling policies, namely round-robin (RR), PF and proportional fair based coordinated scheduler (PCS), are considered. In the RR scheduling, the users access the channel in a circular order and use the whole channel during their access period. The channel conditions of a user are not considered in the RR scheduler. Therefore, although it is fair in the sense of the channel access period that is utilised by every user, rate performance depends on both the period of channel use and its SINR conditions. In the PF scheduling, instantaneous and average data rate performance of the users are taken into account to allocate resources. Therefore, it considers both the channel conditions and amount of the resources allocated to each user.

To achieve a system-wide fair scheduling for a multi-cell system, the scheduler should have all the necessary information used to allocate resources. However, a centralized unit is not considered in the LTE-A system. Therefore, for a system-wide user data rate fairness, a PCS is proposed. The PCS is a modified version of the conventional PF scheduler where a data rate threshold is used to assert users who achieved data rate performance below the threshold. The scheduling metric, w_u^c, of the considered scheduling policies are obtained as

$$w_u^c = \begin{cases} 1, \quad \text{if} \quad \mathrm{u} = \mathrm{U}_{\mathrm{RR}}^{\mathrm{c}}(1), & \multirow{2}{*}{RR} \\ 0, \quad \text{otherwise}, & \\ 1/\bar{\xi}_u^c, & \text{PF}, \\ \Xi_{\text{th}}/\left(\bar{\xi}_u^c\right)^2, & \text{PCS}, \end{cases} \tag{4.21}$$

where U_{RR}^c is the vector that turns users in the circular order in every TTI and cell[5]; $\bar{\xi}_u^c$ is the average data rate for user u over a certain averaging period based on TTI; and Ξ_{th} is the data rate threshold value that is a constant value for all users. According to the given scheduling metric calculation in (4.21), if $\bar{\xi}_u^c = \Xi_{\text{th}}$, the scheduling metric of the PCS becomes $1/\bar{\xi}_u^c$, which is the metric of the conventional PF. However, if $\bar{\xi}_u^c \ll \Xi_{\text{th}}$, then the user that achieves the minimum average data rate is prioritized in the scheduling algorithm. Similarly, when $\bar{\xi}_u^c \gg \Xi_{\text{th}}$, the user that achieves such a high average rate will almost be neglected in the algorithm due to using the square of the average user rate in the denominator, if and only if there are users with $\bar{\xi}_u^c < \Xi_{\text{th}}$.

[5]It is assumed that all cells are synchronized.

Therefore, if there is a case $U^{c} \ll U^{c^*}$, as shown in Fig. 4.2 for eNB 1/channel 1, then the scheduling metric used in PCS will also fail to improve data rate fairness among all users in the system. In order to improve the system fairness, when a user has already achieved the given data rate threshold, there will be no more allocation to this user during the scheduling epoch.

It is important to note that the cell indexing problem given in (4.18) is solved centrally. In other words, it is assumed that there is a central unit that collects CQI reports and average achieved data rate performance of the users to decide the cells to be blanked. In order to make the decision to employ ABS or RP-ABS in a decentralized way, Algorithm 1 is followed.

Algorithm 1 Decentralized Cell Blanking

1: Create a list of randomly sorted cell indexes, L
2: Classify users into groups in each cell
3: **while** $L \neq \{\}$ **do**
4:     Find the user with the highest scheduling metric at cell $c = L(1)$
5:     **if** The user is a cell-edge user **then**
6:         Find the most interfering cell $\acute{c}$ to cell $c = L(1)$
7:         **if** The most interfering cell $\acute{c}$ is not considered before the cell $c = L(1)$ **then**
8:             Index the cell $\acute{c}$, $I^{\acute{c}} = 1$
9:         **end if**
10:     **end if**
11:     Flag the cell $c = L(1)$ to prevent to be indexed by the rest of the cells in the list
12:     Remove the $c = L(1)$ from the list
13: **end while**

In step 2 in Algorithm 1, it is stated that the users are classified into groups. According to [54], users associated with a channel can be grouped as cell-centre or cell-edge based on their reference signal received power (RSRP) levels. In this study, half of the users connected to a cell are classified as cell-edge, with the other half classified as cell-centre users.

4.4 Performance Evaluations

The system performance evaluation is based on 400 iterations, where in each iteration 400 TTIs are considered. This allows for the results to be well averaged and hence representative of a realistic scenario. A full buffer traffic model, where all users constantly request data, is considered in this study. Also, it is assumed that there is always a backhaul link between the aircraft and ground/satellite stations, which provides the data traffic generated by passengers.

System Parameters	Value
Aircraft model	Airbus A321
Number of users	210
Number of eNBs	2 eNBs, 3 eNBs
Total bandwidth per eNB	75 MHz
eNB transmission power per 20 MHz channel	12 dBm
eNB transmission power per 15 MHz channel	10 dBm
Centre frequency	1.8425 GHz (LTE Band 3)
Resource bandwidth	180 kHz
Subcarriers per RB	12
OFDM symbols per time slot (TS)	7
TS duration	0.5 ms
Antenna type	2×1 directional patch antenna
Antenna gain	12 dBi
Antenna tilt	50^o
Antenna positions	Centreline, Provisioned
Traffic model	Full buffer
Number of TTIs	400
Scheduling epoch	1 TTI
Number of iterations	400
CQI Reporting	Aperiodic Mode 3-0
RA Type	Type 0
Rate averaging window (per frame)	10 TTIs
RP-ABS power reduction	3 dB, 6 dB
User grouping percentages	50% cell-edge; 50% cell-centre

Table 4.4: *Simulation parameters*

A list of all the parameters used within the simulation are given in Table 4.4. In the system throughput and user data rate result figures, the function $F(X)$ refers to the empirical cumulative distribution function (CDF) which is defined as the probability of the random variable X taking on values less than or equal to x.

4.4.1 Performance Comparison of Subframes

The performance of the system with NSF and ABS or RP-ABS is compared when the PF scheduler is used in the RA. For RP-ABS, two different power reduction levels, $p = 3$ dB and $p = 6$ dB, are considered.

In Fig. 4.3(a) and Fig. 4.3(c), the user data rate distribution of the system with and without eICIC techniques are shown when the eNB antennas are mounted on the provisioned positions for 2 eNBs and 3 eNBs deployments, respectively. With the use of ABS, the data rate perfor-

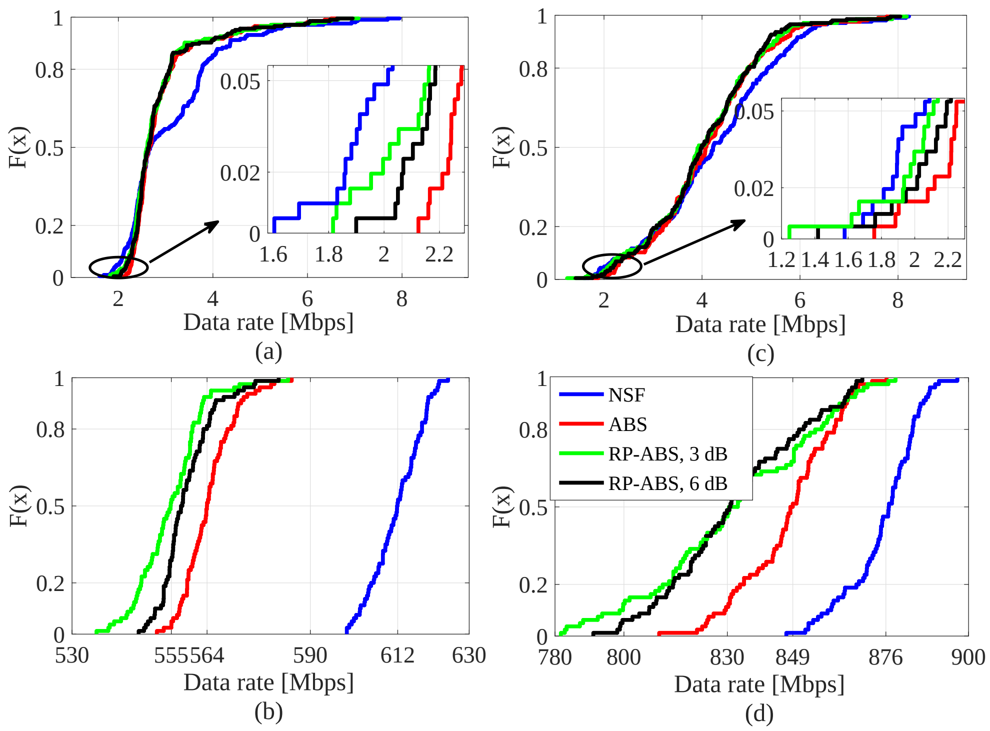

Figure 4.3: *Performance comparison of normal and blanked/reduced power subframes when the provisioned positions, PF scheduler and 64-QAM are used in the system. (a) 2 eNBs - user data rate [Mbps]. (b) 2 eNBs - system throughput [Mbps]. (c) 3 eNBs - user data rate [Mbps]. (d) 3 eNBs - system throughput [Mbps].*

mance of the cell-edge users[6] in the system with NSF is improved by around 13% for 2 eNBs and 9% for 3 eNBs deployments. Using ABS also improves the minimum achieved user rate by 32% and 12% for 2 eNBs and 3 eNBs deployments, respectively. However, such a performance improvement comes with the cost of 48 Mbps and 27 Mbps decrease in the system throughput performance for 2 eNBs and 3 eNBs deployments, as shown in Fig. 4.3(b) and Fig. 4.3(d), respectively.

With the use of RP-ABS, the cell-edge user data rate performance in the system with NSF is improved by 7.3% and 8.5% when 3 dB and 6 dB power reduction levels are used for 2 eNBs deployment, respectively. The same trend is seen for the 3 eNBs deployment where the cell-edge user performance is increased by 2.5% and 6.4% when 3 dB and 6 dB power reduction levels are used, respectively. However, with the use of RP-ABS, there is a 57 Mbps and 48 Mbps decrease in the system throughput for 2 eNBs and 3 eNBs deployments, respectively, irrespec-

[6]For the user data rate distribution, the 5^{th}-percentile and 95^{th}-percentile represent the performance of the cell-edge and cell-centre users, respectively. The 50^{th}-percentile represents the average user data rate performance.

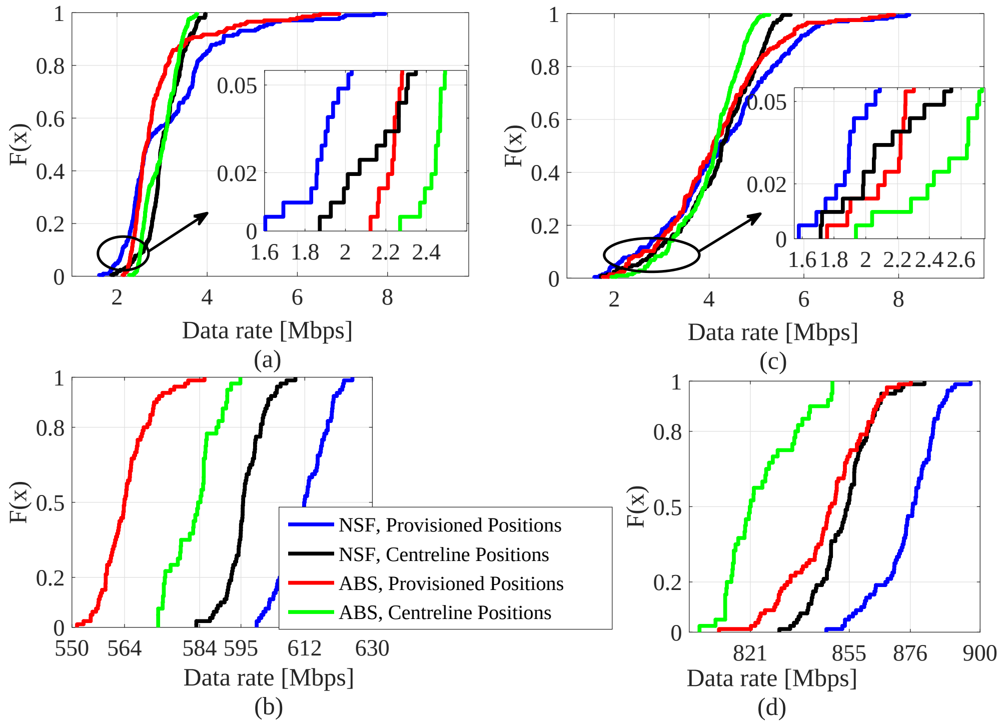

Figure 4.4: *Performance comparison of normal and blanked subframes for different antenna deployment positions when PF scheduler and 64-QAM are used in the system. (a) 2 eNBs - user data rate [Mbps]. (b) 2 eNBs - system throughput [Mbps]. (c) 3 eNBs - user data rate [Mbps]. (d) 3 eNBs - system throughput [Mbps].*

tive of the used power reduction level. As noted, the purpose of using RP-ABS is to provide throughput to the interfering cells during the ABS subframe. However, as shown in Fig. 4.3, RP-ABS does not achieve higher performance than ABS by means of the achieved cell-edge user rate and average system throughput. This is due to (1) reducing the power level of an interfering cell does not fully eliminate the interference, thus limits the achievable rate of the users impacted by interference; and (2) the constraint on the modulation order to conserve EVM during RP-ABS by the AMC function $\tilde{f}_{\text{AMC}}(\Gamma, p)$ limits the achievable rate during the RP-ABS.

In Fig. 4.4, the performance of the system with and without ABS is compared for provisioned and centreline antenna mounting positions when the number of deployed eNBs is 2 and 3. It is shown that deploying the antennas at the centreline antenna positions achieves a slightly better user data rate fairness and cell-edge user throughput performance than deploying the provisioned positions. This is due to having better number of users distribution among the eNBs in the centreline positions than the provisioned positions. It is also shown that employing

ABS further improves the user data rate fairness and cell-edge user throughput performance in the system irrespective of the antenna mounting positions.

4.4.2 Performance Comparison of Schedulers

The performance comparison of the considered RR, PCS and PF scheduler are given in Fig. 4.5 for the systems with different numbers of eNBs and NSF when the eNB antennas are mounted on the provisioned positions[7]. Based on the given results, the RR scheduler achieves the worst user data rate fairness performance. The difference between the minimum and maximum achieved user rate is around 8 Mbps for both 2 eNBs and 3 eNBs deployments. When the performance of the PCS is compared with the PF scheduler, the cell-edge user performance is improved by 4.6% and 17% for 2 eNBs and 3 eNBs deployments, respectively.

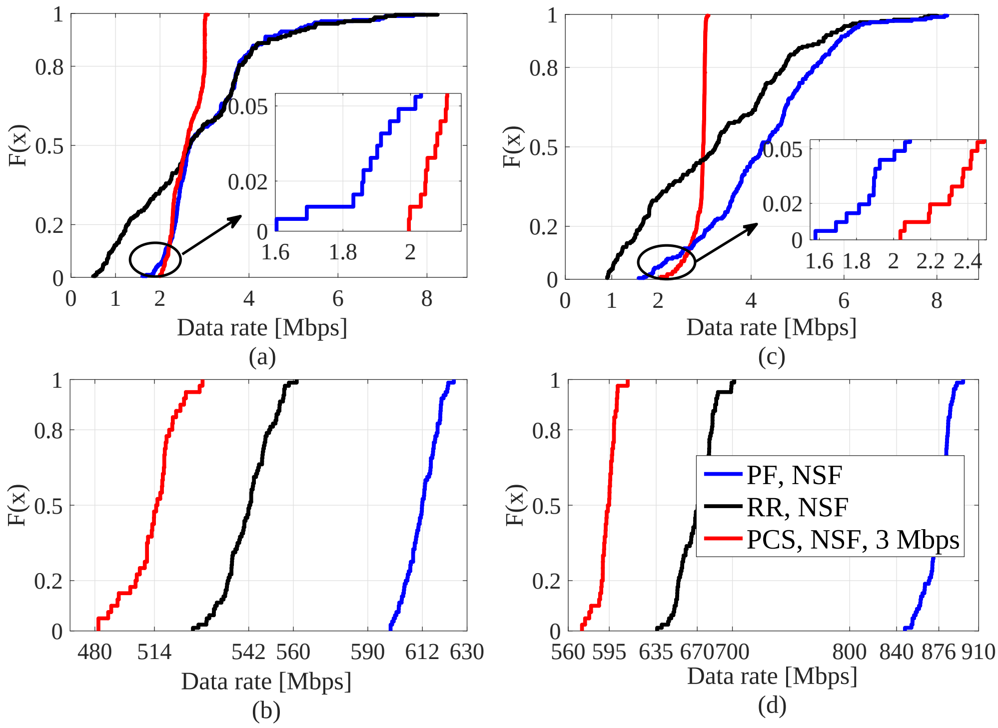

Figure 4.5: *Performance comparison of the considered schedulers with NSF when the provisioned positions and 64-QAM are used in the system. (a) 2 eNBs - user data rate [Mbps]. (b) 2 eNBs - system throughput [Mbps]. (c) 3 eNBs - user data rate [Mbps]. (d) 3 eNBs - system throughput [Mbps].*

[7]At the rest of this chapter, the performance comparison is only given for the provisioned antenna mounting positions. However, the overall system performance comparison, which considers all the noted techniques, number of deployed eNBs and antenna mounting positions, will be provided in Section 4.5.

Inherently, the cost of improving the fairness in the given system model is a degradation in the system throughput performance. When the performance of the PCS is compared to the PF one, the system throughput degradation is approximately 98 Mbps and 280 Mbps for 2 eNBs and 3 eNBs deployments, as shown in Fig. 4.5(b) and Fig. 4.5(d), respectively. This is due to stopping the allocation to the users who have already achieved the target rate. When a user achieves the data rate threshold, the resources that are favourable for the user will be assigned to remaining users who have not yet achieved the target rate. Therefore, those favourable resources may be used with lower MCS indexes for the remaining users. In order to qualify which system is best, the desired metric as well as the implementation limitations of the system must be known.

In addition, a performance comparison of the systems with and without ABS, centralized and decentralized cell blanking algorithms as well as a different data rate threshold of the PCS are given in Fig. 4.6 when 3 eNBs are deployed at the provisioned antenna positions. The PCS scheduler achieves a fairer user data rate distribution compared to the PF scheduler, irrespective of the used subframe and the considered rate threshold, as shown in Fig. 4.6(a). The difference between the maximum and minimum achieved data rate is around 6 Mbps for the PF scheduler for both NSF and ABS. However, for the PCS, the difference is between 1 Mbps and 2 Mbps, depending on the considered target data rate. Increasing the target data rate slightly degrades the minimum achieved and cell-edge user performance but improves the average system throughput. As noted, improvement in the user data rate fairness costs system throughput degradation. In Fig. 4.6(b), it is shown that the system throughput difference between the PCS and PF schedulers is decreased by using a higher target data rate. The system throughput difference is 280 Mbps, 212 Mbps and 158 Mbps for the target data rate of 3 Mbps, 3.5 Mbps and 4 Mbps, respectively.

When the performance of the centralized and decentralized cell blanking is compared for the PCS with a target rate of 3 Mbps, the centralized cell blanking achieves a better performance than the decentralized way of blanking. However, both the cell-edge user and average system throughput performance are close to each other, as shown in Fig. 4.6(a) and Fig. 4.6(b), respectively. When the cost of deploying a centralized unit in the system as well as the cost of transmitting all scheduling information of users to the unit are considered, decentralized cell blanking becomes more efficient than centralized blanking.

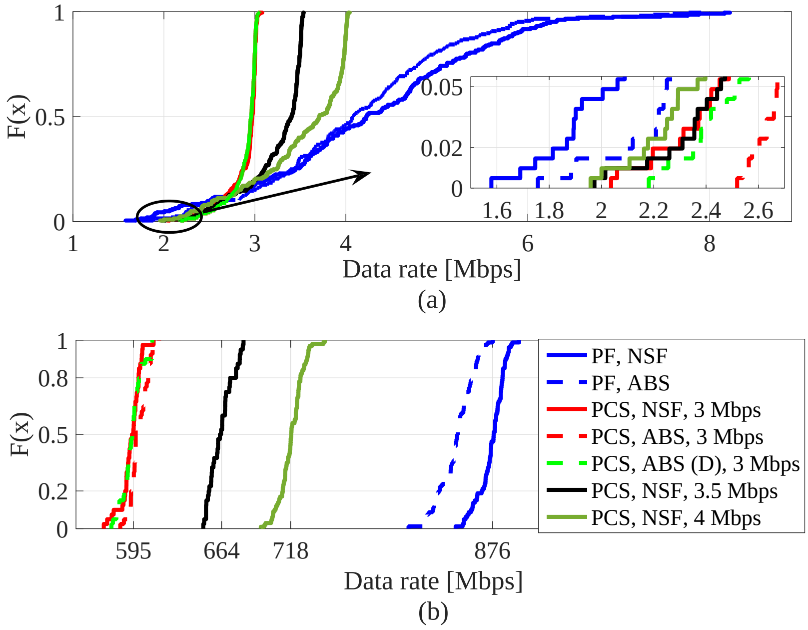

Figure 4.6: *Performance comparison of PCS and PF scheduler with normal and blanked subframes when 3 eNBs are deployed at the provisioned antenna positions and 64-QAM is used in the system. "(D)" represents decentralized cell blanking. (a) User data rate [Mbps]. (b) System throughput [Mbps].*

4.4.3 Performance of System with CA

As shown above, the fairness of the user data rate distribution is not as smooth as desired. In fact, the desired smoothness could not be achieved by using the eICIC techniques. As per the results presented in Fig. 4.7(a), the fairness of the user data rate distribution in the considered system model is improved by employing CA. Previously, using the PCS provided a fairer user rate distribution than the PF with ABS. However, employing CA in the system further improves the performance of the cell-edge users. In order to investigate how different techniques perform together, CA and ABS are combined together in a system where the PCS is used. Accordingly, in Fig. 4.7, the performance of the system with only CA as well as the system with a combination of CA and ABS are shown. When the performance of the system with only CA and with combined CA and ABS is compared, employing only CA in the system achieves a better user rate fairness, minimum user rate and system throughput performance.

As noted and shown in Fig. 4.6, increasing the data rate threshold value used in the PCS slightly decreases the cell-edge user performance but improves the average system throughput. When CA is employed with the PCS in the system, the threshold value of 3.5 Mbps achieves the same cell-edge user performance with the threshold value of 3 Mbps. Whereas both threshold values achieve the same cell-edge user performance, using 3.5 Mbps data rate threshold achieves 80 Mbps higher system throughput.

The most important result to note is that when CA is employed in the system, there is no need to employ eICIC techniques for the PCS. The purpose of employing eICIC techniques with PCS is to improve the data rate performance of users who have not achieved the target data rate by stopping or limiting the transmission of the interfering cell for a certain time. In other words, eICIC techniques waste some of the resources in order to improve the performance of vulnerable users. However, employing CA provides (1) better user per channel bandwidth distribution; and (2) a higher number of RBs which are available to be assigned to a single user. Therefore, if the users achieve the same SINR performance, the achieved even user-resource distribution can provide fair user data rate distribution. If the SINR performance of some of the users are lower than the average SINR performance, then having a higher number of RBs to be assigned to those users can compensate for the low SINR performance. Accordingly, when CA is employed with PCS, the additional employment of eICIC wastes the capability of resources at the interfering cell, which in turn degrades the performance. Another notable result is the degradation level of the system throughput performance. It is shown in Fig. 4.7(b) that the user data rate fairness is improved with a drop of 190 Mbps[8] in the system throughput performance by employing CA.

4.4.4 Performance of System with 256-QAM

So far, the maximum modulation order of the system is considered as 64-QAM. However, the recent LTE standard releases support the use of a higher modulation order, which is 256-QAM [5, Table 7.2.3-2]. Therefore, the performance of the system with 256-QAM is investigated for the NSF. The modified AMC function to employ 256-QAM is given in Table 4.5.

In Fig. 4.8, the performance of the systems with 64-QAM and 256-QAM is shown when the PCS with 3.5 Mbps target rate is used for the 3 eNBs deployment at the provisioned antenna positions. Also, the performance of the system with and without employing CA is given for the different maximum modulation orders. Inherently, using a higher modulation order improves

[8] As shown in previous sections, the highest achievable average system throughput performance among the considered system models is 876 Mbps. This is achieved by using PF scheduler with NSF when 3 eNBs deployed at the provisioned antenna positions.

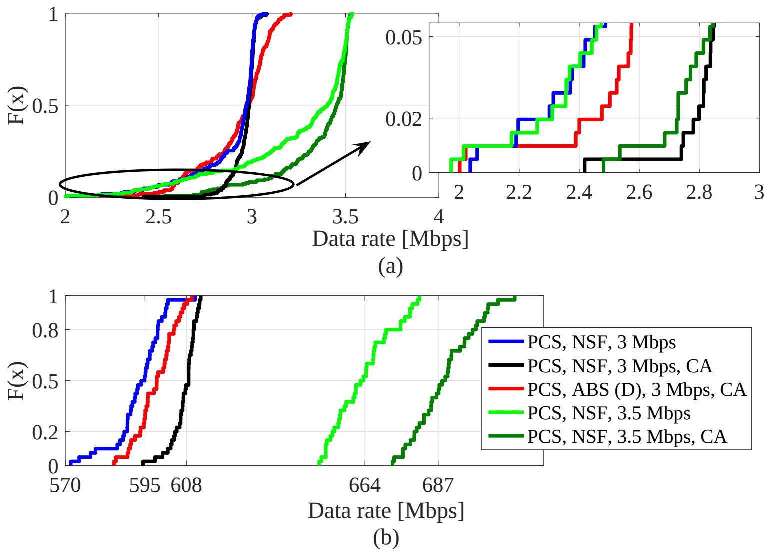

Figure 4.7: *Performance comparison of normal and blanked subframes with and without CA when 3 eNBs are deployed at the provisioned antenna positions and PCS and 64-QAM are used in the system. "(D)" represents decentralized cell blanking. (a) User data rate [Mbps]. (b) System throughput [Mbps].*

the performance for users who have good channel quality. As shown in Fig. 4.8(a), using 256-QAM as the maximum modulation order does not significantly improve the performance for cell-edge users. The reason for this can be explained as follows. It can be expected that the channel quality of a cell-edge user will be lower than a cell-centre user. Although there may be some RBGs that can support 256-QAM, using a lower modulation order may achieve a better data rate due to the common MCS assignment constraint of LTE. Accordingly, maximizing the modulation order of the AMC function neither improves the cell-edge user experience nor the fairness of the user data rate distribution. However, there is a slight improvement in the achievable system data rate as shown in Fig. 4.8(b).

4.5 Recommended System Decision Diagram

After analyzing all of the different algorithms and techniques, the question of how to put together the best system should be answered. It is shown that tradeoff between the fairness in the system and the achievable total system data rate exists. If the system throughput is the metric of choice, the system with PF solely performs the best by achieving an average system rate of 876 Mbps for the 3 eNBs and 612 Mbps for the 2 eNBs deployments. However, when the user data rate fairness is chosen as the system metric, then there are several options such as

CQI Index	Γ [dB]	MCS Index	$f_{\mathrm{AMC}}^{256\mathrm{QAM}}$	
			$M_{f_{\mathrm{AMC}}}$	k_j
0	-	-	-	0
1	-6	0	QPSK	0.1523
2	-3	1		0.3770
3	1	3		0.8770
4	5	6	16QAM	1.4766
5	8	8		1.9141
6	9	11		2.4063
7	11	12	64QAM	2.7305
8	12	15		3.3223
9	14	17		3.9023
10	16	19		4.5234
11	18	22		5.1152
12	20	24	256QAM	5.5547
13	22	26		6.2266
14	23	27		6.9141
15	25	27		7.4063

Table 4.5: *Modulation order and spectral efficiency in bits/symbol for NSF based on [5, Tables 7.1.7.1-1A and 7.2.3-2]*

the system with only ABS, with only CA and with ABS and CA. It is important to note that based on the given performance results, achieving 3 Mbps for all users is the upper limit of user data rate fairness. In theory, for a system with 64-QAM, the achievable system throughput is around 625 Mbps for 2 eNBs and 940 Mbps for 3 eNBs deployments. When the achievable system throughput is divided into the number of users in the system, the achievable user rate is around 2.97 Mbps and 4.45 Mbps for 2 eNBs and 3 eNBs deployments, respectively. However, this calculation is based on all the users in the system achieving a SINR value above 20 dB. When the interference in the real world is taken into account, achieving such a high SINR for all users is not possible. As shown in performance evaluations, achieving a minimum user rate of 3 Mbps is the system limit. Therefore, 3 Mbps is considered as the QoS target for all users.

In the decision diagram given in Table 4.6, the recommended system deployment is given based on the achieved minimum QoS outage. In the case where systems have similar QoS outage, minimum user rate and the difference between the maximum and minimum user rate are considered to decide the recommended system. Thus, once the QoS target or optimality criterion[9] is

[9]The optimality criterion can be the minimum user rate, fairness or system throughput based on a system designer's choice.

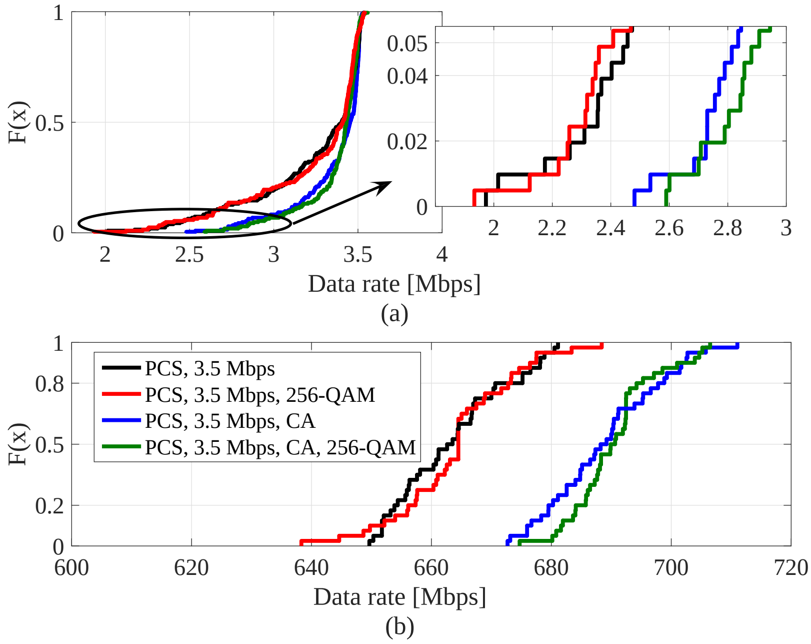

Figure 4.8: *Performance comparison of the supported modulation order when 3 eNBs are deployed at the provisioned antenna positions and PCS is used with and without CA in the system. (a) User data rate [Mbps]. (b) System throughput [Mbps].*

changed, the given QoS outage values as well as the recommended system deployment change. For example, if the optimality criterion is chosen as the minimum achieved user data rate instead of the minimum QoS outage, the recommended optimal system may have a higher QoS outage and lower system rate. To allow for the diagram to be read in the easiest way, the optimal recommended system deployment for different antenna mounting positions is given in bold font. It is important to note that scheduling decisions are made on each eNB in a decentralized way. The centralized unit is only considered for the systems with eICIC to decide which cells should be blanked.

In Fig. 4.9, the performance of the optimal system deployments for different antenna mounting positions are shown when the 3 eNBs are deployed inside the aircraft and 64-QAM is used as the maximum modulation order. As it can be seen from the figure, when the proposed scheduler is employed with CA, the user data rate fairness is improved along the aircraft cabin. Mounting antennas at the centreline positions achieve the most flat user data rate distribution inside the cabin.

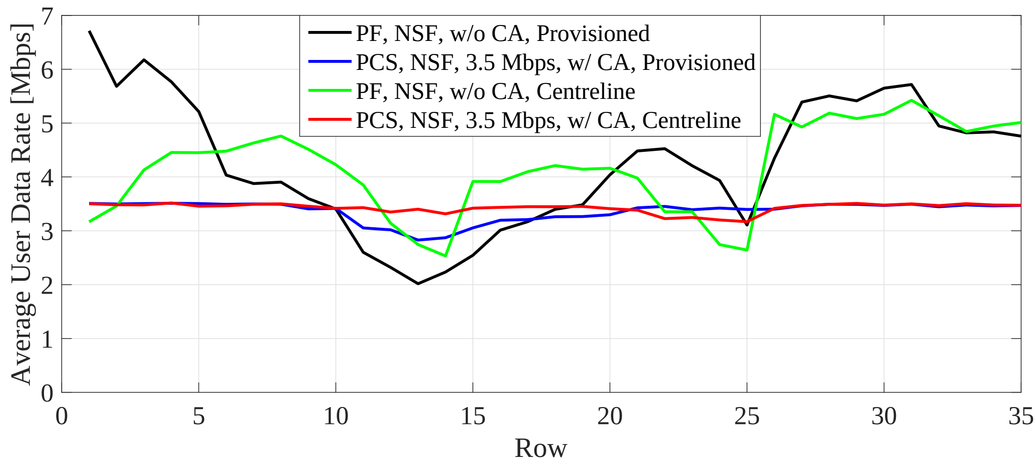

Figure 4.9: *Performance comparison of the optimum system deployments when 3 eNBs are deployed and 64-QAM is used in the system.*

4.6 Summary

This study has explored a number of existing combinations of algorithms/techniques and system deployments as well as proposed new ones such as a scheduler. The optimal system, which provides the optimal tradeoff between the user data rate fairness and overall system throughput, inside a medium-sized commercial aircraft is investigated. Once the optimum antenna orientation is obtained for cell sectorization based multi-cell system, eICIC techniques ABS and RP-ABS as well as CA are employed in the system to improve achieved data rate performance of the cell-edge users. Three different schedulers, namely PF, RR and PCS, two different antenna mounting positions and two different number of eNBs to be deployed such as 2 and 3 are considered.

It is shown that the system with RP-ABS does not achieve better performance than ABS due to its modulation order limitations that can be used with the reduced power level. When the ABS is used with the PF scheduler, it slightly improves the performance of the cell-edge users. However, there is still a significant difference of around 6 Mbps between the maximum and minimum achieved user rates. Once the proposed scheduler with a target data rate is employed, the minimum achieved data rate performance is improved by around 1 Mbps and the difference between the maximum and minimum user rates is reduced to 1 Mbps. Nonetheless, this costs around 280 Mbps of degradation in the system throughput. When the performance of different schedulers are compared, the RR scheduler achieves a better system data rate than the PCS but it has the worst user data rate fairness performance among the considered schedulers.

When CA is employed with the proposed scheduler, it is shown that the fairness can be improved without a significant drop in the system throughput performance. Also, it is shown that employing CA with eICIC techniques does not improve the already achieved performance with employing only CA in the system. Although employing CA with ABS achieves slightly better performance than employing only ABS for some users, there is no need to employ ABS in the presence of CA in the system based on the achieved performance with only CA.

Accordingly, the best proposed system is able to achieve the required 3 Mbps QoS for over 93% of the users inside the cabin. The remaining 7% are able to enjoy a data rate higher than 2.5 Mbps. For the considered antenna mounting positions, the centreline positions can provide better performance than the provisioned positions. Although the centreline antenna positions improve the user data rate fairness, their implementation is prohibitive due to the high additional costs of redesigning the airframe in order to accommodate LTE equipment at those locations. This is the case for the considered number of eNBs to be deployed. Although deploying 3 eNBs can achieve better performance than 2 eNBs deployment, the weight and size of the eNB hardware can be seen as limitations which should be taken into account by the aircraft in-cabin connectivity system design engineers.

From a general point of view, the system capacity results achieved are significant compared to the theoretical limits. In theory, the system capacity of the 3 eNBs deployment inside the cabin in the presence of no interference is approximately 940 Mbps. The proposed system is able to achieve approximately 75% of this capacity in the presence of interference. Higher system capacity is achievable if a degradation in the minimum achieved QoS and/or user data rate fairness is acceptable.

Ant. Pos.	Num. of eNBs	eICIC	CA	Cell Blanking	Max. Mod. Order [QAM]	Min. User Rate [Mbps]	Max.-Min. User Rate [Mbps]	3 Mbps QoS Outage	System Sum Rate [Mbps]	Scheduler	SF
Centreline	2	w/o eICIC	w/o CA	D	64	1.76	2.25	53%	564	PF	NSF
					256	1.6	2.73	29%	590	PF	NSF
			w/ CA	D	64	2.17	1.1	32%	556	PF	NSF
					256	2.33	0.9	23%	567	PCS (3.25)	NSF
		w/ eICIC	w/o CA	C	64	2.27	1.51	48%	551	PF	ABS
					256	2.34	1.37	45%	561	PCS (4)	ABS
				D	64	2.06	1.61	58%	539	PCS (6)	ABS
					256	2.25	1.67	50%	567	PCS (5)	ABS
			w/ CA	C	64	2.31	0.58	100%	480	PCS(3)	ABS
					256	2.48	0.56	95%	513	PCS (3.5)	ABS
				D	64	2.26	0.76	96%	490	PCS (4)	ABS
					256	2.35	0.85	86%	522	PCS (5)	ABS
	3	w/o eICIC	w/o CA	D	64	2.33	1.72	7%	751	PCS (4)	NSF
					256	2.37	1.17	6%	689	PCS (3.5)	NSF
			w/ CA	D	64	2.62	1.17	1.5%	702	PCS (3.5)	NSF
					256	**2.77**	**0.79**	**0.49%**	**700**	**PCS (3.5)**	**NSF**
		w/ eICIC	w/o CA	C	64	2.7	0.84	2.93%	693	PCS (3.5)	ABS
					256	2.87	0.46	1.46%	657	PCS (3.25)	ABS
				D	64	2.7	0.59	6.34%	654	PCS (3.25)	ABS
					256	2.71	0.58	4.39%	653	PCS (3.25)	ABS
			w/ CA	C	64	2.47	1.96	15%	665	PCS (3.5)	ABS
					256	2.63	1.03	9%	677	PCS (3.5)	ABS
				D	64	2.42	2.12	35%	677	PCS (5)	ABS
					256	2.16	2.36	25%	695	PCS (5)	ABS
Provisioned	2	w/o eICIC	w/o CA	D	64	1.6	6.34	57%	577	PF	NSF
					256	1.52	8.15	54%	610	PF	NSF
			w/ CA	D	64	2.14	1.29	51%	563	PF	NSF
					256	2	1.85	30%	603	PF	NSF
		w/ eICIC	w/o CA	C	64	2.09	2.68	72%	513	PCS (5)	ABS
					256	2.06	1.56	52%	546	PCS (3.5)	ABS
				D	64	1.91	3.52	60%	533	PCS (6)	ABS
					256	2	2.79	56%	567	PCS (5)	ABS
			w/ CA	C	64	1.43	1.95	84%	480	PCS (3)	ABS
					256	2.29	1.10	89%	504	PCS (4)	ABS
				D	64	1.41	1.86	78%	483	PCS (3)	ABS
					256	1.99	1.69	78%	515	PCS (4)	ABS
	3	w/o eICIC	w/o CA	D	64	1.95	2.1	18%	720	PCS (4)	NSF
					256	1.94	2.11	18%	724	PCS (4)	NSF
			w/ CA	D	64	2.48	1.06	8%	689	PCS (3.5)	NSF
					256	**2.59**	**0.97**	**7%**	**691**	**PCS (3.5)**	**NSF**
		w/ eICIC	w/o CA	C	64	2.22	1.31	14%	667	PCS (3.5)	ABS
					256	2.37	1.19	9%	676	PCS (3.5)	ABS
				D	64	1.92	1.64	18%	666	PCS (3.5)	ABS
					256	2.1	1.48	17%	671	PCS (3.5)	ABS
			w/ CA	C	64	1.97	2.54	14%	693	PCS (5)	ABS
					256	1.99	2.71	12%	718	PCS (5)	ABS
				D	64	1.76	2.67	27%	671	PCS (5)	ABS
					256	1.74	2.88	20%	688	PCS (5)	ABS

Table 4.6: *Recommended system decision diagram. Performance and details of the recommended system are given as minimum user rate [Mbps]; difference between the maximum and minimum user rate [Mbps]; 3 Mbps QoS outage [%]; average system (sum) rate [Mbps]; scheduler; subframe type. "$w/$" stands for with and "w/o" stands for without. "C" and "D" represents centralized and decentralized cell blanking, respectively. If the scheduler is the PCS, then the used user data rate threshold is given in parenthesis. "SF" stands for subframe.*

Chapter 5
Operating In-Cabin LTE-A System within Cellular Terrestrial Network

5.1 Introduction

Based on the Electronic Communications Committee (ECC) reports and decisions, an onboard mobile communication system can only be operated in certain phases of a flight [2, 14]. The compatibility between the terrestrial and onboard communication networks is firstly investigated for Global System for Mobile Communications (GSM) systems in [15], then it is further analysed for different frequency bands and technologies such as Universal Mobile Telecommunications System (UMTS) and Long Term Evolution (LTE) in [2, 3]. For GSM systems, a network control unit (NCU) is considered as part of the onboard communication system. The NCU is used to increase the noise floor inside the aircraft which in turn prevents the onboard mobile stations communicating with the terrestrial networks [15]. The same approach of using the NCU as part of the in-cabin system is considered in the compatibility analysis given for UMTS and LTE systems. Accordingly, the investigations have been done for the emissions: (1) from the NCU to the downlink of the terrestrial system, which is the link from a terrestrial evolved nodeB (eNB) to a terrestrial user equipment (UE); (2) from an in-cabin eNB to a terrestrial UE; and (3) from an onboard UE to the uplink of the terrestrial system, which is the link from a terrestrial UE to a terrestrial eNB.

According to the noted investigations, the in-cabin onboard system should not be operated while the aircraft is on the ground or during take-off and landing. The system should only be operated when the aircraft is flying at an altitude of 3000 m or more[1]. This conclusion is based on a set of assumptions which include using the maximum transmission power for the onboard UE as well as using the free space path loss for the link between the in-cabin and terrestrial systems. Along with enhancements in wireless technology, LTE systems can aggregate operated frequency bands of the same or different eNBs with carrier aggregation (CA) and establish

[1]The limitations on the UE and eNB inside the aircraft are given in Table 2.2.

a cooperation among cells with coordinated multi-point transmission (CoMP) to manage interference. Also, adaptively allocating the transmission power per UE is also possible in LTE. The maximum and minimum output power of a UE for the whole uplink channel[2] is defined as 23 dBm and -40 dBm, respectively [36]. Due to the decreased distance between the transmitter and receiver in small cells, it is possible to provide a sufficient quality of service (QoS) to small cell users with low transmission powers and vice versa. As a matter of fact, minimizing the potential interference from aircraft mobile users to terrestrial users is possible for LTE systems.

In order to provide a truly seamless and user-friendly integration of an onboard communication system, it is important that the users can make use of the system as soon as they step on board the aircraft. Therefore, an onboard communication system should be in operation in all phases of a flight, from the taxi out and take-off as well as landing and the taxi in. In this chapter, the effects of the operation of the in-cabin Long Term Evolution Advanced (LTE-A) system on the existing terrestrial LTE-A network are investigated, while the aircraft is stationary and in the parked position on the apron. The particular focus of this study is to determine the downlink interference power due to the in-cabin eNBs that terrestrial users experience, as well as the effects of the terrestrial systems on the operation of the in-cabin deployment. The signal-to-noise-plus-interference ratio (SINR) performance and interference level of the users, who are (1) inside the airport building; (2) waiting to board the aircraft; and (3) ground service employers, are investigated using computer simulations. Moreover, the simulation based analysis of the compatibility of both systems is validated through on-site power leakage measurements from onboard to terrestrial and vice versa. For the computer simulations, Edinburgh Airport and LTE cells which cover Edinburgh Airport are modelled to investigate the overall downlink interference with and without the operation of the in-cabin LTE system. For the on-site measurements, an A321 aircraft, which is inside a hangar and covered by a terrestrial network provider, is used to investigate the power leakage from one system to another. Furthermore, based on the measurement results, the procedure and parameters used to handover the passengers when they board the aircraft are provided.

The rest of the chapter is structured as follows. In Section 5.2, the considered simulation environment, which includes details of Edinburgh Airport, existing terrestrial eNBs that cover the airport and the used terrestrial channel model are provided. Also, the computer simula-

[2]The whole uplink channel represents all the available resource blocks (RBs) of the considered channel bandwidth. Therefore, the given minimum and maximum uplink transmission power should be divided by the number of the available RBs.

Figure 5.1: *Overview of Edinburgh Airport.*

tion based analysis are presented in this section. The on-site measurement setup is introduced in Section 5.3. The analysis on how to handover the onboard passengers is also given in this section. Finally, this chapter is concluded in Section 5.4.

5.2 Compatibility of the In-cabin System with Terrestrial Network: Simulation

5.2.1 Edinburgh Airport

Edinburgh Airport is located in Ingliston, a town 5 miles west of the City Centre. The airport is one of the busiest in the UK, with an average of $33,880$ passengers and over 333 flights per day [73]. The airport comprises two runways and one terminal, with one domestic and two international arrival halls. There are a total of 23 aircraft gates. The satellite image of Edinburgh Airport was obtained from the Google maps service as shown in Fig. 5.1.

5.2.2 Existing LTE eNBs

In the UK, there are four main wireless cellular network operators: EE, O2, H3G and Vodafone [74]. Each operator uses different frequencies to deliver mobile services. The permitted frequency bands used in the UK for LTE are: 800 MHz, 1800 MHz and 2600 MHz. The LTE frequency bands used by the mobile network operators are shown in Table 5.1 [74]. As the frequency band of the in-cabin LTE system uses the frequencies between 1805 and 1880 MHz for downlink, the downlink interference from operators of H3G and EE is investigated. The interference from the onboard system to terrestrial LTE users inside and around Edinburgh Airport is also investigated.

Operator	Frequency		
	800 MHz	1800 MHz	2600 MHz
EE	2×5 MHz	2×45 MHz Downlink: 1831.7 - 1876.7 MHz Uplink: 1736.7 - 1781.7 MHz	2×35 MHz
H3G	2×5 MHz	2×15 MHz Downlink: 1816.7 - 1831.7 MHz Uplink: 1721.7 - 1736.7 MHz	-
O2	2×10 MHz	-	-
Vodafone	2×10 MHz	-	2×20 MHz
			1×25 MHz

Table 5.1: *Cellular operators in the UK and their licensed LTE frequency bands*

5.2.3 Terrestrial Channel Model

As part of the Wireless World Initiative New Radio (WINNER) II [75] and WINNER+ [76] projects, path loss models of different scenarios have been investigated. These models are based on literature and real measurements taken during the WINNER II and WINNER+ projects. The general form of the logarithmic path loss model can be expressed as follows:

$$\mathrm{PL}_{\mathrm{terrestrial}} = A_{\mathrm{PL}} \log_{10}(d) + B_{\mathrm{PL}} + C_{\mathrm{PL}} \log_{10} \frac{f_c}{5} + X, \tag{5.1}$$

where A_{PL} is the path loss exponent; d is the distance between eNB and UE; B_{PL} is the intercept which is determined by the free space path loss for the reference distance; C_{PL} is the frequency dependent path loss; f_c is the carrier frequency; and X is the environment dependent term. Specifically, the logarithmic path loss model is modified according to different environments, such as line of sight (LoS) or non-line of sight (NLoS) links, suburban or urban environments, and indoor or outdoor scenarios. The considered WINNER scenarios in this study are listed below [75]:

- **B1 Urban Microcell Scenario (UMi):** The height of the eNB and UE antennas is assumed to be well below the tops of surrounding buildings.
- **B4 Outdoor-to-Indoor Scenario (O2Ia):** In an outdoor to indoor urban microcell scenario. It is assumed that the UE antenna height is at 1-2 m (plus the floor height), and eNB antenna height below roof-top, at 5-15 m depending on the height of surrounding buildings. The variations in the height of the eNB antenna depends on surrounding buildings over four floors.
- **C1 Suburban Macrocell Scenario (SMa):** Macro eNBs are located well above the roof tops to allow wide area coverage and UE handsets are outdoors at street level. Buildings are typically low residential detached houses (1-2 floors) or low rise flats.
- **C2 Urban Macrocell Scenario (UMa):** The UE is located outdoors at street level and an eNB is fixed above the height of surrounding buildings. NLoS or obstructed LoS is a common case.
- **C4 Urban Macro Outdoor-to-Indoor Scenario (O2Ib):** Outdoor environment is the same as in C2, and the indoor environment is an office environment. The eNB antenna is clearly above the average building height. Long LoS channels to indoor environment walls is a common case.

The path loss models for the considered scenarios can be found in Table 5.2 [75, 76].

There are different outdoor path loss models for LoS and NLoS cases, respectively. The NLoS case provides a shadowing standard deviation higher than that for LoS. Due to the blocking effect of walls and ceilings, there is a severe shadowing in the outdoor-to-indoor case. For example, the shadowing standard deviation is $\sigma_{\text{SF}} = 7$ for scenario B4 and $\sigma_{\text{SF}} = 10$ for scenario C4 [75].

Therefore, if an eNB is an urban microcell, and the distance between the UE and eNB is relatively short, scenario B1 with LoS is appropriate. Otherwise, there is a high probability it could be a NLoS link. The LoS link probability of scenario B1, $P_{\text{B1,LoS}}$ can be written as follows:

$$P_{\text{B1,LoS}} = \min(18/d, 1)(1 - \exp(-d/36)) + \exp(-d/36), \tag{5.2}$$

Scenario		**Pathoss** [dB]	**Shadowing Std.**	**Distance Range**	**Antenna Height**
UMi (B1)	LoS	$\mathrm{PL}_{\mathrm{B1,LoS}} = 22.7\log_{10}(d) + 27 + 20\log_{10}(f_c)$	$\sigma_{\mathrm{SF}} = 3$	$10\mathrm{m} < d < d'_{\mathrm{BP}}$	$h_{\mathrm{BS}} = 10\mathrm{m}$, $h_{\mathrm{MS}} = 1.5\mathrm{m}$
		$\mathrm{PL}_{\mathrm{B1,LoS}} = 40\log_{10}(d) + 7.56 - 17.3\log_{10}(h'_{\mathrm{BS}})$ $-17.3\log_{10}(h'_{\mathrm{MS}}) + 2.7\log_{10}(f_c)$		$d'_{\mathrm{BP}} < d < 5\mathrm{km}$	
	NLoS	$\mathrm{PL}_{\mathrm{B1,NLoS}} = [44.9 - 6.55\log_{10}(h_{\mathrm{BS}})]\log_{10}(d)$ $+5.83\log_{10}(h_{\mathrm{BS}}) + 14.78 + 34.97\log_{10}(f_c)$	$\sigma_{\mathrm{SF}} = 4$	$10\mathrm{m} < d < 2\mathrm{km}$	
O2Ia (B4)	NLoS	$\mathrm{PL}_{\mathrm{B4,NLoS}} = \mathrm{PL}^{[d_{\mathrm{out}}+d_{\mathrm{in}}]}_{\mathrm{B1,LoS}} + 21.04 + 0.5d_{\mathrm{in}}$ $+14[1 - 1.8\log_{10}(f_c)]$	$\sigma_{\mathrm{SF}} = 7$	$10\mathrm{m} < d < 2\mathrm{km}$	
		$\mathrm{PL}_{\mathrm{B4,NLoS}} = \mathrm{PL}^{[d_{\mathrm{out}}+d_{\mathrm{in}}]}_{\mathrm{B1,NLoS}} + 21.04 + 0.5d_{\mathrm{in}}$ $-0.8h_{\mathrm{MS}} + 14[1 - 1.8\log_{10}(f_c)]$			
SMa (C1)	LoS	$\mathrm{PL}_{\mathrm{C1,LoS}} = 23.8\log_{10}(d) + 27.2 + 20\log_{10}(f_c)$	$\sigma_{\mathrm{SF}} = 4$	$30\mathrm{m} < d < d_{\mathrm{BP}}$	$h_{\mathrm{BS}} = 25\mathrm{m}$, $h_{\mathrm{MS}} = 1.5\mathrm{m}$
		$\mathrm{PL}_{\mathrm{C1,LoS}} = 40\log_{10}(d) + 9 - 16.2\log_{10}(h_{\mathrm{BS}})$ $-16.2\log_{10}(h_{\mathrm{MS}}) + 3.8\log_{10}(f_c)$	$\sigma_{\mathrm{SF}} = 6$	$d_{\mathrm{BP}} < d < 5\mathrm{km}$	
	NLoS	$\mathrm{PL}_{\mathrm{C1,NLoS}} = [44.9 - 6.55\log_{10}(h_{\_\mathrm{BS}})]\log_{10}(d)$ $+11.78 + 5.83\log_{10}(h_{\_\mathrm{BS}}) + 34.97\log_{10}(f_c)$	$\sigma_{\mathrm{SF}} = 8$	$50\mathrm{m} < d < 5\mathrm{km}$	
UMa (C2)	LoS	$\mathrm{PL}_{\mathrm{C2,LoS}} = 26\log_{10}(d) + 25 + 20\log_{10}(f_c)$	$\sigma_{\mathrm{SF}} = 4$	$10\mathrm{m} < d < d'_{\mathrm{BP}}$	
		$\mathrm{PL}_{\mathrm{C2,LoS}} = 40\log_{10}(d) + 9.27 - 14\log_{10}(h'_{\mathrm{BS}})$ $-14\log_{10}(h'_{\mathrm{MS}}) + 6\log_{10}(f_c)$	$\sigma_{\mathrm{SF}} = 6$	$d'_{\mathrm{BP}} < d < 5\mathrm{km}$	
	NLoS	$\mathrm{PL}_{\mathrm{C2,NLoS}} = [44.9 - 6.55\log_{10}(h_{\mathrm{BS}})]\log_{10}(d)$ $+14.78 + 5.83\log_{10}(h_{\mathrm{BS}}) + 34.97\log_{10}(f_c)$	$\sigma_{\mathrm{SF}} = 8$	$10\mathrm{m} < d < 5\mathrm{km}$	
O2Ib (C4)	NLoS	$\mathrm{PL}_{\mathrm{C4,NLoS}} = \mathrm{PL}^{[d_{\mathrm{out}}+d_{\mathrm{in}}]}_{\mathrm{C2,LoS}} + 21.04 + 0.5d_{\mathrm{in}}$ $+14[1 - 1.8\log_{10}(f_c)]$	$\sigma_{\mathrm{SF}} = 10$	$10\mathrm{m} < d < 5\mathrm{km}$	$h_{\mathrm{BS}} = 25\mathrm{m}$, $h_{\mathrm{MS}} = 3n_{\mathrm{Fl}}$ $+1.5\mathrm{m}$
		$\mathrm{PL}_{\mathrm{C4,NLoS}} = \mathrm{PL}^{[d_{\mathrm{out}}+d_{\mathrm{in}}]}_{\mathrm{C2,NLoS}} + 21.04 + 0.5d_{\mathrm{in}}$ $-0.8h_{\mathrm{MS}} + 14[1 - 1.8\log_{10}(f_c)]$			

Table 5.2: *Terrestrial path loss model. d_{out} is the distance between the outdoor terminal and the wall nearest to the indoor terminal; d_{in} is the distance between wall to the indoor terminal; $n_{Fl} \in [1, \infty)$ represents floor index; h_{BS} is antenna height of eNB; $h'_{BS} = h_{BS} - 1m$ is the effective antenna height of eNB; h_{MS} is the antenna height of UE; $h'_{MS} = h_{MS} - 1m$ is the effective antenna height of UE; f_c represents the centre frequency in Hz; $d_{BP} = 4h_{BS}h_{MS}f_c/c$ is the break point distance; $d'_{BP} = 4h'_{BS}h'_{MS}f_c/c$; and Std. stands for standard deviation.*

where $\min(x, y)$ is the function to take the minimum between x and y. Also, if the UE is indoors, such as in an airport gateway or inside the aircraft, the outdoor-to-indoor scenario B4 is used. If the eNB is a suburban macrocell, scenario C1 is applied and the LoS probability is:

$$P_{\text{C1,LoS}} = \exp(-d/200). \tag{5.3}$$

If the eNB is an urban macrocell, scenario C2 should be used and the LoS probability is:

$$P_{\text{C2,LoS}} = \min(18/d, 1)(1 - \exp(-d/63)) + \exp(-d/63). \tag{5.4}$$

Once the distance dependent path loss is calculated, a clustered delay line (CDL) model specific to each scenario is used to generate frequency selective fading coefficients. The CDL models based on cluster and power delay profile values for each scenario can be found in Appendix B [75]. According to the CDL model, the time-domain channel response is calculated as follows:

$$h'(t) = \sum_i \sqrt{a_i} h_{w_i} \delta(t - \tau_i), \tag{5.5}$$

where a_i is the power delay value of the ith cluster of the applicable CDL model; h_{w_i} is a random variable with zero mean and unity variance; and τ_i is the delay of the ith cluster of the applicable CDL model. When the time-domain channel response $h'(t)$ is calculated, the frequency-domain response of the channel can be found by its Fourier transform as follows:

$$H_0(f) = \sum_i \sqrt{a_i} h_{w_i} e^{-j2\pi f \tau_i}, \tag{5.6}$$

where $H_0(f)$ is the frequency-domain fast fading channel information for the frequency f. Thus, in order to calculate the channel response of each RB, the frequency band of the channel should be appropriately quantized.

Accordingly, the final channel impulse response, including the shadowing, can be calculated as follows:

$$H_{\text{RB}}^{\text{T}}(f_{\text{RB}}) = \sqrt{10^{\frac{-\text{PL}_{\text{terrestrial}} + X_{\sigma_{\text{SF}}}}{10}}} H_0(f_{\text{RB}}), \tag{5.7}$$

where $H_{\text{RB}}^{\text{T}}(f_{\text{RB}})$ is the channel frequency response of RB; $\text{PL}_{\text{terrestrial}}$ is the distance dependent path loss based on the considered scenario; $X_{\sigma_{\text{SF}}}$ is the log-normal shadowing value based on the considered scenario; and $H_0(f_{\text{RB}})$ is the channel frequency response of the centre frequency of the RB as given in (5.6).

5.2.4 System Model

5.2.4.1 Frequency Reuse

LTE uses frequency reuse 1, which means all available RBs are used by every eNB. In general, the terrestrial eNBs are sectorized in three sectors and use full frequency reuse. As noted, cell sectorization is also used for the in-cabin eNBs to increase the effective distance of the interfering source. For the in-cabin eNBs, full frequency reuse is applied where the 4 available channels (3×20 MHz and 1×15 MHz) are divided into two sectors with each pointing in opposite directions.

5.2.4.2 User-eNB Attachment

In the considered system model, each in-cabin user is connected to an eNB which serves the best average signal power to the user. However, for the terrestrial users, two different user-eNB association schemes are considered. The first scheme is the same approach used to attach in-cabin users, each terrestrial user is served by the eNB that provides the best average signal power. In the second scheme, a terrestrial user can associate with the eNB that serves the best average signal power as long as there is room for the user at the eNB. In other words, there is a limitation on the number of attached users to an eNB in the second scheme. This can be considered as load balancing in the network. Accordingly, the first scheme can be considered as the best case scenario where a user always has the best possible desired signal power, and the second scheme can be considered as the real-world scenario where there is no guarantee to serve a user from the eNB which could best serve the user.

5.2.4.3 Scheduling

In order to investigate changes in the interference level with and without an in-cabin LTE system, scheduling is out of the scope of this chapter. Accordingly, it is assumed that all available RBs in each eNB/channel are always being transmitted for each user. In other words, it is assumed that each user is served by all available RBs at its connected eNB.

5.2.5 System Performance Analysis

In light of the given system model assumptions, to investigate the effects of the in-cabin LTE system on the already existing terrestrial LTE network as well as the effects of the existing terrestrial LTE network on the in-cabin LTE system when the aircraft is in the parked position, four different cases are considered as follows:

- **CASE 1: Only terrestrial LTE system:** In this case, the in-cabin LTE system is not considered in operation, and only the terrestrial LTE system performance is investigated to consider it as a benchmark for terrestrial users.

- **CASE 2: Full-scale LTE system:** In addition to the existing terrestrial LTE network, an in-cabin LTE system with 2 eNBs deployed in the aircraft on the airport apron is considered. This case can also be considered as the overall network model where all of the eNBs are considered in operation.

- **CASE 3: Only in-cabin LTE systems:** To investigate how the nearby in-cabin LTE deployments interact between each other, only the in-cabin LTE systems are considered. In this case, all the terrestrial eNBs are out of operation and all the in-cabin eNBs are in operation.

- **CASE 4: Only single in-cabin LTE system:** An isolated in-cabin LTE system is considered to be used as a benchmark while investigating the in-cabin user performance affected by the terrestrial LTE network, as well as the other nearby in-cabin deployments. Different from case 3, a single in-cabin LTE system deployed in an aircraft is considered in operation. All the remaining eNBs are considered out of operation.

5.2.5.1 Interference Analysis

For the described cases, received signal strength indicator (RSSI) is considered as a performance metric. The reasons for considering RSSI as a performance metric are twofold: (i) interference power levels can be obtained by comparing different system cases which are described above; and (ii) RSSI measurement results can be found in any mobile device which is connected to a mobile network. Therefore, interference analysis given in this report can be verified by a simple mobile device (with no need to use expensive software to carry out measurements).

Based on third generation partnership project (3GPP) definitions, RSSI represents the wideband received power which includes the power from a serving cell, non-serving (interfering) cells and noise, observed in certain orthogonal frequency division multiplexing (OFDM) symbols [38]. Therefore, comparing the RSSI performance from different cases provides information on changes in the received power level between the cases. For example, obtaining the received power level difference between the system with (case 2) and without (case 1) in-cabin eNBs gives information on how much interference is caused by the in-cabin eNBs.

As described in Section 2.4, in LTE systems, a RB consists of 7 OFDM symbols, each OFDM symbol has 12 subcarriers/resource elements (REs) and each subcarrier/RE has 15 kHz spacing [1]. Thus, a RB consists of 84 subcarriers. Among the OFDM symbols, only 2 of them (the first and fifth OFDM symbols) carry the reference signal. RSSI is obtained by averaging the total received power of 12 subcarriers located in each OFDM symbol that carries the reference signal.

Obtaining the RSSI of a user is dependent on used RBs at the connected cell and the cells using the same RBs in the given case. Let x be the case index, $\mathcal{C}$ be the set of all cells considered in the system, c be the cell index and r be the used RB index at the cell c that serves the user u. Firstly, obtain the set $\mathcal{C}_x$ which represents the active cells in the case x. For example, in case 1, all the terrestrial cells will be considered whereas in case 2, the terrestrial and in-cabin cells will be considered. Then, obtain the set $\mathcal{C}_x^r$ which represents the cells that use the RB r. Accordingly, it can be written that $\mathcal{C}_x^r \subseteq \mathcal{C}_x \subseteq \mathcal{C}$. Therefore, RSSI of a user for case x, $P_{u,x}^{\mathrm{RSSI}}$ is obtained by:

$$P_{u,x}^{\mathrm{RSSI}} = \left(\frac{1}{7}\right)\left(\sum_{c\in\mathcal{C}_x^r}\sum_{r=1}^{N_{\mathrm{RB},c}} P_{u,c,r}\right), \tag{5.8}$$

where $P_{u,c,r}$ is the received power on RB r from cell c to user u; and $N_{\mathrm{RB},c}$ is the number of RBs that are used in cell c. The factor of $1/7$ used in (5.8) is to calculate RSSI based on 3GPP definitions where 2 out of 7 OFDM symbols use reference signals in a RB and the total received power on subcarriers in these symbols are averaged. In this study, channel gain is obtained based on a RB level. In order to obtain the average received power level of the 2 OFDM symbols, the received power of a RB should be divided by the number of symbols in a RB, which is equal to 7. The parameter $P_{u,c,r}$ is calculated based on the transmission power and number of RBs used in cell c as well as channel coefficients between the cell c and user u

on RB r as follow:

$$P_{u,c,r} = \left(\frac{\sqrt{P_c}}{N_{\mathrm{RB},c}} H_r^{u,c} \right)^2, \tag{5.9}$$

where P_c is the transmission power at cell c; and $H_r^{u,c}$ represents channel coefficients. $H_r^{u,c}$ is obtained by (3.10) or (5.7) when cell c is an in-cabin LTE cell or terrestrial LTE cell, respectively.

5.2.5.2 SINR Analysis

As noted, RSSI gives information on the average total received power. It can only be affected by the number of deployed eNBs, their transmission power and channel coefficients between the mobile device and eNBs. When there is a limitation on the number of attached users per eNB, a user may not attach to its best serving eNB and may be forced to connect to its second best eNB. The RSSI level of this user will be the same. Therefore, the effect of having a limitation on the number of attached users cannot be observed from the RSSI level. However, in such a situation, the SINR performance of the user will be degraded. Therefore, SINR performance is considered in order to investigate the interaction between the in-cabin and terrestrial LTE systems when there is a constraint on the number of users per eNB. SINR of a user u on RB r for a case x, $\gamma_{u,r,x}$, is calculated as follows:

$$\gamma_{u,r,x} = \frac{P_{u,c^*,r}}{\sum\limits_{\substack{c \in C_x^r \\ c \neq c^*}} P_{u,c,r} + N_r}, \tag{5.10}$$

where c^* is the cell that user u is connected to[3].

5.2.5.3 Handover Analysis

As described in Section 2.4.6, handover in LTE is a UE assisted, eNB triggered process. Based on the measurement reports sent by the UE, the eNB decides to trigger the handover process, where the triggering can be based on the reported reference signal received power (RSRP) level, reference signal received quality (RSRQ) level or both. As depicted in Fig. 2.16, several parameters are used at both the connected eNB and neighbour eNB sides. The parameters hysteresis (*hysteresis*), offset (*a3-Offset*) and cell-specific offset (*cellIndividualOffset*) are added to

[3]Description of the other parameters can be found after (4.1).

the serving cell triggering quantity, which are used to discard small fluctuations over the measured value and make the serving cell attractive to decrease handover occurrences, respectively. At the neighbour eNB side, the *cellIndividualOffset* parameter is used to artificially increase the received signal quality. The reported triggering quantity is observed over a certain period, which is described as *time-to-trigger*, to avoid the UE to handover between the same neighbour and serving cell continuously. The range of the handover parameters are given in Table 5.3. Accordingly, the parameters *a3-Offset*, *hysteresis*, *cellIndividualOffset* and *time-to-trigger* are needed to be known to make the transition from the terrestrial system to the onboard system smoothly while the passengers board the aircraft. In this research, RSRP is considered as the triggering quantity, which can be obtained as follows:

$$P_u^{\mathrm{RSRP}} = \left(\frac{1}{7 \times 12}\right) \left(\sum_{r=1}^{N_{\mathrm{RB},c}} P_{u,c,r}\right). \tag{5.11}$$

The factor of $1/(7 \times 12)$ is used to calculate received power of a subcarrier/RE, as explain in Section 2.4.3.

Parameter	**Range**	**Unit**	**Notes**
cellIndividualOffset	-24, -22,...,-2, -1, 0, 1, 2,...,22, 24	dB	Set as Q-OffsetRange
a3-Offset	-30,...,30	-	0.5×*a3-Offset* dB
Hysteresis	0,...,30	-	0.5×*Hysteresis* dB
TimeToTrigger	0, 40, 64, 80, 100, 128, 160, 256, 320, 480, 512, 640, 1024, 1280, 2560, 5120	ms	

Table 5.3: *Event A3 handover parameters*

5.2.6 Simulation Model

5.2.6.1 Physical Model

In the simulation platform, Edinburgh Airport is physically modelled based on its coordinates. In addition, the existing LTE eNBs of each operator are modelled. The height of each eNB is randomly assigned as 10 m or 25 m. Then, three Airbus A321 aircraft are modelled as parked on the airport apron where each of them is connected to the airport building by a passenger boarding bridge (referred to as the gateway in this study).

Once all the physical buildings and cells are modelled, in-cabin and terrestrial users are modelled. As shown in Fig. 2.7, all passenger seats represent a user. Terrestrial users are divided

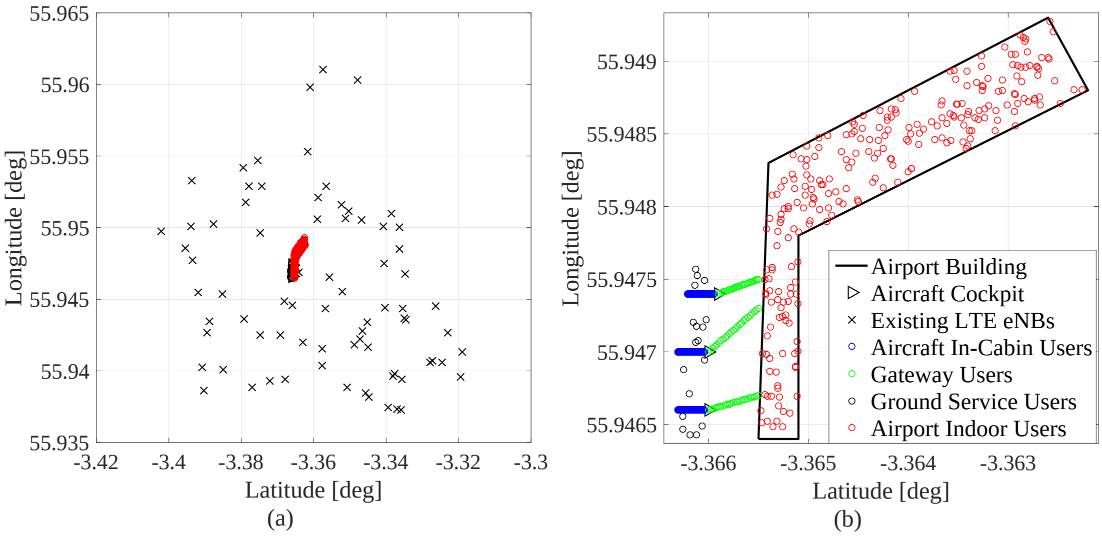

Figure 5.2: *Simulation model. (a) Full-scale. (b) Zoomed version.*

into 3 different classes – airport indoor users, gateway users who are waiting to board the aircraft and aircraft ground service users. In total, 4 different classes of user are considered, including in-cabin users alongside the aforementioned ones. The location of the airport indoor and ground service users are randomly distributed inside the airport and around each aircraft, respectively. However, the gateway users are uniformly distributed to model them as if they are waiting in a line within the gateway. The geometrical model of Edinburgh Airport, existing LTE eNBs, in-cabin eNBs and users are shown in Fig. 5.2.

5.2.6.2 Path Loss and Channel Model

The channel models given in WINNER+ are used to model the channels between terrestrial eNBs and all users, both in-cabin and terrestrial. When a link from an in-cabin eNB to a terrestrial user is considered, the indoor-to-outdoor scenario B4 is used to model path loss. Also, when a link from a terrestrial eNB to an in-cabin user is considered, the same scenario B4 is used to model outdoor-to-indoor link path loss. For both cases, the aircraft fuselage attenuation which will be explained in more detail in the next section, is added to the calculated path loss. However, when a link from a terrestrial eNB to terrestrial users is considered, a WINNER scenario and link case (LoS or NLoS) decision is made as follows:

- Step 1 - Check the height of the eNB,
  - if it is 10 m, the eNB is a microcell and the scenario should be B1 or B4;

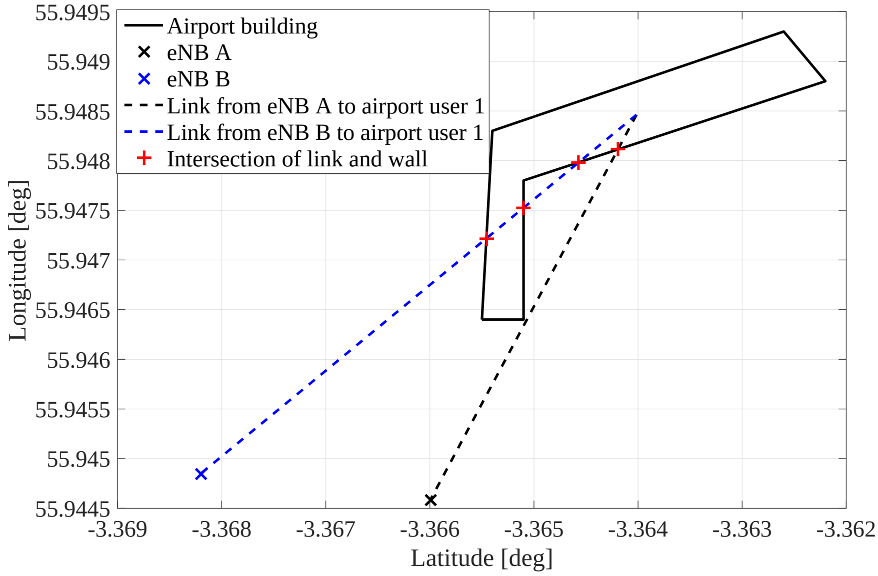

Figure 5.3: *LoS and NLoS channels.*

- if it is 25 m, the eNB is a macrocell and the scenario should be C1, C2 or C4.

- Step 2 - Check the link from the eNB to the user,

  - if the number of the wall intersection points is larger than 1, the link is definitely NLoS;

  - otherwise, the link can be LoS or NLoS based on its distance dependent LoS probability which is given in (5.2), (5.3) and (5.4) for scenarios B1, C1 and C2, respectively.

In Fig. 5.3, the calculation of the number of wall intersection points is depicted. When the channel between the user and eNB A is considered, there is only one intersection point on the path of the signal propagation, which means that between eNB A and the airport building wall, the channel could be a LoS one. However, when the channel between the user and eNB B is considered, there are 3 intersection points along the line of signal propagation. Accordingly, the link from eNB B to the airport building wall is definitely NLoS. The same approach can be used to characterize the channel between the eNBs inside the 1st and 3rd aircraft where the 2nd aircraft is in the parked position between the other two. Thus, all the channels from/to eNBs inside the 1st aircraft as well as to/from the 3rd aircraft are definitely NLoS channels.

5.2.6.3 Aircraft Fuselage Attenuation

Based on ECC reports [2, 15], three different aircraft fuselage attenuation cases, namely case A, case B and case C, are considered. The aircraft fuselage attenuation level is assumed as 5 dB, 10 dB and 15 dB for case A, case B and case C, respectively. In this study, the described aircraft fuselage attenuation cases A and C are considered. Accordingly, the channel from/to the in-cabin eNBs/users are attenuated an additional 5 dB or 15 dB to model the aircraft fuselage for cases A or C, respectively. Moreover, when channels between the aircraft are considered, the attenuation is added twice in order to model from aircraft-to-air and from air-to-aircraft transmissions.

5.2.6.4 Transmission Power and Antenna Gain

Based on [2, 63], antenna input power is assumed as 43 dBm for a 5 MHz channel, and 46 dBm for 10 MHz, 15 MHz and 20 MHz channels in downlink of the LTE 1800 MHz system. However, in [77], the maximum permitted downlink transmission power for LTE 1800 MHz is increased by 3 dB for operators in the UK which covers operators EE and H3G. Accordingly, the antenna input power is assumed as 46 dBm for 5 MHz channel and 49 dBm for 10 MHz, 15 MHz and 20 MHz channels in the system downlink. Also, maximum allowable effective isotropic radiated power (EIRP) is stated as 65 dBm [77] which is the summation of the antenna input power and antenna gain. In the simulations, the antenna gain of the terrestrial eNBs is set to 16 dBi [63] and assumed to be uniform in each direction to simulate an omni-directional antenna. Although the terrestrial eNBs are generally deployed in three sectors with directional antennas, assuming uniform gain in each direction makes the system operate at its worst case scenario.

The described in-cabin deployment in Section 2.3.2 is used for the in-cabin LTE 1800 MHz system. Accordingly, the antenna input power is assumed as 10.2 dBm due to the short distance between eNBs and users inside the aircraft. The antenna gain of the used 2×1 directional patch antennas is 12 dBi. Therefore, for the in-cabin eNBs, an EIRP of 22.2 dBm is considered.

5.2.6.5 Simulation Parameters

The system parameters used within the simulation adhere to the LTE specifications and operator licenses. A list of the terrestrial system parameters is summarized in Table 5.4 where the in-cabin system related parameters can be found in Table 4.4.

Terrestrial LTE System Parameter	Value
Operator H3G frequency band	1816.7-1831.7 MHz (1×5 MHz + 1×10 MHz; 75 RBs)
Operator EE frequency band	1831.7-1876.7 MHz (3×15 MHz; 225 RBs)
Antenna input power - 5 MHz	46 dBm
Antenna input power - 10, 15, 20 MHz	49 dBm
Tx antenna gain	16 dBi
Rx antenna gain	0 dBi
Tx antenna height (from ground)	10 or 25 m
Rx antenna height (from ground/floor)	1.5 m
Tx antenna type	Omni-directional
Tx antenna tilt	0^o
Total number of EE eNBs	50
Total number of H3G eNBs	26
Total number of gateway users	50 per aircraft
Total number of ground service users	8 per aircraft
Total number of airport indoor users	250
Frequency Reuse	1

Table 5.4: *Simulation parameters*

5.2.7 Simulation Results

Performance of the in-cabin LTE system within the existing LTE network is simulated and the results are given below. The system performance evaluation is based on 500 Monte Carlo simulations, where in each simulation the terrestrial users are randomly located. As noted in Section 5.2.5, RSSI and SINR are considered as the performance metrics for four different cases and RSRP is considered to investigate handover occurrence. Accordingly, the RSSI and SINR performance of the terrestrial users are observed when the in-cabin LTE eNBs are not in operation, which represents case 1. RSSI and SINR performance are also observed for the in-cabin users when there is no transmission from the terrestrial and nearby in-cabin LTE eNBs, which is represented in case 4. As explained in Section 5.2.5, cases 1 and 4 are the benchmark for the terrestrial and in-cabin users, respectively. In addition to the performance observation for cases 1 and 4, RSSI is observed for case 3, by considering the only in-cabin LTE eNBs in operation. After that, full-scale LTE system (case 2) is considered by operating all the in-cabin and terrestrial eNBs. Then, in order to understand the interaction among the terrestrial and in-cabin LTE systems, the benchmark cases are compared with the full-scale system case.

In the performance result figures, the function $F(X)$ refers to the cumulative distribution function (CDF) which is defined as the probability of the random variable X taking on values less than or equal to x.

5.2.7.1 Interference Power Results

In order to evaluate the transmission power leakage from the aircraft to outside, as well as from the outside to the aircraft, users inside the second aircraft are considered. The second aircraft is parked inbetween the other two aircraft. Therefore, the passengers inside the second aircraft are the users that can be mostly affected by the onboard systems deployed in the neighbouring aircraft. In Fig. 5.4(a), the received interference power level of users inside the second aircraft are shown for different numbers of aircraft and the described simulation cases 2, 3 and 4. It can be seen from Fig. 5.4(a) that the interference signal from one aircraft to another has almost no effect. This is due to the aircraft fuselage attenuation, which is considered as 5 dB, the distance between the aircraft and the transmission power used in the in-cabin eNBs. In the proposed in-cabin LTE system, eNB antennas are pointed to the cockpit and tail of the aircraft by using directional antennas. Thus, signal propagation is constrained in the pointed direction and the side lobe propagation is minimized. Moreover, the interference power from the terrestrial eNBs to the users inside the aircraft has slightly increased the received interference power for 20% of the in-cabin users, as shown in Fig. 5.4(a). However, it is important to note that the main interference source of the in-cabin users is the other eNB deployed inside the aircraft. The received interference power level within the same onboard system inside the second aircraft is around 70 dB and 20 dB higher than the received power level from the other two aircraft and terrestrial eNBs, respectively. Therefore, it can be said that based on the position of the aircraft parking spots and the given onboard system deployment, increasing the number of aircraft does not degrade the performance of other onboard systems.

In order to investigate the transmission power leakage from in-cabin eNBs to the outside of the aircraft, the received power level from the in-cabin eNBs at outside of the aircraft is obtained inside a circle with a radius of 50 m around the second aircraft[4]. In Fig. 5.4(b), the received interference power level of different numbers of aircraft and fuselage attenuation levels are shown. When the number of aircraft parked on the apron is increased, the median of the received interference power level increases. However, the maximum value of the interference remains unchanged. This is due to the architectural plan used in airport aprons. The

[4]Based on the given system model, the second aircraft is located 44 m away from the both first and third aircraft.

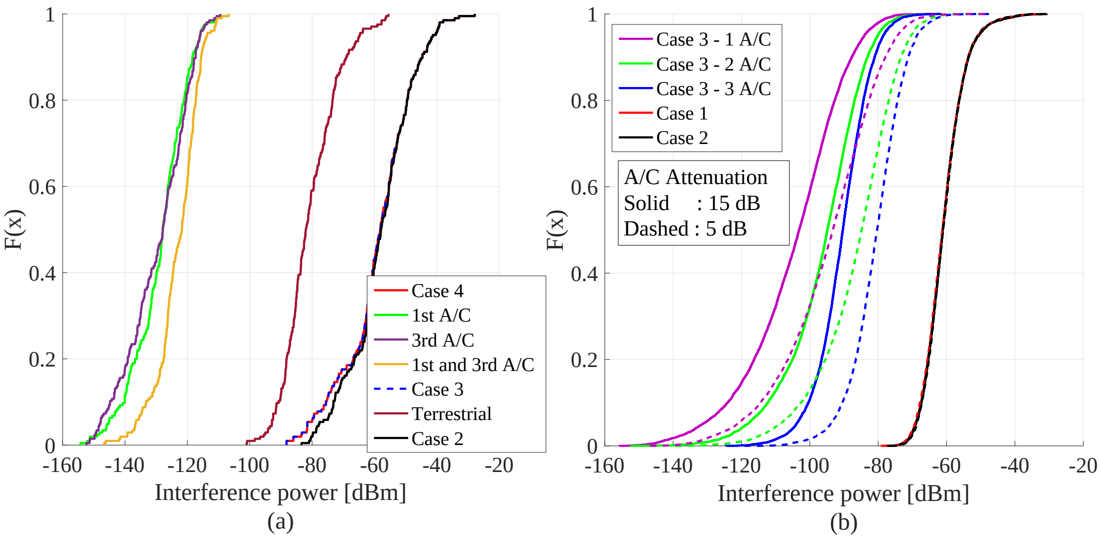

Figure 5.4: *Received interference power levels for the second aircraft. (a) For in-cabin users inside the second aircraft when the fuselage attenuation is considered as 5 dB. (b) For terrestrial users. "A/C" stands for aircraft.*

minimum distance between the aircraft parking spots depends on regulations to standardize it independent from the type and size of an aircraft. When the power leakage from the 1st and 3rd aircraft is considered for the users on the ground around the 2nd aircraft, it will only affect the users close to these aircraft. Therefore, the median of the received interference power CDF is increased but the maximum received level remains the same. The same observation can be made for both aircraft fuselage attenuation levels. Inherently, for a low attenuation level, the power leakage increases but increasing the number of aircraft in the system does not change the maximum received interference level. Moreover, when the interference power level from all 3 aircraft is taken into account for the users around the 2nd aircraft, there is no change to the overall received interference power level independent from the considered fuselage attenuation. This is due to having relatively higher interference from other terrestrial eNBs compared to the in-cabin eNBs in the system.

The RSSI performance of the users in the considered system is also investigated. Fig. 5.5 shows the CDF of the experienced RSSI difference between the systems with and without in-cabin LTE eNBs. As described in Section 5.2.5.1, the difference between the RSSI performance of the described cases provides information on changes in the received power level between the two. When the performance of the in-cabin users is considered, a notable RSSI degradation is not observed. Therefore, it can be understood that the terrestrial LTE eNBs do not contribute to the interference level inside the aircraft in the downlink direction. However, the in-cabin LTE

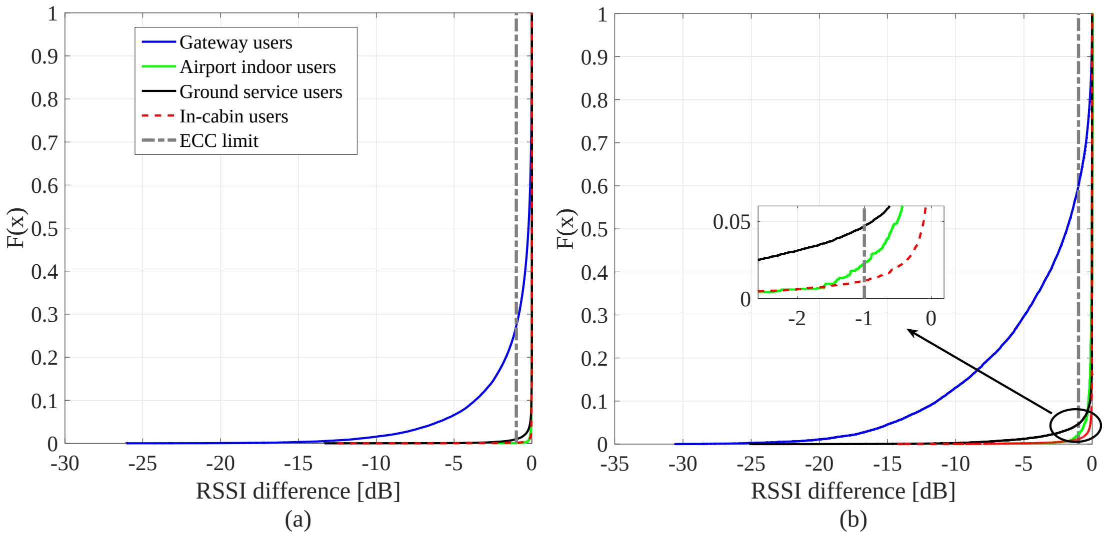

Figure 5.5: *RSSI difference between the systems with and without in-cabin LTE system for fuselage attenuation (a) 15 dB and (b) 5 dB.*

eNBs cause interference to the gateway users. This could potentially result in the connectivity in an area close to the aircraft doors being compromised. Although the in-cabin eNB causes an increase in the interference power level, exceeding the limit considered by the ECC, which is a 1 dB increase in the noise level, is observed for 30% and 60% of the gateway users when the aircraft fuselage attenuation is considered as 15 dB and 5 dB, respectively. It is clear that the least vulnerable users are those inside the airport due to the aircraft fuselage attenuation, the used in-cabin transmission power, the airport wall attenuation and distance between the apron and the airport. Based on the simulation results, for 15 dB fuselage attenuation, the RSSI performance of airport indoor users is essentially the same as when the in-cabin LTE system is transmitting and when it is not. This is the case for the ground service users as well. There is no significant additional interference power caused by the in-cabin LTE eNBs. Although the RSSI performance of airport indoor and ground service users are slightly increased for the 5 dB fuselage attenuation, only 5% of both classes of users are above the ECC's limit.

5.2.7.2 SINR Results

SINR performance is observed in order to investigate the effects of having limitations on the number of users that a terrestrial eNB can serve. Cases where there are 20 users per eNB, 50 users per eNB and unlimited users per eNB are simulated and compared. As described in Section 5.2.4.2, the given user number is the maximum capability limit for a terrestrial eNB.

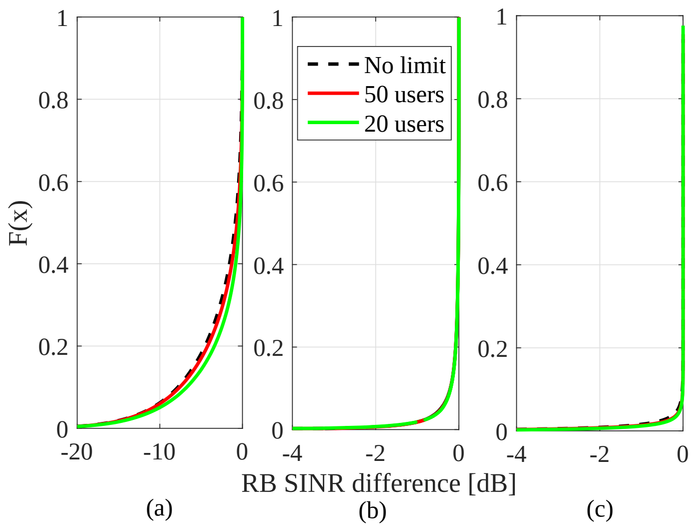

Figure 5.6: *Effect of number of users limit per eNB. (a) Gateway Users. (b) Ground Service Users. (c) Airport Indoor Users.*

It is important to note that the given user capability limitation is only applied to the terrestrial eNBs, not to the in-cabin eNBs. When a terrestrial eNB has reached its maximum capability number, it will not accept the connection request from a user. The declined user has to connect to another terrestrial eNB, which is not its best serving eNB. Therefore, when the systems with and without limitations on the number of users that an eNB can serve are compared, a SINR performance degradation is expected. However, as noted, the focus of this study is to understand how the in-cabin eNBs interact with the terrestrial network. From this perspective, when a terrestrial user cannot connect to its best serving eNB and is forced to connect to another terrestrial eNB, its main interference source will become its best serving eNB. Therefore, it is expected that the SINR performance degradation due to interference generated by the in-cabin eNBs in operation is negligible.

Fig. 5.6 shows the observed SINR difference between the systems with and without in-cabin eNBs for different classes of users when there is a limitation on the number of users per eNB. According to the Fig. 5.6, having a number of users per eNB limitation has a negligible effect on the RB SINR performance. When three cases for the number of users per eNB are considered for the gateway users, the SINR performance degradation due to the existence of in-cabin eNBs is reduced while the number of users per eNB decreases, as expected. Although a small degradation in the SINR performance can be seen for the gateway users, the considered three cases for the number of users that an eNB can serve have exactly the same SINR performance

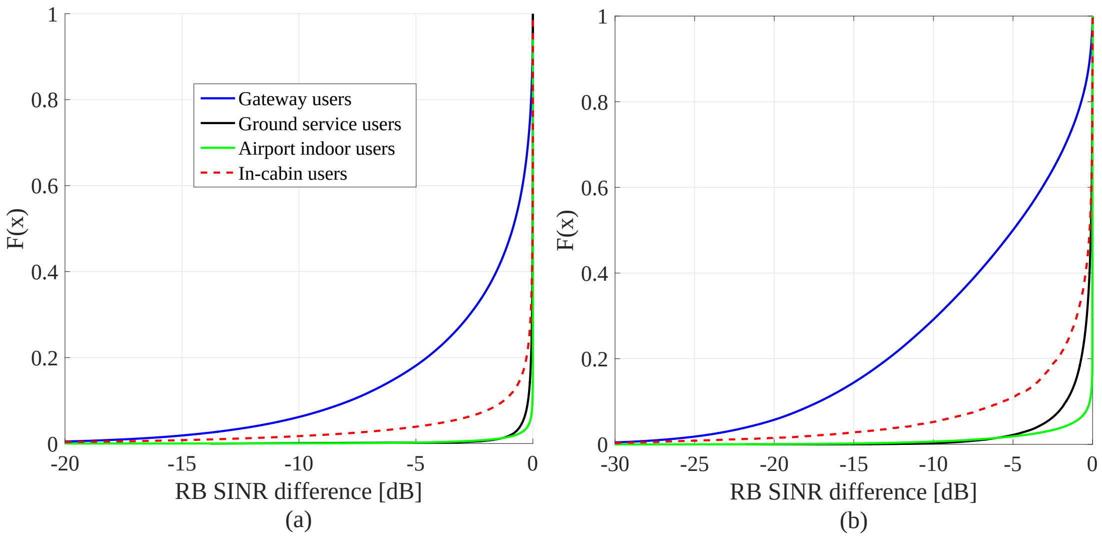

Figure 5.7: *SINR difference per RB between the systems with and without in-cabin LTE system when the fuselage attenuation is considered as (a) 15 dB and (b) 5 dB.*

per RB for the ground service and airport indoor users. The capacity of RBs appears to be minimally affected by the given eNB user capability limits.

In Fig. 5.7, the SINR difference per RB is shown for the eNBs with unlimited user capability in order to make a fair comparison between the performance of the terrestrial and in-cabin users. When the observed RSSI difference performance given in Fig. 5.5 is taken into account, it is expected that the SINR difference observed for the in-cabin, ground service and airport indoor users should be the same. However, as shown in Fig. 5.7, the SINR difference of the in-cabin users is slightly larger than the SINR difference performance of the ground service and airport indoor users, irrespective of the considered fuselage attenuation. This can be explained by the considered EIRP for the in-cabin LTE system which is 22.2 dBm and relatively lower than the EIRP values considered for the terrestrial LTE system.

In addition to the given analysis for 2 eNBs deployment, RSSI and SINR performance of the 3 eNBs deployment are also investigated. As shown in Fig. 5.8, for RSSI peformance, increasing the number of deployed in-cabin eNBs slightly increases the percentage of gateway users that are above the ECC's limit. However, the RSSI performance of both airport indoor and ground service users remain the same. For SINR performance, the conclusion drawn for the 2 eNBs deployment can also be drawn for the 3 eNBs case with an exception for in-cabin users. The SINR difference between the systems with and without terrestrial eNBs has less effect for the 3 eNBs deployment. Due to increasing the number of eNBs inside the aircraft, the interfer-

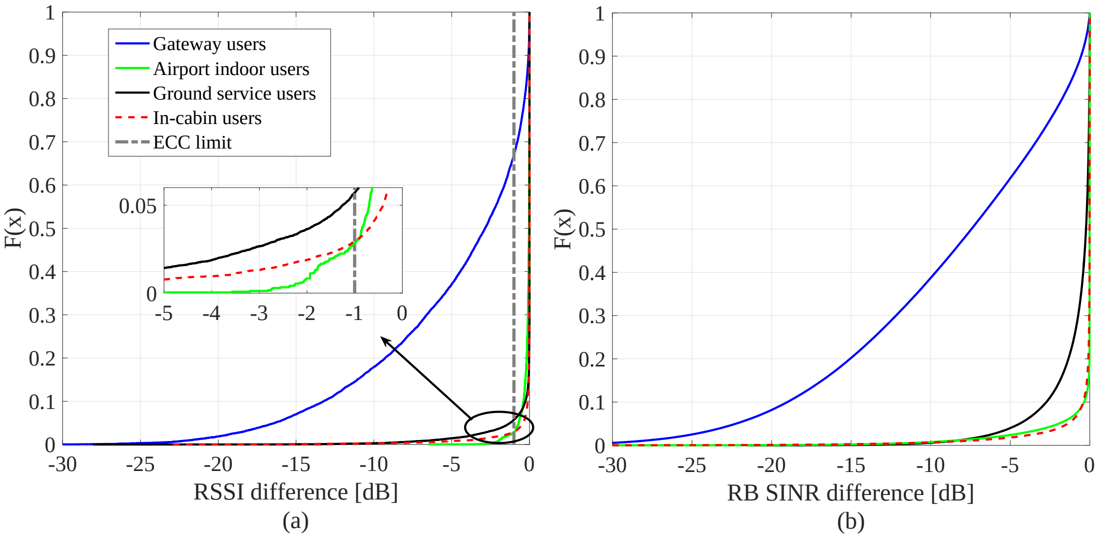

Figure 5.8: *Difference between the systems with and without in-cabin LTE system when 3 eNBs are deployed inside the aircraft and the fuselage attenuation is considered as 5 dB. (a) RSSI. (b) SINR.*

ence power of the onboard system is increased and becomes more dominant than the terrestrial interference power.

In general, activating the in-cabin LTE system does not have a significant harmful effect on the existing terrestrial LTE network and its users. Especially since, realistically, there are limitations on the number of users that an eNB can serve, the contribution of the in-cabin eNBs to the interference level is negligible. The main interference source becomes the terrestrial eNBs. Although, the performance of several RBs is decreased, the majority of the RBs have the same performance with and without the in-cabin system being operational.

5.2.7.3 Handover Results

In order to analyse the handover triggering for a passenger boarding the aircraft, a moving user is modelled in the system where it starts its move from inside the airport, then travels through the gateway to board the aircraft and walks to the end of the cabin. The speed of the moving user is assumed to be 3 km/h (0.82 m/s) and its path is shown in Fig. 5.9.

Fig. 5.10 shows handover instances along the moving user path. The handover triggering quantity is considered as the RSRP. The range of the handover parameters are given in Table 5.3. The parameters *a3-Offset*, *hysteresis* and *time-to-trigger* are set to 12 dB, 6 dB and 1024 ms,

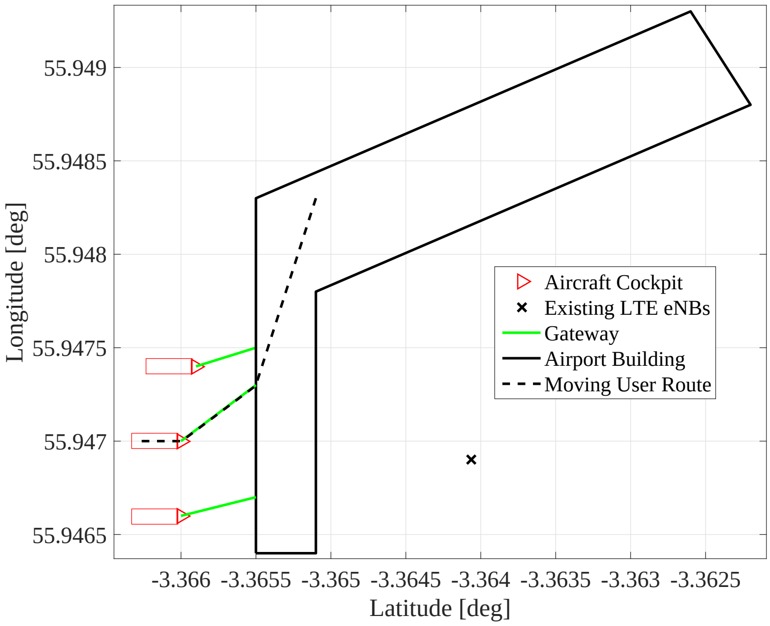

Figure 5.9: *Moving user route.*

respectively. The *individualCellOffset* is considered as 0 dB for terrestrial eNBs and 3 dB for in-cabin eNBs. As it is shown in Fig. 5.10(b), when the moving user steps onto the aircraft, it is handed over to the in-cabin eNB.

For the considered system model, the received signal power level varied from eNB to eNB. However, in order to understand all perspectives of the compatibility of the terrestrial and in-cabin systems, -50 dBm, -70 dBm and -90 dBm of RSRP levels are considered outside the aircraft irrespective of the location of the eNBs. In Table 5.5, an approximated distance between the terrestrial eNB and the aircraft is given for the noted RSRP levels when the transmission power and transmit antenna gain of the terrestrial eNB are set to 49 dBm and 16 dBi, respectively.

Based on the given handover parameters and RSRP levels from terrestrial and in-cabin eNBs, the handover triggering threshold can be written as follows:

$$\mathrm{RSRP_{out}} + \mathrm{CIO_{out}} + \text{a3-Offset} + \text{hysteresis} < \mathrm{RSRP_{in}} + \mathrm{CIO_{in}}, \qquad (5.12)$$

where $\mathrm{RSRP_{out}}$ is the RSRP level from the terrestrial eNB; $\mathrm{RSRP_{in}}$ is the highest RSRP level from the in-cabin eNBs in front of the aircraft entrance door when a user onboard the aircraft; $\mathrm{CIO_{out}}$ represents *cellIndividualOffset* of the terrestrial eNB; and $\mathrm{CIO_{in}}$ represents *cellIndivid-*

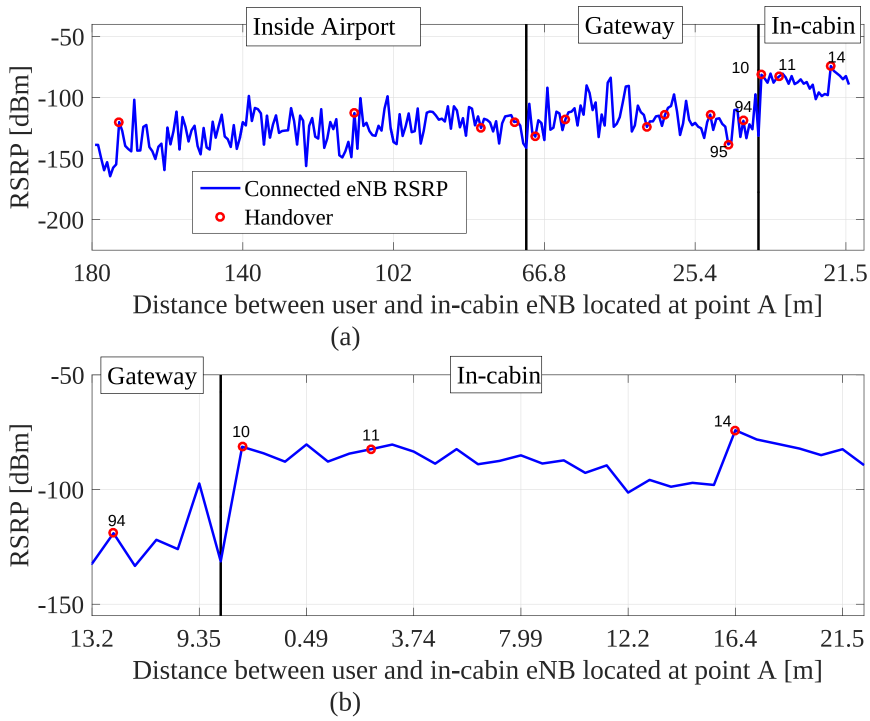

Figure 5.10: *Handover occurrence for the moving user for (a) Full scale and (b) Zoomed. Written number on the red circles represents serving eNB after handover - eNB index equal or smaller than* 24 *represents in-cabin eNBs (there are 3 aircraft, in each aircraft there are 2 eNBs and in each eNB there are 4 cells) and larger than* 24 *represents terrestrial eNBs.*

ualOffset of the in-cabin eNBs. The possible *cellIndividualOffset* values can be obtained based on the achieved RSRP_{out}, RSRP_{in} and the used handover parameters, namely *a3-Offset* and *hysteresis*[5]. For example, lets consider that RSRP_{out}, *a3-Offset*, CIO_{in} and *hysteresis* are equal to -90 dBm, 10 dB, 0 dB and 5 dB, respectively. When the in-cabin eNB transmission power is set to 10.2 dBm, RSRP_{in} is -78.9 dBm around the aircraft front entrance door. Accordingly, for the given example, *cellIndividualOffset* of the in-cabin eNB, CIO_{in}, should be set to 6 dB to satisfy (5.12) to handover the users as soon as they board the aircraft. However, for the given example, if the considered RSRP_{out} level is equal to -50 dBm, then there is no *cellIndividualOffset* value in its prescribed range – the maximum value of the *cellIndividualOffset* is 24 dB. Therefore, for such a case, the *a3-offset* and *hysteresis* parameters of the terrestrial eNB should be set to lower values, as depicted in Fig. 2.16.

[5]Range of *a3-Offset*, *hysteresis* and *cellIndividualOffset* parameters can be found in Table 5.3.

Desired RSRP Level	Distance
-50 dBm	50 m
-70 dBm	135 m
-90 dBm	500 m

Table 5.5: *Distance between the terrestrial eNB and aircraft for a given RSRP level*

5.3 Compatibility of the In-cabin System with Terrestrial Network: Measurement

5.3.1 Measurement Setup

The measurement campaign for compatibility of the in-cabin and terrestrial system is conducted in the Airbus GmbH campus which is based in Finkenwerder, Hamburg, Germany. The objectives of the measurement campaign are to investigate the A321 aircraft fuselage attenuation, power leakage from/to in-cabin system to/from terrestrial system and handover process. Different transmission power levels for both in-cabin and terrestrial systems are considered.

5.3.1.1 Terrestrial System

In the measurement setup, the A321 aircraft is parked inside a hangar and the terrestrial eNB antennas are mounted on a tower roughly 550 m away, as illustrated in Fig. 5.11. Based on Table 5.5, the expected RSRP value around the aircraft is roughly -100 dBm. In order to analyse all perspectives of the compatibility of both systems, higher received power levels are needed around the aircraft. Therefore, a repeater antenna is installed inside the hangar to amplify the received power level of the terrestrial eNBs. The measurement campaign is conducted in collaboration with Vodafone Germany which has the license to operate LTE 1800 MHz system in Germany. Due to having the measurement in a live network, increasing the terrestrial RSRP level around the aircraft may degrade the performance of the LTE systems operating at 1800 MHz. Thus, in order to setup the measurement case with high terrestrial RSRP values, a femto cell antenna is mounted inside the aircraft. In the measurement, the considered terrestrial RSRP levels around the aircraft are -100 dBm, -80 dBm, -70 dBm and -60 dBm. The evolved universal terrestrial radio access absolute radio frequency channel number (EARFCN) and physical cell ID (PCI) of the terrestrial cell was configured to 1836 and 384, respectively.

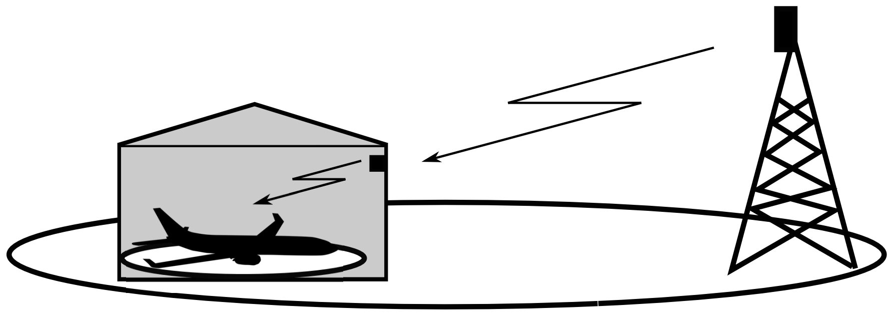

Figure 5.11: *On-site measurement scenario with a terrestrial eNB outside and a repeater antenna inside the hangar. The terrestrial eNB is located about 550 m away from the hangar. The distance between the repeater antenna and aircraft is about 25 m.*

5.3.1.2 In-Cabin System

The in-cabin system is deployed as described in Section 3.4. Accordingly, 3 eNBs are deployed at the provisioned antenna mounting positions. The deployed in-cabin eNBs are manufactured by a vendor company called AZCOM Technology. As in Section 3.4, the QualiPoc Android handsets are used to measure the RSRP and RSSI levels of both in-cabin and terrestrial systems. In the measurement, the considered transmission power of in-cabin eNBs are 17 dBm, 14 dBm and 8 dBm. The EARFCN and PCI configuration of the in-cabin system used in the measurement is given in Table 5.6.

EARFCN	Channel Index	PCI		
		eNB 1	eNB 2	eNB 3
1300	CH 1	119	111	115
1500	CH 2	118	110	114
1675	CH 3	121	113	117
1850	CH 4	120	112	116

Table 5.6: *PCI configuration*

5.3.2 Measurement Results

5.3.2.1 Aircraft Fuselage Attenuation

In order to investigate the aircraft fuselage attenuation, the measurements have been conducted with a scenario where a mobile user moved from/to outside to/from inside the aircraft. The terrestrial cell is provided by Vodafone. The RSRP level outside the aircraft is adjusted to have -80 dBm in front of the aircraft door. During the measurement, the aircraft door is left open. As shown in Fig. 5.12, the RSRP level decreases while the user board the aircraft. The attenuation level is 10 dB around the cockpit site. When the user moves away from the aircraft door towards the tail of the aircraft, the attenuation level becomes 20 dB.

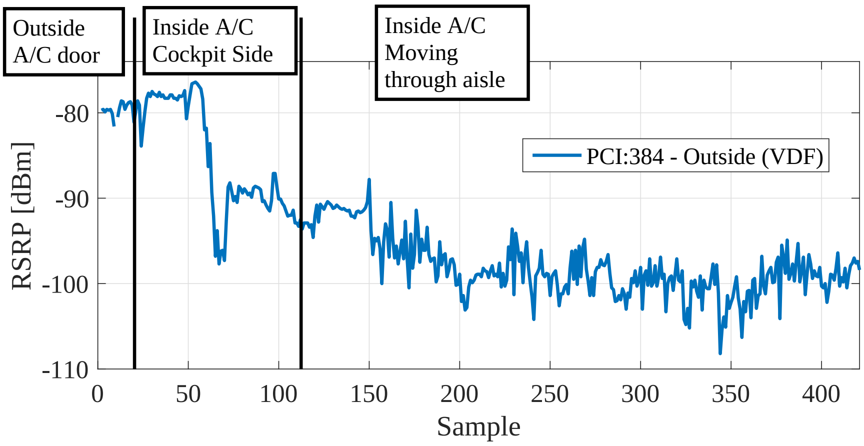

Figure 5.12: *Moving user from outside to inside the aircraft when the terrestrial RSRP level is* -80 *dBm around the aircraft.*

The same scenario is measured with a different terrestrial RSRP level. The repeater antenna is deactivated and the terrestrial eNB located outside the hangar is considered. The RSRP level outside the aircraft is measured as -100 dBm in front of the aircraft door. Moreover, for this case, the door was open when the moving user was on board the aircraft, then the door was closed and remained closed for the duration of the measurement. Fig. 5.13 shows the measured RSRP levels when the user is outside the aircraft, inside the aircraft when the aircraft door is open and inside the aircraft when the aircraft door is closed. When the door is open, the attenuation level is around 10 dB, as in the -80 dBm terrestrial RSRP level case. However, when the door is closed after the moving user is on board the aircraft, an attenuation of 15 dB is observed. The 5 dB difference between the two measurement cases can be explained with antenna characteristics of the repeater and terrestrial eNB. Considering a 12 to 15 dB attenuation level is more realistic for a general system point of view.

5.3.2.2 Handover

Handover in LTE depends on eNB configured parameters *a3-Offset*, *Hysteresis*, *cellIndividualOffset* and *TimeToTrigger* and UE measurement report on the configured triggering quantity. Configuration of the *a3-Offset*, *Hysteresis* and *TimeToTrigger* parameters can only be done by the terrestrial eNBs and their configuration affects the performance of the whole network. Therefore, in cases where a terrestrial user is forced to handover to an in-cabin cell, the only

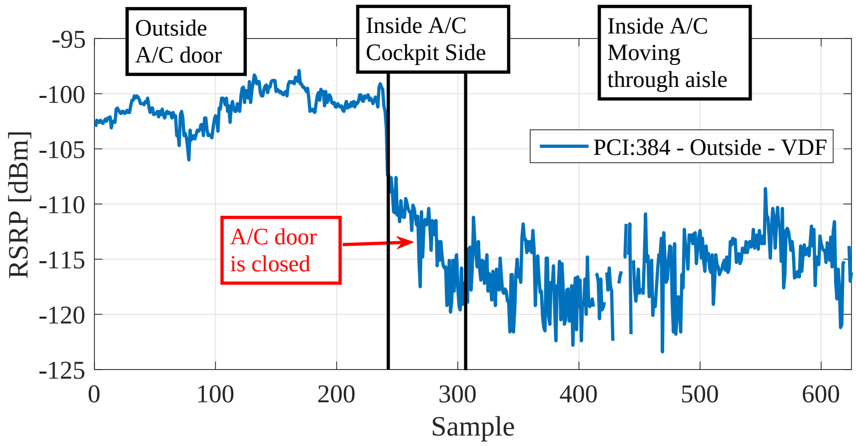

Figure 5.13: *Moving user from outside to inside the aircraft when the terrestrial RSRP level is* -80 *dBm around the aircraft.*

parameter that can be configured by the in-cabin eNB is the *cellIndividualOffset*.

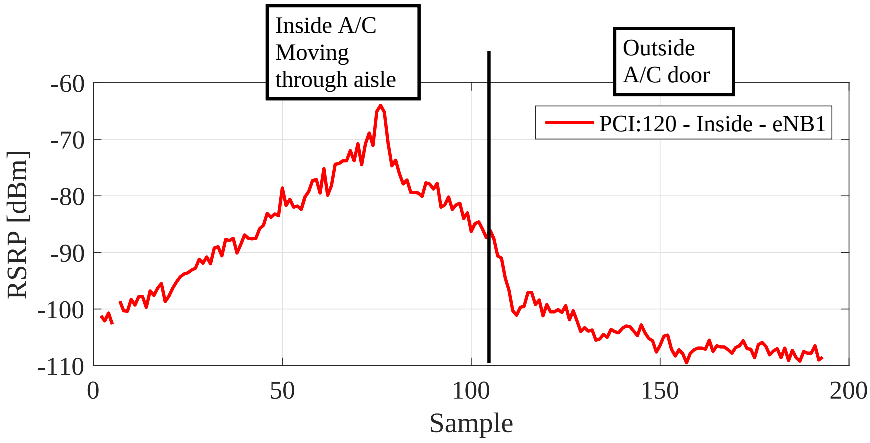

Figure 5.14: *Moving user from inside to outside the aircraft when the transmission power of the in-cabin eNB is set to* 17 *dBm with additional* 8 *dB BCCH power boosting.*

In this research, a broadcast control channel (BCCH) power boosting feature in the in-cabin eNBs is proposed in order to trigger the handover instance earlier. As its name states, BCCH is a control channel that conveys system control information. The idea of the proposed BCCH power boosting feature is to degrade the quality of BCCH transmitted by terrestrial eNBs. Therefore, when the boarding passenger UE cannot get the system information messages, it will start to search for other cells. Accordingly, when the proposed BCCH power boosting feature is employed in the system, the transmit power level of the broadcast channel is increased. Hence, in the proposed feature, there will be no increase in the interference level on the data channels.

Before measuring the handover performance, the power leakage from the in-cabin eNBs to outside the aircraft is investigated. The maximum transmission power capability of the used hardware was limited to 25 dBm. Therefore, in order to investigate the worst case scenario, the maximum transmission power is considered for the in-cabin eNBs, in combination with the proposed BCCH power boosting feature. In Fig. 5.14, the transmission power level of the in-cabin eNB is set to 17 dBm and the BCCH power boosting feature is activated to increase the broadcast channel power level by 8 dB, which makes 25 dBm of transmission power in total. During the measurement, a mobile user moved from inside to outside the aircraft where the QualiPoc handset of the user is forced to connect to EARFCN 1850. The RSRP level from the first eNB observed outside the aircraft is around -102 dBm whereas it is around -90 dBm inside the aircraft. This observation further validates the aircraft fuselage attenuation of 12 dB.

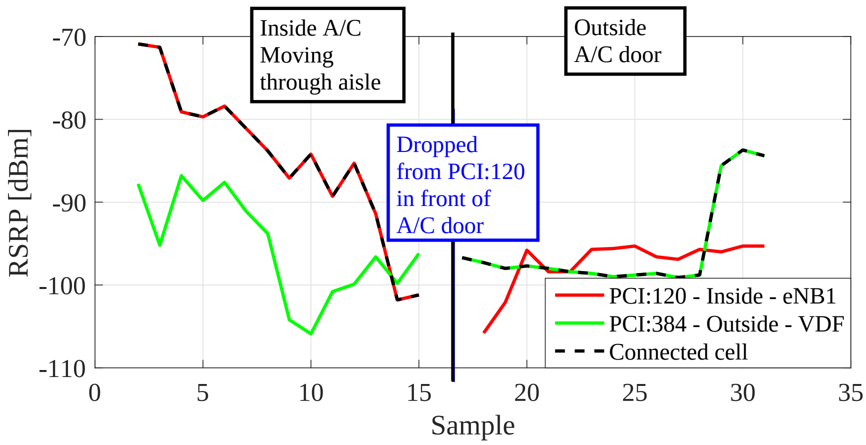

Figure 5.15: *Moving user from inside to outside the aircraft when the transmission power of the in-cabin eNBs is set to* 17 *dBm with additional* 8 *dB BCCH power boosting and RSRP level outside the aircraft is adjusted to* -80 *dBm.*

Further measurements have been conducted to investigate handover performance when the passengers leave the aircraft. Fig. 5.15 shows the RSRP level from the terrestrial and in-cabin cells when the transmission power of the in-cabin eNB is set to 17 dBm with an additional 8 dB of BCCH power boosting. The gap between samples 15 and 20 can be explained as follows: as the UE was trying to handover between cells, the software could not get the RSRP measurements. Once the handover process is completed, the software again started to show the RSRP level. The outside[6] cell is provided by a repeater antenna inside the hangar and the RSRP level outside the aircraft is adjusted to -80 dBm. In order to fully interfere with the terrestrial cell, the EARFCN of the in-cabin cell with PCI equal to 120 is set to the same EARFCN of the

[6]Outside cell and terrestrial cell are used interchangeably where both represent the cell provided by Vodafone Germany.

Vodafone's cell, which is 1836. As can be seen from the figure, when the passenger leaves the aircraft, they are directly connected to the outside cell. It is important to note that the in-cabin system is seen as a private network by the terrestrial network providers. Moreover, the eNB hardware does not support the sending of a system information block (SIB) 3 message which contains handover parameters. Therefore, there is no coordination between the terrestrial and in-cabin eNBs and there is no *cellIndividualOffset* parameters sent by the in-cabin eNBs. Thus, the noted handover analysis represents the cell re-selection procedure and it will be based on the RSRP level.

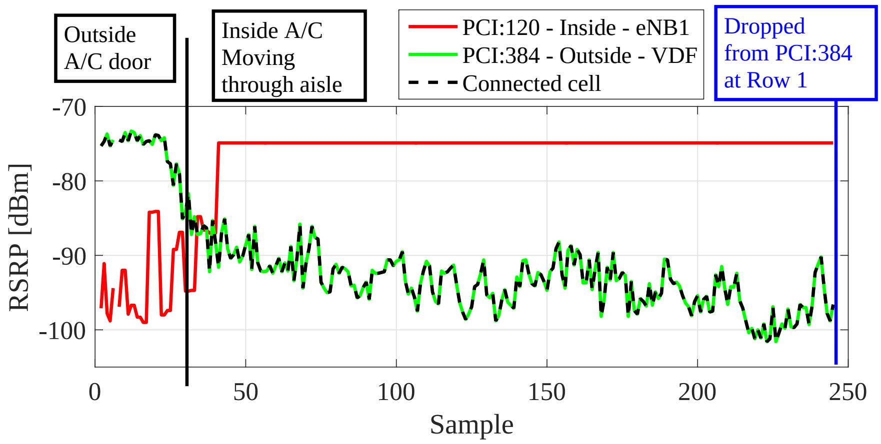

Figure 5.16: *Moving user from outside to inside the aircraft when the transmission power of the in-cabin eNBs is set to* 17 *dBm with additional* 8 *dB BCCH power boosting and RSRP level outside the aircraft is adjusted to* -80 *dBm.*

In Fig. 5.16, the mobile user moves from outside to inside the aircraft, which represents a passenger boarding. When the RSRP level outside the aircraft is adjusted to -80 dBm and the transmission power of the in-cabin eNBs is set to 17 dBm with 8 dB BCCH power boosting feature. Due to the noted lack of cooperation between the Vodafone and in-cabin networks, as well as the lack of system information messages that are used in the handover process at the in-cabin eNBs, the mobile user is not moving at the same pace in this measurement. In order to understand the exact point where the handover process starts for the given power levels, the mobile user is moved from one row to another by spending some time in each row. Accordingly, once the RSRP level from the in-cabin eNB became higher than the terrestrial eNB, the UE handset needs some time to drop from the connected terrestrial cell. As it can be seen from the figure, once the user boards the aircraft, the in-cabin RSRP level becomes 25 dB higher than the terrestrial RSRP. This means that if the two networks were in cooperation and the in-cabin eNBs transmitted handover messages, such as SIB 3, it is most likely that the mobile user will be handed over to the in-cabin network. However, due to the noted shortage, the mobile user has to spend some time to drop from its connected cell and search for other cells. In Fig. 5.16, the measurements are taken while the user was standing in the 1^{st} row. As it can be seen from the figure, the mobile user needed some time to drop from the connected terrestrial cell.

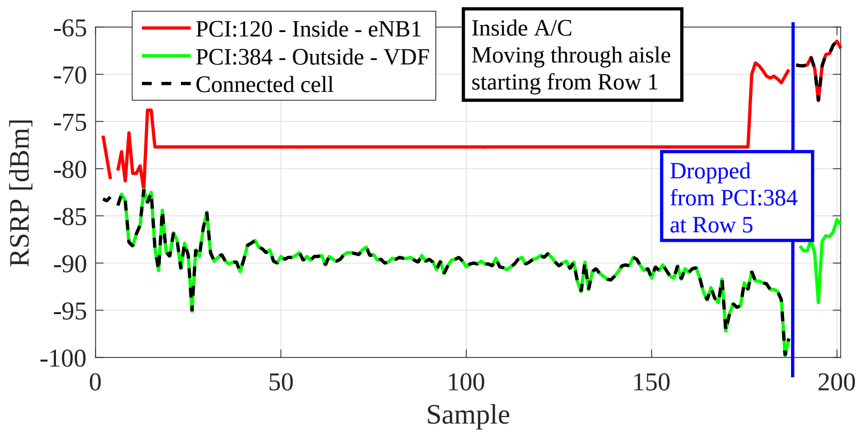

Figure 5.17: *Moving user from outside to inside the aircraft when the transmission power of the in-cabin eNBs is set to* 17 *dBm with additional* 8 *dB BCCH power boosting and RSRP level outside the aircraft is adjusted to* -70 *dBm.*

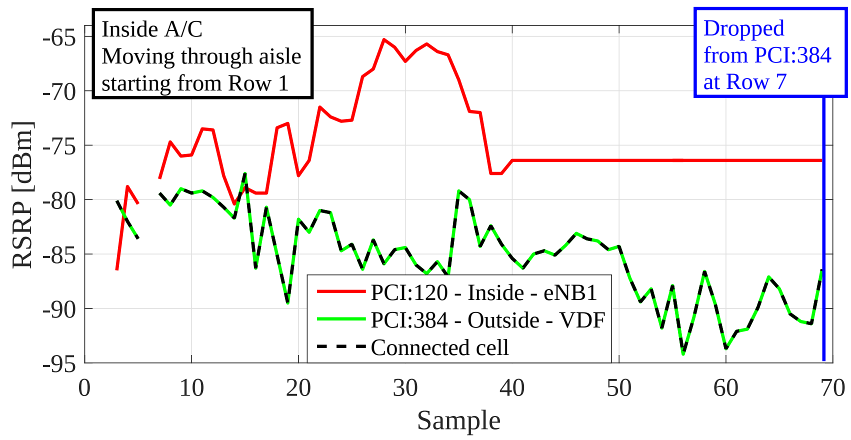

Figure 5.18: *Moving user from outside to inside the aircraft when the transmission power of the in-cabin eNBs is set to* 17 *dBm with additional* 8 *dB BCCH power boosting and RSRP level outside the aircraft is adjusted to* -60 *dBm.*

The same measurement case is repeated for different RSRP levels outside the aircraft. The RSRP level outside the aircraft is adjusted to -70 dBm and -60 dBm in Fig. 5.17 and Fig. 5.18, respectively. To prevent any performance degradation on the live terrestrial network, the repeater antenna is mounted inside the aircraft. In order to represent the aircraft fuselage, the actual RSRP level is set to 10 dB lower than the considered outside RSRP level. For example, when the RSRP level of -60 dBm is considered outside the aircraft, the transmission power of the repeater antenna is adjusted to have -70 dBm inside the aircraft. According to the presented results, the mobile user is dropped from the terrestrial cell at the 5^{th} and 7^{th} rows for the outside RSRP level of -70 dBm and -60 dBm, respectively.

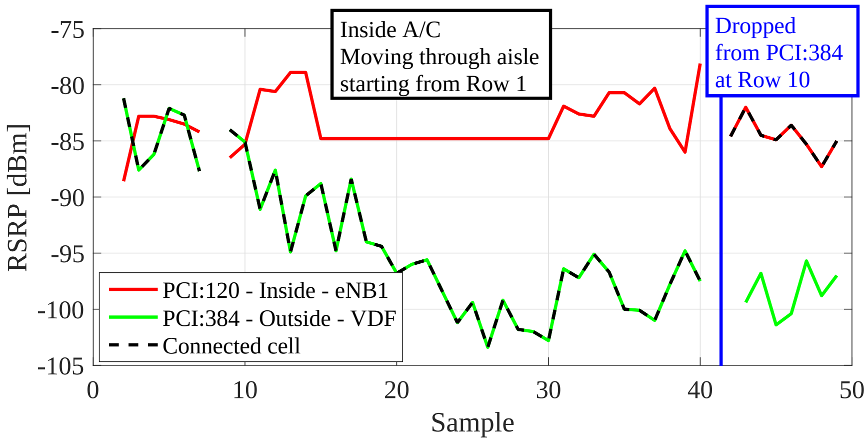

Figure 5.19: *Moving user from outside to inside the aircraft when the transmission power of the in-cabin eNBs is set to* 14 *dBm and RSRP level outside the aircraft is adjusted to* -70 *dBm.*

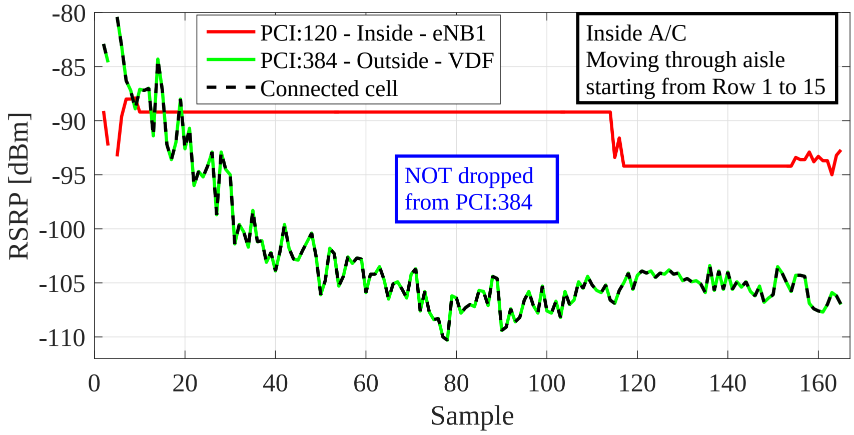

Figure 5.20: *Moving user from outside to inside the aircraft when the transmission power of the in-cabin eNBs is set to* 8 *dBm and RSRP level outside the aircraft is adjusted to* -70 *dBm.*

Another set of measurements have been conducted to understand the effects of the transmission power level of the in-cabin eNBs on handover performance. Therefore, the BCCH power boosting feature is disabled and the transmission power level of the in-cabin eNB is reduced. The RSRP level outside the aircraft is adjusted to -70 dBm. In Fig. 5.19 and Fig. 5.20, the handover performance is observed for the in-cabin eNB transmission power level of 14 dBm and 8 dBm, respectively. It is observed that the mobile user is dropped from the terrestrial cell at row 10 for the transmission power level of 14 dBm, whereas for 8 dBm transmission power, the mobile user is not disconnected from the terrestrial cell. When the user moves from the 1^{st} to 15^{th} row, the RSRP level should increase through the in-cabin eNB location, then it should decrease through to the 15^{th} row. However, as it can be seen from Fig. 5.20, the RSRP level of the in-cabin cell remained the same for a while due to having the noted lack of cooperation among the terrestrial and in-cabin networks. Therefore, it can be concluded that the lack of coordination between the terrestrial and in-cabin eNBs makes the transition intermittent. This statement is valid for the all figures presented for the handover analysis. Based on the measured RSRP levels, the mobile user can be handed over to the in-cabin cell when the transmission power of 8 dBm and RSRP level of -70 dBm are considered for in-cabin and terrestrial systems, respectively.

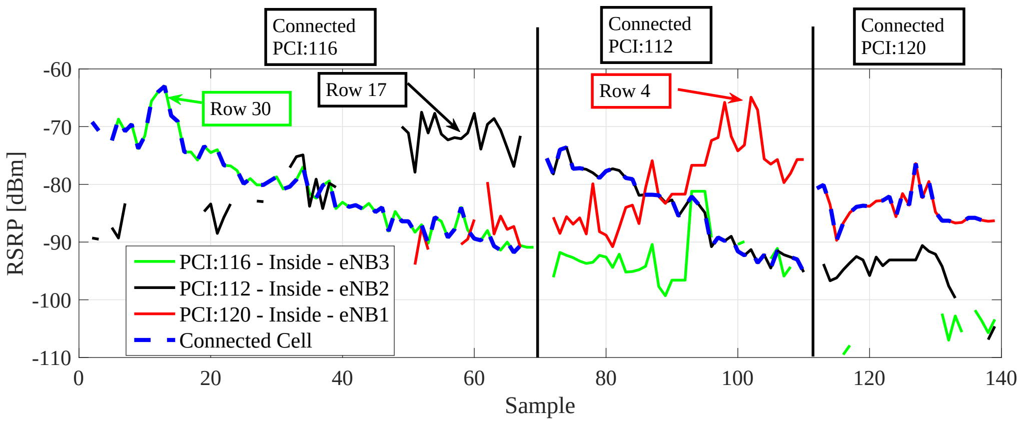

Figure 5.21: *Moving user inside the aircraft when the transmission power of the in-cabin eNBs is set to* 17 *dBm with additional* 8 *dB of BCCH power. No outside cell is considered.*

In Fig. 5.21, cell re-selection performance inside the aircraft is investigated. Accordingly, the measurements are taken with the QualiPoc handset inside the aircraft while the mobile user moves from row 35 to row 1. The in-cabin eNBs locations are indicated on the measured value. Only the channels with index 4 are activated in each eNB with 17 dBm transmission power and additional 8 dB BCCH power. In Fig. 5.21, the connected cell PCI and re-selection instances are shown inside a text box and straight line, respectively. As in the previously shown figures, the gap in the measured values can be seen while the UE establishes the cell-reselection or handover process. The software did not report the measured value during these processes. In Fig. 5.21, the dashed line shows the connected cell and it can be observed that the moving user is smoothly handed over through the in-cabin cells.

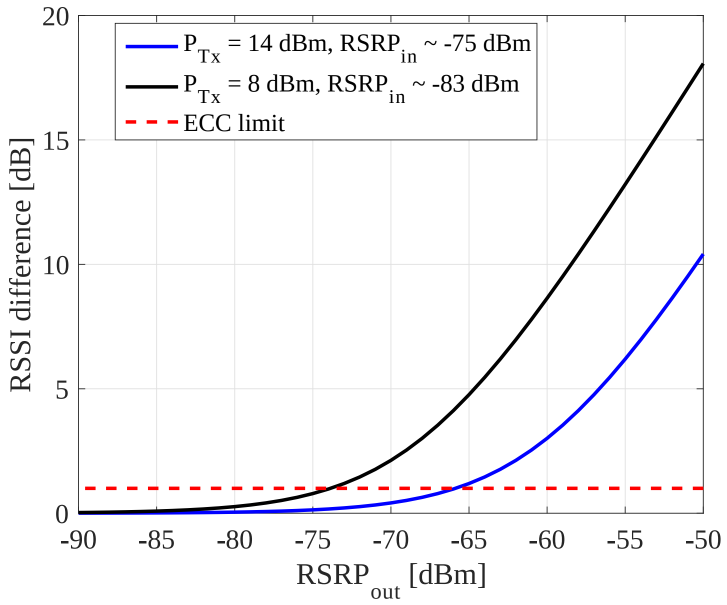

Figure 5.22: *RSSI difference of in-cabin users with respect to RSRP level outside the aircraft.*

In order to specify handover parameters to make the transition from/to terrestrial to/from in-cabin system, the parameters used in Vodafone Germany's network are considered. According to the system information messages sent by the cell with PCI equal to 384, the *cellIndividualOffset*, $\mathrm{CIO_{out}}$, and *hysteresis* are considered as 0 dB and 2 dB, respectively. Whereas, two different configurations are specified for the *a3-Offset* parameter, which are 2 dB and -10 dB. In Fig. 5.22, power leakages from the terrestrial eNBs to in-cabin system for different RSRP levels outside the aircraft is shown. The average of the RSRP level inside the aircraft for different transmission power levels is obtained from the measurement results shown in Fig. 3.15 and the aircraft fuselage attenuation is considered to be between 12 and 15 dB. Accordingly, when the RSRP level of the terrestrial cell is -50 dBm around the aircraft, the in-cabin system performance suffers due to harmful interference, irrespective of the considered transmission power level of the in-cabin eNB. Therefore, when the ECC's limit on the power leakage is considered, the acceptable RSRP levels from the terrestrial cell should be -65 dBm and -75 dBm around the aircraft for in-cabin eNB transmission power level of 14 dBm and 8 dBm, respectively. In Table 5.7, range of the in-cabin *cellIndividualOffset* parameter, $\mathrm{CIO_{in}}$, is given for different in-cabin transmission power and terrestrial RSRP levels according to the noted terrestrial eNB handover parameters. The minimum value of *cellIndividualOffset* parameter that provides smooth transition from terrestrial to in-cabin system is obtained by (5.12).

P_{Tx} [dBm]	$\mathrm{RSRP}_{\mathrm{in}}$ [dBm]	$\mathrm{RSRP}_{\mathrm{out}}$ [dBm]	Increase in RSSI [dB]	Terrestrial *a3-offset* [dB]	Min. $\mathrm{CIO}_{\mathrm{in}}$ [dB]
14	-75	-50	10	2	16
				-10	4
		-66	1	2	-1
				-10	-12
		-90	0	2	-24
				-10	-24
8	-83	-50	18	2	24
				-10	12
		-74	1	2	-1
				-10	-12
		-90	0	2	-16
				-10	-24

Table 5.7: *Minimum cellIndividualOffset value for in-cabin eNBs when the configuration of the Vodafone Germany's cell is considered.*

5.4 Summary

In this chapter, compatibility between the proposed in-cabin LTE system and the existing terrestrial LTE network is investigated while the aircraft is parked on the ground. Although the ECC reports and decisions state that an in-cabin mobile communication system should not be activated/operated while the aircraft is on the ground or during take-off and landing (only active when the altitude of the aircraft is above 3000 m), it is of interest to establish the effects such an operation would have on the existing terrestrial networks. Accordingly, Edinburgh Airport and existing LTE eNBs covering the airport are modelled in this study. Generally accepted and validated WINNER channel models are used to model link between terrestrial eNBs and all classes of users, and a channel model obtained from in-cabin measurement campaign data is used to model channel between the in-cabin eNBs and in-cabin users. Although the presented simulation results are based on only Edinburgh Airport, they could be extended to any airport because of (1) regulations and standards on the minimum distance between the aircraft parking spots; and (2) considering the different received power levels around the aircraft in the simulation platform.

Based on interference power performance results of the systems with and without in-cabin LTE eNBs, an in-cabin LTE system can be operated within the existing LTE network without causing almost any interference. There should be an exception for the users who are in the process of boarding the aircraft by use of a passenger bridge. To mitigate possible harmful interference to the existing LTE network users on the passenger bridge, the in-cabin LTE system could be operated only after boarding is completed and the passenger bridge is empty.

In addition, users who are connected to the terrestrial network are split between the different operators and only allowed to connect to their operator's eNBs. The process through which a UE attaches to an eNB is also studied in detail, in order to understand if there are any other challenges associated with having a limitation on the number of users that an eNB can serve. Based on the SINR performance results with and without in-cabin LTE eNBs, when a user cannot connect to an eNB that serves the best average received power, the performance degradation due to the presence of the in-cabin eNBs is negligible.

In order to validate the simulated results, on-site measurements have been conducted. As a result of the measurements, the aircraft fuselage, power leakage from in-cabin eNBs to the terrestrial system as well as handover performance are validated. Although the in-cabin system is seen as a private network by the already deployed terrestrial system, radio conditions of both terrestrial and in-cabin systems are measured to analyse the handover performance. Accordingly, the parameters that provide a smooth transition from terrestrial to in-cabin systems for the passengers who board the aircraft are obtained for different transmission power levels of in-cabin and terrestrial eNBs. It is important to note that the handover parameters are obtained for the cells which are operated at the same frequency band. In LTE, when the neighbouring cell is at the same frequency as the connected cell, then intra-frequency measurements can be used to trigger handover. However, if the neighbouring cell is at a different frequency, then eNB should inform the UE to do intra-frequency measurements from time to time. This is known as the measurement gap in LTE and it is configured based on *MeasGapConfig* information element (IE). During the measurement gap, there is no transmission and reception and UE switches to frequency bands other than its connected cell to perform measurements.

Another important issue in the in-cabin LTE system design is that the considered 75 MHz bandwidth is not assigned to a single network operator in the terrestrial systems[7]. When a UE is connected to a cell which is operated by its subscribed network operator, then it will keep searching the frequency band used by its network operator. The UE should be informed by its connected eNB to perform measurements at frequency bands that are operated by other service

[7]In general, frequency bandwidth is divided into 5 MHz, 10 MHz, 15 MHz and 20 MHz portions. An auction mechanism is used by governments to sell these portions. Therefore, most of the time, the available portions are shared between network operators in the market, as given in Table 5.1 for the UK.

providers. In LTE, this is done with a public land mobile network (PLMN) number which is an identity for a service provider. When a multi-operator network is considered in LTE, PLMN information is sent as *PLMN-IdentityList*, which is an IE carried by SIB 1. Once the user have the PLMN list, it knows which frequency bands should be measured. In LTE, there can only be a maximum of 6 PLMNs listed in *PLMN-IdentityList* [41].

In conclusion, it is shown that the in-cabin LTE network does not interact significantly with the terrestrial LTE network in the downlink direction. Although there can be performance degradation for the in-cabin network when the terrestrial eNB is deployed roughly 50-135 m away from the airport apron, this can be solved by regulations considered for direct air-to-ground communication (DA2GC). This means that there should not be any significant challenges from a signal quality and network management perspective that need to be solved in order for the two networks to co-exist. Therefore, the legislation that prohibits the use of mobile devices onboard aircraft may not be required.

Chapter 6
Conclusions, Limitations and Future Research

6.1 Summary and Conclusions

In this thesis, a series of fundamental studies related to operating a multi-cell, multi-user onboard communication system in every phase of a flight have been presented. According to regulations, an onboard system could only be operated when the altitude of the aircraft is above 3000 m. However, the key requirement of a next generation communication system is to provide seamless connectivity for anyone and anything. Therefore, this thesis includes an analysis and evaluation of in-flight connectivity. An aircraft cabin is characterised by a high user density which poses a particular problem in this environment. Accordingly, channel propagation characteristics inside the aircraft have been investigated to propose an onboard wireless system design. Specifically, the performance of the onboard Long Term Evolution Advanced (LTE-A) system for an optimal tradeoff between fairness and system throughput has been obtained. Advanced techniques to mitigate co-channel interference for cell-edge users have been considered in a resource allocation (RA) problem. In the problem statement, practical LTE-A system constraints have been taken into account to be able to arrive at a realistic system performance results. Finally, compatibility between the onboard system with the already deployed terrestrial wireless networks has been investigated while the aircraft is in the parked position on the apron.

In Chapter 2, the relevant background related to in-flight connectivity has been presented. Firstly, a brief history of the evolution of wireless communication systems has been provided. Then, the focus of the chapter was to introduce the basic concepts of LTE-A systems, which includes radio frame structure, channel state reporting, RA, handover process and interference mitigation. The introduction of these concepts helps the reader to understand how the LTE-A system works. Specific studies and system concepts in subsequent chapters are based on these basic concepts.

In Chapter 3, the channel propagation characteristics inside the aircraft have been investigated. In many in-cabin channel propagation studies, the transmit antenna location was fixed in the front of the aircraft aisle. Therefore, the characteristics obtained in these studies do not represent an accurate in-cabin multi-cell deployment. In this research, a measurement and modelling procedure has been proposed where the transmit antenna location has been considered at the front, middle and end of the aircraft aisle. The proposed measurement procedure has been conducted to model channel propagation of an onboard multi-cell deployment. Then, in order to minimize the interference among the neighbouring evolved nodeBs (eNBs) and the path loss for users, the proposed channel propagation model has been used to optimize the antenna orientation. In addition, another set of measurements have been conducted to validate the proposed model. It has been shown that co-channel interference is realistically modelled by the proposed channel model.

In Chapter 4, a comprehensive performance evaluation of the multi-cell, multi-user onboard system has been given for LTE-A system where the proposed channel propagation model developed in Chapter 3 has been used. The tradeoff between fairness, which is defined as the lowest variation in user data rates across a large user population, and system throughput has been considered as the optimality criterion of the system. In order to improve fairness, enhanced inter-cell interference coordination (eICIC) techniques, namely almost blank subframe (ABS) and reduced power-ABS (RP-ABS), as well as carrier aggregation (CA) have been employed. In addition, the performance evaluations have been carried out for different resource scheduling policies. Accordingly, round-robin (RR), proportional fair (PF) and a proposed proportional fair based coordinated scheduler (PCS) have been used in the system. The LTE-A system constraints, which are channel quality indicator (CQI) reporting; RA types; and single modulation and coding scheme (MCS) index assignment to the resources allocated to a user, have been considered in the formulation of the scheduling algorithms. Furthermore, the cases have been examined as follows: (1) two different antenna mounting positions, which are 'centreline' and 'provisioned positions'; and (2) deployments of different numbers of eNBs. As a result of the given comprehensive study, an optimum system configuration out of a large set of system options has been provided. It has been shown that with respect to system throughput, the system with PF scheduler and normal subframes (NSF) performs the best, irrespective of the considered antenna mounting positions and number of deployed eNBs. It achieves an average system data rate of 876 Mbps for the 3 eNBs and 612 Mbps for the 2 eNBs deployments when the maximum modulation order has been considered as 64-quadrature amplitude modulation (QAM). However, when the fairness and quality of service (QoS) threshold of 3 Mbps have been considered as the metric of choice, the system with PCS, CA and NSF performs the best for 3 eNBs deployment. When the maximum modulation order has been considered as 64-QAM, the 3 Mbps QoS outage has been recorded as 1.5% and 8% for centreline and provisioned antenna positions, respectively. In other words, 98.5% and 92% of the passengers enjoy a minimum data rate of 3 Mbps when the antennas are mounted at the centreline and provisioned positions, respectively. It has also been shown that a system which employs CA and eICIC techniques together offers no performance improvement compared to the systems which employ only CA. For the considered antenna mounting positions, although the centreline antenna positions have achieved better performance by means of the tradeoff between the fairness and system throughput, their implementation has been considered to be prohibitive due to the additional cost of redesigning the airframe of all aircraft.

In Chapter 5, operating the onboard system within the already deployed terrestrial network has been investigated while the aircraft is considered in the parked position on the apron. Firstly, the power leakage from onboard to terrestrial systems and vice versa has been analysed based on computer simulations. The systems with and without onboard LTE-A deployment have been considered for different classes of users such as those inside the aircraft, waiting on the boarding brigde, working as ground service employees and waiting inside the airport terminal. It has been shown that the onboard LTE-A system can coexist within the already deployed terrestrial LTE-A network without causing almost notable interference. Furthermore, in order to provide a seamless integration of the onboard system, handover parameters have been evaluated for different received power levels of the terrestrial system. It has been shown that when the received power level of the terrestrial system is -50 dBm, it is not possible to provide transition for passengers from the terrestrial to onboard system for the given in-cabin deployment. Secondly, on-site measurements have been conducted in order to validate the simulated results. Based on the measurement results, the aircraft fuselage attenuation has been found to be in the range of 12 to 15 dB. It has been shown that when the received power level from the terrestrial systems is below -65 dBm around the aircraft, (1) a passenger who boards/leaves the aircraft can be handed over to the onboard/terrestrial system; and (2) the terrestrial system does not cause harmful interference to the onboard system for the considered in-cabin deployment. Consequently, it has been demonstrated that the onboard LTE-A system can be operated while the aircraft is in the parked position on the apron. Therefore, the legislation that prohibits the operation of the onboard system should be reviewed to offer seamless mobile connectivity.

6.2 Limitations and Future Research

In the analysis presented in this thesis, a majority of the practical limitations related to the LTE-A system have been taken into account to provide insights into the deployment of onboard LTE-A systems and the coexistence of the onboard and terrestrial networks. Some of the investigations in this thesis have been supported by on-site measurements. However, as inherent with any work that is not fully tested in the real world, there are limitations on the accuracy of the given results. More detailed measurements are needed to further investigate and validate the presented results in order to provide broad guidance for possible regulation changes.

In the modelling of the in-cabin channel propagation characteristics, only a single aircraft type has been used in the measurements. In order to generalize the proposed in-cabin channel propagation, different aircraft types should be used in further measurements. Moreover, the proposed channel model has been given for an empty aircraft. Therefore, the effects of human bodies should also be found and considered for a general in-cabin propagation model. In addition, due to the cost of conducting on-site measurements, only the first phase of the proposed measurement and modelling procedure, which characterizes the antenna propagation direction, has been conducted. The remaining phases which characterize the reflection from the cabin ends and sidewalls could be subjects in the future work in order to precisely investigate the channel propagation inside the aircraft.

In the analysis of the downlink performance of the onboard systems, it has been assumed that there is always an ideal backhaul (IB) link. In other words, the link between the core network and onboard system has infinite capacity and no connection delay. The same assumption has also been held for transmissions in the uplink direction. The effects of having a non-ideal link with limited capacity and connection delay for the backhaul and uplink transmission can be added to the analysis in the future research. Moreover, a full buffer traffic model has been assumed in the onboard network. Although it can be a reasonable assumption for the usage of in-flight entertainment system during a flight, the effects of a finite buffer traffic model should be investigated in the future research to validate the recommended system diagram.

Appendix A
Considered Probability Functions

This section contains a list of papers either accepted for publication, pending publication or submitted for publication.

$$f_{\mathrm{rayleigh}}^{\mathrm{PDF}}\left(x;\mathcal{D}=\{\sigma\}\right)=\frac{x}{\sigma^2}e^{-\frac{x^2}{2\sigma^2}} \tag{A.1}$$

$$f_{\mathrm{weibull}}^{\mathrm{PDF}}\left(x;\mathcal{D}=\{\lambda,k\}\right)=\frac{k}{\lambda}\left(\frac{x}{\lambda}\right)^{(k-1)}e^{-\left(\frac{x}{\lambda}\right)^k} \tag{A.2}$$

$$f_{\mathrm{exponential}}^{\mathrm{PDF}}\left(x;\mathcal{D}=\{\lambda\}\right)=\lambda e^{-x\lambda} \tag{A.3}$$

$$f_{\mathrm{nakagami}}^{\mathrm{PDF}}\left(x;\mathcal{D}=\{\mu,\omega\}\right)=\frac{2\mu^\mu}{\Gamma(\mu)\omega^\mu}x^{2\mu-1}e^{-x^2\frac{\mu}{\omega}} \tag{A.4}$$

Appendix B
Power Delay Profiles for Terrestrial Channel Model

Power delay profile table of each scenario for both line of sight (LoS) and non-line of sight (NLoS) link cases can be found in this subsection from Table B.1 to Table B.5.

Cluster #	Delay [ns]			Power [dB]		
1	0			0.0		
2	30	35	40	-10.5	-12.7	-14.5
3	55			-14.8		
4	60	65	70	-13.6	-15.8	-17.6
5	105			-13.9		
6	115			-17.8		
7	250			-19.6		
8	460			-31.4		

(a)

Cluster #	Delay [ns]			Power [dB]		
1	0			-1.0		
2	90	95	100	-3.0	-5.2	-7.0
3	100	105	110	-3.9	-6.1	-7.9
4	115			-8.1		
5	230			-8.6		
6	240			-11.7		
7	245			-12.0		
8	285			-12.9		
9	390			-19.6		
10	430			-23.9		
11	460			-22.1		
12	505			-25.6		
13	515			-23.3		
14	595			-32.2		
15	600			-31.7		
16	615			-29.9		

(b)

Table B.1: *Scenario B1 clustered delay line model. (a) LoS. (b) NLoS*

Cluster #	Delay [ns]			Power [dB]		
1	0	5	10	-3.0	-5.2	-7.0
2	0			-8.7		
3	5			-3.7		
4	10			-11.9		
5	35			-16.2		
6	35			-6.9		
7	65	70	75	-3.4	-5.6	-7.3
8	120			-10.3		
9	125			-20.7		
10	195			-16.0		
11	250			-21.0		
12	305			-22.9		

Table B.2: *Scenario B4 NLoS clustered delay line model*

Cluster #	Delay [ns]			Power [dB]		
1	0	5	10	0.0	-25.3	-27.1
2	85			-21.6		
3	135			-26.3		
4	135			-25.1		
5	170			-25.4		
6	190			-22.0		
7	275			-29.2		
8	290	295	300	-24.3	-26.5	-28.2
9	290			-23.2		
10	410			-32.2		
11	445			-26.5		
12	500			-32.1		
13	620			-28.5		
14	655			-30.5		
15	960			-32.6		

(a)

Cluster #	Delay [ns]			Power [dB]		
1	0	5	10	-3.0	-5.2	-7.0
2	25			-7.5		
3	35			-10.5		
4	35			-3.2		
5	45	50	55	-6.1	-8.3	-10.1
6	65			-14.0		
7	65			-6.4		
8	75			-3.1		
9	145			-4.6		
10	160			-8.0		
11	195			-7.2		
12	200			-3.1		
13	205			-9.5		
14	770			-22.4		

(b)

Table B.3: *Scenario C1 clustered delay line model. (a) LoS. (b) NLoS.*

Cluster #	Delay [ns]			Power [dB]		
1	0			0.0		
2	0	5	10	-16.2	-18.4	-20.2
3	30			-15.3		
4	85			-16.7		
5	145	150	155	-18.2	-20.4	-22.2
6	150			-18.2		
7	160			-15.3		
8	220			-23.1		

(a)

Cluster #	Delay [ns]			Power [dB]		
1	0			-6.4		
2	60			-3.4		
3	75			-2.0		
4	145	150	155	-3.0	-5.2	-7.0
5	150			-1.9		
6	190			-3.4		
7	220	225	230	-3.4	-5.6	-7.4
8	335			-4.6		
9	370			-7.8		
10	430			-7.8		
11	510			-9.3		
12	685			-12.0		
13	725			-8.5		
14	735			-13.2		
15	800			-11.2		
16	960			-20.8		
17	1020			-14.5		
18	1100			-11.7		
19	1210			-17.2		
20	1845			-16.7		

(b)

Table B.4: *Scenario C2 clustered delay line model. (a) LoS. (b) NLoS.*

Cluster #	Delay [ns]			Power [dB]		
1	0	5	10	-3.0	-5.2	-7.0
2	15			-6.9		
3	95			-3.6		
4	145			-16.2		
5	195			-8.5		
6	215			-15.9		
7	250			-6.9		
8	445			-14.1		
9	525	530	535	-3.8	-6.0	-7.8
10	815			-13.6		
11	1055			-17.8		
12	2310			-32.2		

Table B.5: *Scenario C4 NLoS clustered delay line model*

Appendix C
List of Publications

This section contains a list of papers either accepted for publication, pending publication or submitted for publication.

C.1 Journal Papers

- T. Cogalan, S. Videv, and H. Haas, "Operating An In-Cabin Femto-Cellular System Within A Given LTE Cellular Network," accepted for publication by *IEEE Trans. Veh. Technol.*.
- T. Cogalan, S. Videv, and H. Haas, "Aircraft In-Cabin Communication System Design: Optimizing User Throughput Fairness to System Throughput Tradeoff," submitted to *IEEE Access*, 2018.

C.2 Conference Papers

- T. Cogalan, S. Videv, and H. Haas, "Performance Optimization of Aircraft In-Cabin LTE Deployment Using Taguchis Method," in *Proc. of IEEE Int. Conf. on Commun. (ICC)*, London, UK, pp. 3125-3130, June, 8–12 2015.
- T. Cogalan, H. Haas, and E. Panayirci, "Power Control-Based Multi-User Li-Fi Using a Compound Eye Transmitter," in *Proc. of IEEE Global. Commun. Conf. (GLOBECOM)*, San Diego, CA, pp. 1–6, Dec., 6–10 2015.
- T. Cogalan, H. Haas, and E. Panayirci, "Precoded Single-Cell Multi-User MISO Visible Light Communications," in *Proc. of the 21th European Wireless Conf. (EW)*, Budapest, Hungary, pp. 1–6, May., 20–22 2015.
- T. Cogalan, H. Haas, "Why Would 5G Need Optical Wireless Communications?," in *Proc. of IEEE Int. Symp. on Personal, Indoor and Mobile Radio Commun. (PIMRC)*, Montreal, QC, Canada, pp. 1–6, Oct., 8–13 2017.

- T. Cogalan, S. Videv, and H. Haas, “Aircraft In-Cabin Radio Channel Characterization: From Measurement to Model,” in *Proc. of IEEE Global. Commun. Conf. (GLOBECOM)*, Singapore, pp. 1-6, Dec., 4–8 2017.
- T. Cogalan, S. Videv, and H. Haas, “Coordinated Scheduling for Aircraft In-Cabin LTE Deployment Under Practical Constraints,” accepted by *Proc. of IEEE 87th Veh. Technol. Conf. (VTC)*, Porto, Portugal, June, 3–6 2018.
- T. Cogalan, S. Videv, and H. Haas, “Inflight Connectivity: Deploying Different Communication Networks Inside an Aircraft,” accepted by *Proc. of IEEE 87th Veh. Technol. Conf. Workshop (VTC)*, Porto, Portugal, June, 3–6 2018.

References

[1] 3rd Generation Partnership Project (3GPP), “LTE; Evolved Universal Terrestrial Radio Access (E-UTRA); Physical Channels and Modulation (Release 13).” 3GPP TS 36.211 V13.0.0, January 2016.

[2] ECC, “Compatibility Study Between Mobile Communication Services On Board Aircraft (MCA) and Ground-Based Systems,” Tech. Rep. ECC Report 187, Electronic Communications Committee (ECC), 2013.

[3] CEPT, “Report from CEPT to the European Commission in Response to the Second Mandate to CEPT on Mobile Communication Services on board Aircraft (MCA),” Tech. Rep. CEPT Report 48, CEPT Electronic Communications Committee (ECC), Mar 2013.

[4] 3rd Generation Partnership Project (3GPP), “LTE; Evolved Universal Terrestrial Radio Access (E-UTRA); Physical Layer Procedures (Release 8).” 3GPP TS 36.213 V8.8.0, October 2009.

[5] 3rd Generation Partnership Project (3GPP), “LTE; Evolved Universal Terrestrial Radio Access (E-UTRA); Physical Layer Procedures (Release 13).” 3GPP TS 36.213 V13.0.1, January 2016.

[6] C.-X. Wang, F. Haider, X. Gao, X.-H. You, Y. Yang, D. Yuan, H. Aggoune, H. Haas, S. Fletcher, and E. Hepsaydir, “Cellular Architecture and Key Technologies for 5G Wireless Communication Networks,” *IEEE Commun. Mag.*, vol. 52, pp. 122–130, February 2014.

[7] ECC, “Broadband Direct-Air-to-Ground Communications (DA2GC),” Tech. Rep. ECC Report 214, Electronic Communications Committee (ECC), May 2014.

[8] Alcatel-Lucent, “Using Air-to-Ground LTE for In-Flight Ultra Broadband - Opening the Skies to New Possibilities,” tech. rep., Strategic White Paper, May 2015.

[9] E. Dinc, M. Vondra, S. Hofmann, D. Schupke, M. Prytz, S. Bovelli, M. Frodigh, J. Zander, and C. Cavdar, “In-Flight Broadband Connectivity: Architectures and Business Models for High Capacity Air-to-Ground Communications,” *IEEE Commun. Mag.*, vol. 55, no. 9, pp. 142–149, 2017.

[10] E. Dinc, M. Vondra, and C. Cavdar, “Seamless Gate-to-Gate Connectivity Concept: Onboard LTE, WiFi and LAA,” in *IEEE Vehicular Technology Conference 2017*, pp. 1–6, Sept 2017.

[11] D. B. Walen, R. A. Chitwood, B. DeCleene, and T. Shave, “Study on the User of Cell Phones on Passenger Aircraft,” Tech. Rep. DOT/FAA/AR-12/30, Federal Aviation Administration (FAA), July 2012.

[12] FCC, “Expanding Access to Mobile Wireless Services Onboard Aircraft Notice of Proposed Rulemaking,” Tech. Rep. FCC 13-157, Federal Communications Commission (FCC), Washington, DC, USA, December 2013.

[13] FCC, “Expanding Access to Broadband and Encouraging Innovation through Establishment of an Air-Ground Mobile Broadband Secondary Service for Passengers Aboard Aircraft in the 14.0-14.5 GHz Band Notice of Proposed Rulemaking,” Tech. Rep. FCC 13-66, Federal Communications Commission (FCC), Washington, DC, USA, May 2013.

[14] ECC, “The Harmonised Use of Airborne GSM and LTE Systems in the Frequency bands 1710-1785 MHz and 1805-1880 MHz, and Airborne UMTS Systems in the Frequency Bands 1920-1980 MHz and 2110-2170 MHz (Amended 14 March 2014),” Tech. Rep. ECC Decision (06)07, Electronic Communications Committee (ECC), 2006.

[15] ECC, “Compatibility Between GSM Equipment On Board Aircraft and Terrestrial Networks (Revised May 2008),” Tech. Rep. ECC Report 93, Electronic Communications Committee (ECC), 2006.

[16] ECC, “On Harmonised Conditions of Spectrum Use for the Operation of Mobile Communication Services on Aircraft (MCA Services) in the Community,” Tech. Rep. ECC Decision 2008/294/EC, Electronic Communications Committee (ECC), 2008.

[17] ECC, “Amending Decision 2008/294/EC to Include Additional Access Technologies and Frequency Bands for Mobile Communication Services on Aircraft (MCA Services),” Tech. Rep. ECC Decision 2013/654/EU, Electronic Communications Committee (ECC), 2013.

[18] E. Dinc, M. Vondra, and C. Cavdar, “Multi-user Beamforming and Ground Station Deployment for 5G Direct Air-to-Ground Communication,” in *IEEE Globecom*, December 2017.

[19] P. J. Winzer and D. T. Neilson, “From Scaling Disparities to Integrated Parallelism: A Decathlon for a Decade,” *J. Lightw. Technol.*, vol. 35, pp. 1099–1115, Mar. 2017.

[20] N. Alliance, “5G White Paper, version 1.0,” Final Deliverable, NGMN Alliance, February 2015.

[21] T. Cogalan, S. Videv, and H. Haas, “Performance Optimization of Aircraft In-Cabin LTE Deployment Using Taguchi’s Method,” in *2015 IEEE International Conference on Communications (ICC)*, pp. 3125–3130, June 2015.

[22] T. Cogalan, S. Videv, and H. Haas, “Aircraft In-Cabin Radio Channel Characterization: From Measurement to Model,” in *IEEE Globecom*, December 2017.

[23] T. Cogalan, S. Videv, and H. Haas, “Coordinated Scheduling for Aircraft In-Cabin LTE Deployment Under Practical Constraints,” in *accepted by Proc. of IEEE 87th Veh. Technol. Conf. (VTC)*, June 2018.

[24] T. Cogalan, S. Videv, and H. Haas, “Aircraft In-Cabin Communication System Design: Optimizing User Throughput Fairness to System Throughput Tradeoff,” *submitted to IEEE Trans. on Veh. Technol. (TVT)*, submitted on March 2018.

[25] T. Cogalan, S. Videv, and H. Haas, “Operating An In-Cabin Femto-Cellular System Within A Given LTE Cellular Network,” *submitted to IEEE Trans. on Veh. Technol. (TVT)*, submitted on September 2017.

[26] 3rd Generation Partnership Project (3GPP), Technical Specification Group Radio Access Network, “Coordinated Multi-Point Operation for LTE Physical Layer Aspects (Release 11).” 3GPP TR 36.819 V11.2.0 (2013-09), September 2013.

[27] J. Lee, Y. Kim, H. Lee, B. L. Ng, D. Mazzarese, J. Liu, W. Xiao, and Y. Zhou, “Coordinated Multipoint Transmission and Reception in LTE-Advanced Systems,” *IEEE Commun. Mag.*, vol. 50, pp. 44–50, November 2012.

[28] Huawei, HiSilicon, “LS on BS Implications due to LP-ABS for feICIC.” 3GPP TSG-RAN WG4 Meeting 62, R4-122088, March 2012.

[29] M. Dohler, R. W. Heath, A. Lozano, C. B. Papadias, and R. A. Valenzuela, “Is the PHY Layer Dead?,” *IEEE Commun. Mag.*, vol. 49, pp. 159–165, April 2011.

[30] “Sky High Economics - A Strategic Overview - Chapter One: Quantifying the Commercial Opportunities of Passenger Connectivity for the Global Airline Industry.” LSE Consulting and Inmarsat Aviation, September 2017.

[31] “In-Flight Connectivity: Bringing Fredoom to the Skies.” Inmarsat Aviation, White Paper, July 2017.

[32] N. Tadayon, G. Kaddoum, and R. Noumeir, “Inflight broadband connectivity using cellular networks,” *IEEE Access*, vol. 4, pp. 1595–1606, 2016.

[33] Gogo, “The Anatomy of Inflight Connectivity - First Edition,” tech. rep., Gogo LLC White Paper, 2014.

[34] ETSI, “Broadband Direct Air-to-Ground Communications; Equipment operating in the 1 900 MHz to 1 920 MHz and 5 855 MHz to 5 875 MHz frequency bands; Beamforming antennas; Harmonised Standard covering the essential requirements of article 3.2 of Directive 2014/53/EU,” Tech. Rep. ETSI TR 303 316 V1.0.3, ETSI, Sep. 2016.

[35] J. Lai, “Broadband wireless communication system provided by commercial airlines,” *US Patent 6285878B1*, 2001.

[36] 3rd Generation Partnership Project (3GPP), “Evolved Universal Terrestrial Radio Access (E-UTRA); User Equipment (UE) Radio Transmission and Reception (Release 15).” 3GPP TS 36.101 V15.0.0, Sep 2017.

[37] E. Dahlman, S. Parkvall, J. Skold, and P. Beming, *3G Evolution: HSPA and LTE for Mobile Broadband*. Academic Press, second ed., 2008.

[38] 3rd Generation Partnership Project (3GPP), “LTE; Evolved Universal Terrestrial Radio Access (E-UTRA); Physical Layer; Measurements (Release 13).” 3GPP TS 36.214 V13.0.0, January 2016.

[39] 3rd Generation Partnership Project (3GPP), “Technical Specification Group Radio Access Network; Evolved Universal Terrestrial Radio Access (E-UTRA); Requirements for Support of Radio Resource Management (Release 13).” 3GPP TS 36.133 V13.2.0, January 2016.

[40] 3rd Generation Partnership Project (3GPP), “LTE; Evolved Universal Terrestrial Radio Access (E-UTRA); Overall Description; Stage 2 (Release 13).” 3GPP TS 36.300 V13.2.0, January 2016.

[41] 3GPP, “LTE; E-UTRA; Radio Resource Control (RRC); Protocol Specification (Release 13).” 3GPP TS 36.331 V13.0.0, January 2016.

[42] A. Hamza, S. Khalifa, H. Hamza, and K. Elsayed, “A Survey on Inter-Cell Interference Coordination Techniques in OFDMA-Based Cellular Networks,” *IEEE Commun. Surv. Tutorials*, vol. 15, pp. 1642–1670, Fourth 2013.

[43] Ericsson, ST-Ericsson, “System Performance Evaluations on FeICIC.” 3GPP TSG-RAN WG1 Meeting 66, R1-113482, October 2011.

[44] Huawei, HiSilicon, “Evaluation of the Benefit of Additional Signalling in Case of Reduced Power ABS.” 3GPP TSG-RAN WG1 Meeting 70, R1-123101, August 2012.

[45] Huawei, HiSilicon, “Evaluation of Reduced-Power ABS Based on RAN4 Feedback.” 3GPP TSG-RAN WG1 Meeting 69, R1-122522, May 2012.

[46] Nokia Siemens Networks, Nokia, “LP-ABS Performance in Uniform and Non-uniform Topologies.” 3GPP TSG-RAN WG1 Meeting 70, R1-123637, August 2012.

[47] B. Soret and K. I. Pedersen, “Macro Transmission Power Reduction for HetNet Co-Channel Deployments,” in *IEEE GLOBECOM 2012*, pp. 4126–4130, Dec 2012.

[48] A. Ghosh, R. Ratasuk, B. Mondal, N. Mangalvedhe, and T. Thomas, “LTE-Advanced: Next-Generation Wireless Broadband Technology [Invited Paper],” *IEEE Wireless Commun.*, vol. 17, pp. 10–22, June 2010.

[49] X. Tao, X. Xu, and Q. Cui, “An overview of cooperative communications,” *IEEE Commun. Mag.*, vol. 50, pp. 65–71, June 2012.

[50] M. Sawahashi, Y. Kishiyama, A. Morimoto, D. Nishikawa, and M. Tanno, “Coordinated Multipoint Transmission/Reception Techniques for LTE-Advanced [Coordinated and Distributed MIMO],” *IEEE Wireless Commun.*, vol. 17, pp. 26–34, June 2010.

[51] X. Wang, B. Mondal, E. Visotsky, and A. Ghosh, “Coordinated Scheduling and Network Architecture for LTE Macro and Small Cell Deployments,” in *Communications Workshops (ICC), 2014 IEEE International Conference on*, pp. 604–609, June 2014.

[52] NSN, Nokia, “Simulation Results for CoMP Scenario 2 with Non-Ideal Backhaul.” 3GPP TSG-RAN WG1 Meeting 75, R1-136023, Nov. 2013.

[53] LG Electronics, “Considerations on Inter-eNB Signalling for DL CoMP with Non-Ideal Backhaul.” 3GPP TSG-RAN WG1 Meeting 75, R1-135491, Nov. 2013.

[54] IAESI, DAC-UPC, “Collaborative Distributed Scheduling - Updated Information.” 3GPP TSG-RAN WG1 Meeting 75, R1-135241, November 2013.

[55] Q. W. Lifeng He, “RAN Evolution Project - CoMP Evolution and Enhancement, version 2.0,” Final Deliverable, NGMN Alliance, March 2015.

[56] G. Yuan, X. Zhang, W. Wang, and Y. Yang, “Carrier Aggregation for LTE-Advanced Mobile Communication Systems,” *IEEE Commun. Mag.*, vol. 48, pp. 88–93, February 2010.

[57] EE, “LTE-Advanced Carrier Aggregation Demo.” Available at http://www.fiercewireless.com/europe/story/ee-says-wembley-stadium-lte-carrier-advanced-demo-first-uk/2015-02-27.

[58] Nokia, “LTE-Advanced Carrier Aggregation Demo.” Available at http://company.nokia.com/en/news/press-releases/2015/05/27/nokia-networks-starhub-showcase-lte-advanced-at-600mbps-using-4x4-mimo-technology.

[59] S. Chiu, J. Chuang, and D. G. Michelson, “Characterization of uwb channel impulse responses within the passenger cabin of a boeing 737-200 aircraft,” *IEEE Trans. Antennas Propag.*, vol. 58, pp. 935–945, March 2010.

[60] N. Moraitis, P. Constantinou, F. Perez-Fontan, and P. Valtr, “Propagation Measurements and Comparison with EM Techniques for In-Cabin Wireless Networks,” *EURASIP J. Wireless Comm. and Networking*, 2009.

[61] H. Saghir, C. Nerguizian, J. Laurin, and F. Moupfouma, “In-Cabin Wideband Channel Characterization for WAIC Systems,” *IEEE Trans. Aerosp. Electron. Syst.*, vol. 50, pp. 516–529, January 2014.

[62] A. Awada, B. Wegmann, I. Viering, and A. Klein, “Optimizing the Radio Network Parameters of the Long Term Evolution System using Taguchi’s Method,” *IEEE Trans. Veh. Technol.*, vol. 60, pp. 3825–3839, Oct 2011.

[63] 3GPP, “Further Advancements for E-UTRA Physical Layer Aspects (Release 9).” 3GPP TR 36.814 V9.0.0 (2010-03), Sept. 2012. Retrieved Sept. 3, 2010 from www.3gpp.org/ftp/Specs/.

[64] A. B. Sediq, R. Schoenen, H. Yanikomeroglu, and G. Senarath, “Optimized Distributed Inter-Cell Interference Coordination (ICIC) Scheme Using Projected Subgradient and Network Flow Optimization,” *IEEE Trans. Commun.*, vol. 63, pp. 107–124, Jan 2015.

[65] R. Kwan, C. Leung, and J. Zhang, “Proportional Fair Multiuser Scheduling in LTE,” *IEEE Signal. Proc. Let.*, vol. 16, pp. 461–464, June 2009.

[66] D. Lopez-Perez, X. Chu, A. Vasilakos, and H. Claussen, “On Distributed and Coordinated Resource Allocation for Interference Mitigation in Self-Organizing LTE Networks,” *IEEE/ACM Trans. Networking*, vol. 21, pp. 1145–1158, Aug 2013.

[67] S. N. Donthi and N. B. Mehta, “Joint Performance Analysis of Channel Quality Indicator Feedback Schemes and Frequency-Domain Scheduling for LTE,” *IEEE Trans. Veh. Technol.*, vol. 60, pp. 3096–3109, Sept 2011.

[68] J. Niu, D. Lee, X. Ren, G. Y. Li, and T. Su, “Scheduling exploiting frequency and multi-user diversity in lte downlink systems,” *IEEE Trans. Wireless Commun.*, vol. 12, pp. 1843–1849, April 2013.

[69] Z. Q. Luo and S. Zhang, “Dynamic Spectrum Management: Complexity and Duality,” *IEEE J. Sel. Top. Signal Process.*, vol. 2, pp. 57–73, Feb 2008.

[70] 3rd Generation Partnership Project (3GPP), “Evolved Universal Terrestrial Radio Access (E-UTRA); User Equipment (UE) Radio Transmission and Reception (Release 13).” 3GPP TS 36.101 V13.2.1, January 2016.

[71] J. Olmos, A. Serra, S. Ruiz, M. Garca-Lozano, and D. Gonzalez, “Exponential Effective SIR Metric for LTE Downlink,” in *2009 IEEE 20th International Symposium on Personal, Indoor and Mobile Radio Communications*, pp. 900–904, Sept 2009.

[72] 3rd Generation Partnership Project (3GPP), “Technical Specification; LTE; Evolved Universal Terrestrial Radio Access (E-UTRA); Multiplexing and Channel Coding (Release 13).” 3GPP TS 36.212 V13.0.0, January 2016.

[73] “http://www.edinburghairport.com/about-us/facts-and-figures,” accessed on February 2018.

[74] OFCOM, “Licences of UK Cellular Operators,” January 2015. Available at http://licensing.ofcom.org.uk/radiocommunication-licences/mobile-wireless-broadband/cellular-wireless-broadband/policy-and-background/licensee-freq-tech-information/uk-cellular-operators.

[75] P. Kysti, J. Meinil, L. Hentil, X. Zhao, T. Jms, C. Schneider, M. Narandzic, M. Milojevic, A. Hong, J. Ylitalo, V.-M. Holappa, M. Alatossava, R. Bultitude, Y. de Jong, and T. Rautiainen, “WINNER II Channel Models,” Tech. Rep. D1.1.2 V1.2, WINNER, Information Society Technologies, 2008.

[76] J. Meinila, P. Kyosti, L. Hentila, T. Jamsa, E. Suikkanen, E. Kunnari, and M. Narandzic, “WINNER+ Final Channel Models,” Tech. Rep. D5.3, WINNER+, Celtic Telecommuncation Solutions, 2010.

[77] OFCOM, “Variation of 1800 MHz Mobile Licences to Increase Power Limit.” Statement, August 2014.